

Characterization of an *ATG5* derived circular RNA (hsa_circ_0077535) in childhood acute lymphoblastic leukemia

Inaugural-Dissertation

zur Erlangung des Doktorgrades der Mathematisch-Naturwissenschaftlichen Fakultät der Heinrich-Heine-Universität Düsseldorf

vorgelegt von

Idriss Edler Koumba Mahoungou

aus Brazzaville, Republik Kongo

aus der Klinik für Kinder-Onkologie, -Hämatologie und Klinische Immunologie des Universitätsklinikums Düsseldorf				
Berichterstatter:				
1. Prof. Dr. Arndt Borkhardt				
2. Prof. Dr. Sebastian Wesselborg				

Table of content

1 Introduction	10
1.1 Leukemia	10
1.1.1 Etiology	12
1.1.2 Symptoms	14
1.1.3 Diagnosis	14
1.2 Non-coding RNAs	18
1.2.1 Discovery of circular RNAs (circRNAs)	19
1.2.2 Properties of circRNAs	20
1.2.3 Biogenesis of circRNAs	20
1.2.4 Biological relevance of circRNAs	22
1.2.5 Role of circRNAs in cancers	23
1.3 Autophagy	24
1.3.1 The autophagy machinery and regulation of autophagy in mammalian cells	25
1.3.2 Role of autophagy in cancer	27
1.3.3 Role of ATG5	28
2 Aim of the thesis	30
3 Materials and Methods	31
3.1 Materials	31
3.1.1 Human cell lines	31
3.1.2 Media and cell culture supplements	31
3.1.3 Reagents and chemicals	32
3.1 Kits and ladders	34
3.1.1 Oligonucleotides	35
3.1.2 RNA FISH probes	36
3.1.3 Small interfering RNAs (siRNAs)	36
3.1.4 Plasmids and plasmid cards	37
3.1.5 Antibodies	41
3.2 Enzymes	41
3.3 Other consumables	42

3.4 Software	43
3.5 Hardware	43
4 Methods	45
4.1 Cell culture techniques	45
4.1.1 Cultivation of human cell lines	45
4.1.2 Cryopreservation and thawing of human cell lines	45
4.1.3 RNA isolation	46
4.1.4 RNase R treatment	46
4.1.5 RNA sequencing	46
4.1.6 cDNA synthesis	47
4.1.7 Quantitative real-time PCR (RT-qPCR)	47
4.1.8 MicroRNA quantification system	48
4.1.9 Standard PCR	50
4.1.10 Agarose gel electrophoresis	50
4.1.11 Gel extraction	51
4.1.12 Sanger sequencing	51
4.1.13 DNA cloning	51
4.1.14 Virus production	52
4.1.15 Transformation	53
4.1.16 Plasmid purification	53
4.1.17 Transfection of plasmid DNA	54
4.1.18 RNA interference using small interfering RNA (siRNA)	54
4.1.19 RNA fluorescence in situ hybridization (FISH)	54
4.1.20 mRNA stability assay using transcription inhibition by Actinomycin D	55
4.1.21 Cell based assays	55
4.1.22 Cell cycle analysis	58
4.1.23 Proteomics	58
4.1.24 Western blot	58
4.1.25 Statistical analysis	59
5 Results	60

	5.1 Detection of circATG5 4-5 in B cell acute lymphoblastic leukemia cell lines	60
	5.2 Characterization of circATG5 4-5	62
	5.3 CircATG5 4-5 can be detected and validated by RT-qPCR	62
	5.4 CircATG5 4-5 is expressed in B-ALL cell lines across different molecular subtypes	64
	5.5 CircATG5 4-5 can be detected in the cytoplasm	64
	5.6 Overexpression of circATG5 4-5	65
	5.7 circATG5 4-5 may correlate with ATG5	69
	5.8 Overexpression of circATG5 4-5 increases ATG5 levels	70
	5.9 Knockdown of circATG5 4-5 reduces ATG5 levels	71
	5.10 CircATG5 4-5 regulates the stability of <i>ATG5</i> mRNA	73
	5.11 Transcriptomic changes following circATG5 4-5 overexpression	73
	5.12 Effect of circATG5 4-5 expression on autophagy flux	77
	5.13 MicroRNA prediction binding sites	78
	5.14 Expression of predicted miRNA in HEK293, 697 and HAL-01 cell lines	79
	5.15 Overexpression of circATG5 4-5 affects most predicted miRNAs	79
	5.16 circATG5 4-5 may regulate CDK6 upon affecting miRNA-1299 levels	80
	5.17 circATG5 4-5 and ATG5 positively correlate with CDK6	82
	5.18 CircATG5 4-5 overexpression increases cell viability and proliferation	83
	5.19 Overexpression of circATG5 4-5 increases G2M cell fraction	84
6	Discussion	86
7	References	93
8	Acknowledgements	107
9	Appendix	108
	9.1 Abbreviations	108
	9.2 Table Directory	111
	9.3 Figure Directory	112

Summary

Acute lymphoblastic leukemia (ALL) is the most common malignant disease in children. Autophagy is a cellular recycling process that removes unnecessary and dysfunctional components within cells. Autophagy plays an important role in the regulation of numerous physiological functions, including hematopoiesis. Depending on the cellular context, autophagy can inhibit tumor initiation or promote cell survival of established tumors. Therefore, autophagic activity could be an interesting therapeutic target for the treatment of ALL. Increasing evidence has recently suggested that circular RNAs (circRNAs) are implicated in the regulation of autophagy during the development of tumors.

High-throughput RNA sequencing has led to the discovery of more than 100,000 circRNAs. However, most of them have not yet been functionally characterized. This thesis aimed to identify circRNAs derived from *autophagy-related genes*, especially *ATG5*. Therefore, the current study focused on the circRNA hsa_circ_0077535 ("circATG5 4-5"), a circRNA derived from exons 4 and 5 of *autophagy-related gene 5* (*ATG5*) and characterized its impact on autophagy signaling in the context of *TCF3*-rearranged ALL.

CircATG5 4-5 was identified by RNA sequencing in *TCF3*-rearranged B-ALL cell lines (HAL01 and 697). RT-qPCR and Sanger sequencing were then performed to validate the transcript. The expression of circATG5 4-5 in B-ALL was determined employing additional B-ALL cell lines of different molecular subgroups using RT-qPCR. The subcellular localization of circATG5 4-5 was characterized by RNA fluorescence *in situ* hybridization (RNA FISH). To investigate the effect of circATG5 4-5 on its host gene *ATG5* and its consequence for autophagy, cell proliferation, survival and cell cycle, cellular models of altered circATG5 4-5 expression were developed (overexpression and knockdown models of HEK293T, HAL01 and 697). *ATG5* RNA stability was further analyzed in these models upon actinomycin D treatment. miRNAs predicted to interact with circATG5 4-5 were identified using the in-silico tool circInteractome.

The present work showed that circATG5 4-5 can be detected in a wide variety of B-ALL cell lines. It is predominantly distributed in the cytoplasm. The overexpression of circATG5 4-5 significantly increased the expression of its parental gene *ATG5* and consequently led to an increase of autophagy. Consistently, the knockdown of circATG 4-5 showed the reverse effect. Overexpression of circATG5 4-5 had a protective effect on ATG5 mRNA stability during actinomycin D treatment, whereas the knockdown had a negative impact. Several

miRNAs were predicted to interact with circATG5 4-5 of which miR1299 was further functionally analyzed. While miR1299 expression was repressed in circATG5 4-5 overexpressing cells, *cyclin dependent kinase* 6 (*CDK6*), a target of miR1299 was increased. Proliferation, cell viability and G2/M phase of cell cycle were increased by overexpression of circATG5 4-5. Taken together, the data obtained in this thesis suggest that high expression of circATG5 4-5 may contribute to a malignant phenotype by promoting cell proliferation, cell viability and positive regulation of the cell cycle. Conversely, low circATG 4-5 expression may have an anti-proliferative, anti-cancer effect.

Zusammenfassung

Die akute lymphoblastische Leukämie (ALL) ist die häufigste bösartige Erkrankung bei Kindern. Autophagie ist ein zellulärer Recyclingprozess, der Zellen von unnötigen und dysfunktionalen Komponenten beseitigt. Er spielt eine wichtige Rolle bei der Regulierung zahlreicher physiologischer Funktionen, einschließlich der Hämatopoese. Je nach zellulärem Kontext kann Autophagie die Tumorentstehung verhindern oder das Überleben von Zellen in etablierten Tumoren fördern. Die gezielte Beeinflussung der zellulären Autophagie-Aktivität könnte daher zur Verbesserung der Behandlung der akuten lymphatischen Leukämie beitragen. Es gibt immer mehr Hinweise darauf, dass zirkuläre RNAs (circRNAs) während der Tumorentwicklung an der Steuerung der Autophagie beteiligt sind.

Die Hochdurchsatz-RNA-Sequenzierung hat die Forschung über circRNAs gefördert. Zurzeit sind mehr als 100.000 circRNAs entdeckt worden. Die meisten von ihnen sind jedoch noch nicht funktionell charakterisiert worden.

Das Ziel dieser Arbeit war es, circRNAs zu identifizieren, die von Autophagie-assoziierten Genen stammen, insbesondere *ATG5*. Daher hat sich die aktuelle Studie auf die circRNA *hsa_circ_0077535* ("circATG5 4-5") fokussiert, eine circRNA, die auf Exons 4 und 5 des Autophagie-assoziierten Gens 5 (*ATG5*) codiert ist, und hat des Weiteren ihren Einfluss auf die Autophagie-Signalgebung im Kontext der *TCF3*-rearrangierten ALL charakterisiert.

CircATG5 4-5 wurde durch RNA-Sequenzierung in *TCF3*-veränderten B-ALL-Zelllinien (HAL01 und 697) identifiziert. RT-qPCR und Sanger-Sequenzierung wurden anschließend zur Validierung des Transkripts durchgeführt. Die Expression von circATG5 4-5 bei B-ALL wurde mit weiteren B-ALL-Zelllinien verschiedener molekularer Untergruppen mittels RT-qPCR bestimmt. Die subzelluläre Lokalisierung von circATG 4-5 wurde durch RNA-Fluoreszenz-*in-situ*-Hybridisierung (RNA-FISH) charakterisiert. Um die Wirkung von circATG5 4-5 auf *ATG5* und dessen Auswirkungen auf Autophagie, Zellproliferation, Überleben und Zellzyklus zu untersuchen, wurden von mir Zellmodelle mit veränderter circATG5 4-5-Expression entwickelt (Überexpressions- und Knockdown-Modelle von HEK293T, HAL01 und 697). Die *ATG5*-mRNA-Stabilität wurde in diesen Modellen unter Actinomycin D-Behandlung weiter analysiert. Darüber hinaus wurden miRNAs, die mit circATG5 4-5 interagieren, mithilfe des *in silico*-Vorhersagetools CircInteractome identifiziert.

Die vorliegende Arbeit zeigte, dass circATG5 4-5 in verschiedenen B-Zelllinien exprimiert wird und überwiegend im Zytoplasma verteilt ist. Die Überexpression von circATG5 4-5 führte zu einer signifikanten Steigerung der Expression seines Parentalgens ATG5 und somit zu einer positiven Regulierung der Autophagie. Hingegen zeigte der Knockdown einen gegenläufigen Effekt. Des Weiteren zeigten circATG5 4-5 überexprimierende Zellen eine protektive Schutzwirkung von ATG5 gegen Actinomycin D, während der Knockdown eine negative Auswirkung auf die ATG5-Stabilität zeigte. Mehrere miRNAs zeigten eine Interaktion mit circATG5 4-5, von denen miR1299 eingehend untersucht wurde. Während die miR1299-Expression in circATG5 4-5 überexprimierenden Zellen unterdrückt wurde, war die Cyclin-abhängige Kinase 6 (CDK6), ein Ziel von miR1299, erhöht. Proliferation, Zelllebensfähigkeit und G2/M-Phase des Zellzyklus wurden durch die Überexpression von circATG5 4-5 erhöht.

Insgesamt deuten die in dieser Arbeit generierte Daten darauf hin, dass eine hohe Expression von circATG5 4-5 zu einem malignen Phänotyp beitragen kann, indem sie die Zellproliferation und Zelllebensfähigkeit fördert und den Zellzyklus positiv reguliert. Umgekehrt kann der Knockdown circATG5 4-5-Expression eine anti-proliferative, krebshemmende Wirkung haben.

1 Introduction

1.1 Leukemia

The term leukemia is derived from the greek words leukos (white) and haima (blood), which literally means white blood. In Germany, leukemia is the most diagnosed cancer type in children and adolescents younger than 18 years, followed by tumors of the central nervous system, with about 29.7% and 23.6%, respectively ¹. Despite major advances in the treatment of childhood leukemia, it remains the leading cause of death from disease in children in industrialized countries ².

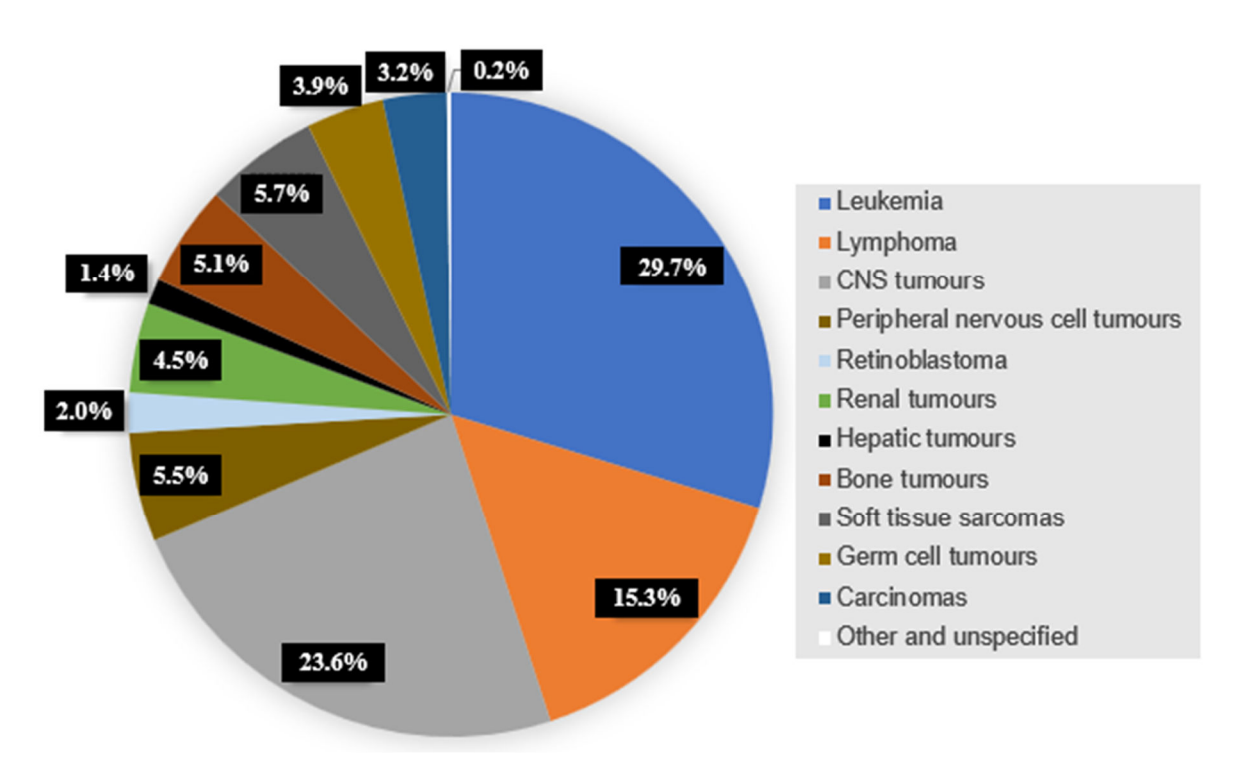


Figure 1: Most prevalent cancer types presenting in childhood (age <18 years) in Germany. Childhood cancer incidence rates in Germany based on 21831 patients during 2009-2018. Annual Report 2019 from the German Childhood Cancer Registry. CNS: central nervous system. Adapted from ¹.

All blood cell lineages arise from hematopoietic stem cells (HSCs) residing in the bone marrow by a process called hematopoiesis (**Figure 2**) ³. This highly conserved process begins *in utero* and continues for life. One distinguishes between long-term (LT)-HSCs, which have self-renewal potential for life, and short-term (ST)-HSCs that self-renew for a limited time ⁴. ST-HSCs give rise to multipotent progenitors (MPPs), which in turn give rise to common lymphoid progenitors (CLPs) or common myeloid progenitors (CMPs). CLPs undergo lymphopoiesis to produce lymphoid lineages including B and T lymphocytes as

well as natural killer cells. Cells of the myeloid lineage develop from CMPs during myelopoiesis and include e.g. granulocytes, monocytes, and megakaryocytes. Dendritic cells can originate from either lymphoid or myeloid precursors ⁵.

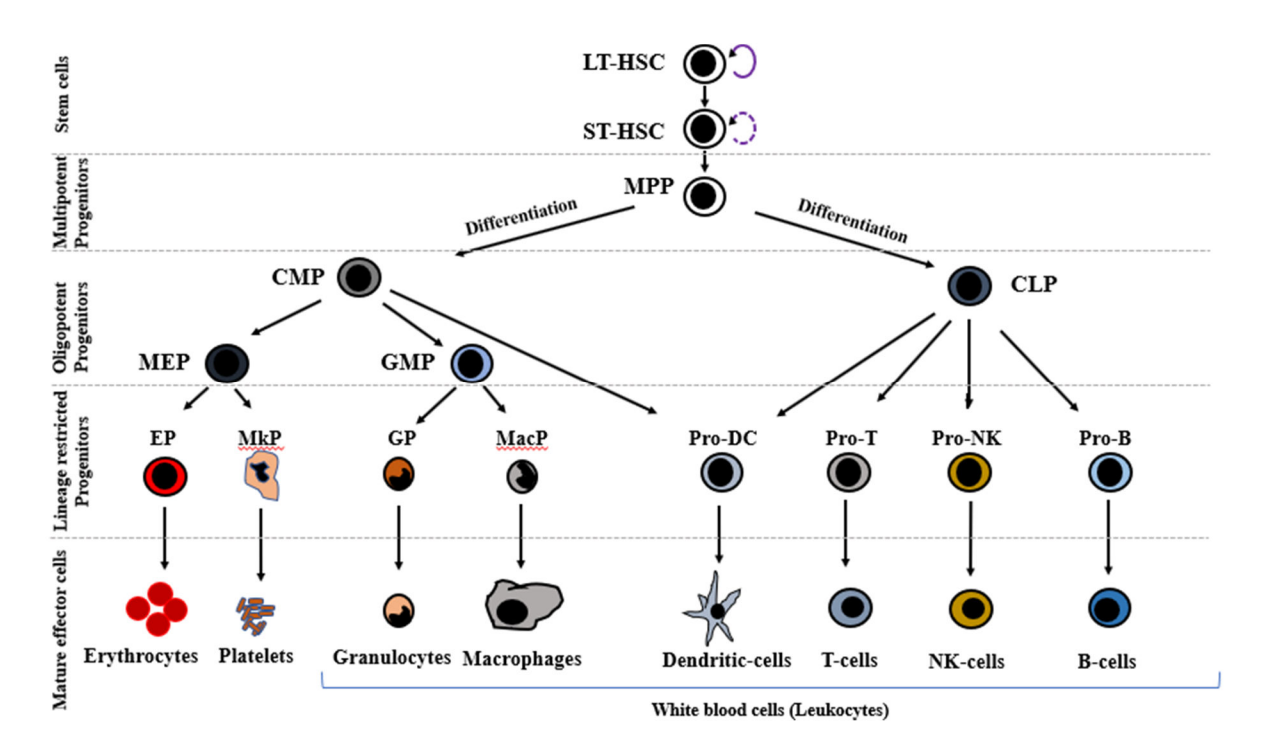


Figure 2: Scheme of hematopoiesis.

All hematopoietic cells derive from common pluripotent hematopoietic stem cells. The LT-/LS-HSCs initially give rise to multi-potent progenitors (MPP). The MPPs differentiate into oligo-potent progenitors: the common lymphoid progenitor (CLP) and the common myeloid progenitor (CMP). T-cells, B-cells, and natural killer (NK) cells derive from lineage restricted progenitors, which are products of CLPs, while the CMPs give rise to megakaryocyte/erythrocyte progenitors (MEPs) and granulocyte/macrophage progenitors (GMPs). MEPs produce megakaryocytes/platelets and erythrocytes by passaging through lineage restricted progenitors and GMPs give rise to granulocytes and monocytes/macrophages by passaging through different restricted progenitors. Dendritic cells are produced by both the CMPs and the CLPs. Leukocytes derive from both lineages (CMP and CLP). Depending on the lineage that they arise in, leukemias can be lymphoid or myeloid. EP: erythrocyte progenitor, MkP: megakaryocyte progenitor, GP: granulocyte progenitor, MacP: macrophage progenitor, DC: dendritic cell, NK: natural killer. Adapted from ^{4,6}.

HSCs balance between the process of self-renewal and differentiation to regulate the production of blood cells and maintenance of the stem cell pool. This balance can be disturbed by the accumulation of genetic and epigenetic changes leading to malignant transformation of HSCs or hematopoietic progenitor cells into leukemic stem cells (LSC) ⁷. LSCs generate partially differentiated progenies, e.g. leukemic blasts, which have a limited proliferative potential ⁸, but a small subset of LSCs can maintain a replenishment of the bulk of leukemic cells with their capacity to self-renew and proliferate ⁹.

Depending on how fast the disease progresses, leukemia can be divided in acute or chronic forms ¹⁰. Acute leukemia progresses faster and gets worse very quickly. It is characterized by an accumulation of immature cells called blasts (≥ 20% blasts in the peripherical blood or bone marrow) ¹¹. Chronic leukemia develops over a long period of time (over months and years) and is characterized by the abnormal proliferation of more mature white blood cells that may be able to maintain some functions of normal blood cells. Leukemias can furthermore be divided into myeloid or lymphoid leukemias. Myeloid leukemias arise from cells derived from the common myeloid progenitor, while lymphoid (or lymphoblastic) leukemias arise from cells derived from the common lymphoid progenitor.

There are in total four subtypes of leukemia, namely acute myeloid leukemia (AML), acute lymphoblastic leukemia (ALL), chronic myeloid leukemia (CML) and chronic lymphoblastic leukemia (CLL).

As this work is about childhood acute lymphoblastic leukemia (ALL), the next part of this chapter will deal with that. Childhood ALL is the most common pediatric cancer, accounting for approximately 25% of all childhood cancers ¹² and 75 to 80% of all cases of childhood leukemia ¹³. There are more boys suffering from ALL than girls ¹⁴. B-cells precursor types are around 85% of the ALL cases ¹⁵, while T-ALLs represent 15% of childhood ALL ¹⁶. As this work focused on B-cell ALL (B-ALL) in children, the rest of this chapter dealing with leukemias will place more emphasis on B-cell ALL rather than on other leukemia types.

1.1.1 Etiology

Many factors can be involved in the development of the childhood ALL such as genetic factors, exposure to infections and environmental influences ¹⁷.

Concerning the genetic factors of childhood ALL, childhood ALL typically results from the interplay between genetic predisposing factors and later acquired somatic alterations ¹⁸. Genetic predisposition in childhood ALL can be classified according to their penetrance and frequency. This includes rare highly penetrant germline mutations, frequent low-penetrant germline variations and somatic predisposition ¹⁹.

> Rare highly penetrant germline mutations

Down syndrome ²⁰, ETV6 (ETS Variant Transcription Factor 6)-deficiency ²¹, IKZF1 (IKAROS Family Zinc Finger 1)-deficiency ²² and PAX5 (Paired Box 5)-deficiency ²³ predispose to ALL. The genetic variations occurring in ETV6 and IKZF1 genes of the germ cells include missense, nonsense and frameshift mutations ^{24,25}. ETV6 can be additionally subjected to deletion, or the mutation can occur in the splice site ²⁶. Constitutionally mismatch repair deficiency (CMMRD) syndrome caused by mutations in the DNA mismatch repair genes PMS2 (PMS1 Homolog 2, Mismatch Repair System Component), MSH6 (MutS Homolog 6), MSH2 (MutS Homolog 2) or MLH1 (MutL Homolog 1) should be considered in childhood ALL, since it is known to be associated with a high risk of cancer development ²⁷. Several other genes whose germline mutations are associated with a risk for childhood ALL have been reviewed ¹⁹.

> Frequent low-penetrant germline variations

In addition to rare highly penetrant germline mutations, further germline variations have already been identified. These variations are frequent but present low-penetrant somatic chromosomal aberrations. Moreover, they are mostly single nucleotide polymorphisms (SNPs) associated with a high risk for ALL development. Genome-wide association studies have shown an association between the increased risk of ALL with the presence of certain SNPs in genes including IKZF1, ARID5B (AT-Rich Interaction Domain 5B), CEBPE (CCAAT Enhancer Binding Protein Epsilon) and CDKN2A (Cyclin Dependent Kinase Inhibitor 2A) ^{28,29}.

> Somatic predisposition

Acquired somatic mutations are commonly required for the initiation of ALL. Several gene fusions resulting from chromosome translocations facilitate the development of childhood ALL, of which *ETV6-RUNX1* (*ETS Variant Transcription Factor 6 - RUNX Family Transcription Factor 1*) with t(12;21) (p13; q22) is the most common, occurring in 22% of cases ³⁰. Approximately 5% of healthy newborns carry *ETV6-RUNX1* fusion, but only 0.2% (~1 in 500) will develop ALL ^{19,31}. BCP-ALL (B-cell precursor (BCP) acute lymphoblastic leukemia) with t(9;22) (q34; q11) accounts for about 2% of childhood ALL, *TCF3-PBX1* (*Transcription Factor 3 - PBX Homeobox 1*) with t(1;19) (q23; p13) is present in approximately 4% of ALL, *MLL* (*KMT2A*) rearrangement of 11q23 is present in 6% of ALL ³⁰. The gene fusion *TCF3-HLF* (*Transcription Factor 3-HLF Transcription Factor*,

PAR BZIP Family Member) t(17;19) (q22; p13) is a rare subtype of ALL and accounts for less than 1% of childhood ALL ³².

In addition to the genetic factors, external factors such as the impact of the environment and infectious exposures induce the pathogenesis of leukemia. These factors can play a role *in utero* or after childbirth. The risk of leukemia in Japanese atomic bomb survivors is an evidence of the radiation-induced leukemia ^{33,34}. Furthermore, Greaves suggested that the delayed exposure to common childhood infections in the early childhood increases the risk to develop pediatric leukemia ^{35,36}.

1.1.2 Symptoms

The symptoms of childhood leukemia are clinically manifested by bleeding and/or bruising caused by thrombocytopenia, pallor and fatigue due to anemia, recurrent infections caused by neutropenia, and fever resulting from infections ³⁷. Bone and joint pain commonly result from the crowding of bone marrow by accumulating leukemic cells (blasts) ³⁸. Additionally, leukemic cells can accumulate in the liver and spleen, causing enlargement of these organs (splenomegaly and hepatomegaly), which can lead to pain in the abdomen ³⁹.

1.1.3 Diagnosis

The correct diagnosis and classification of ALL requires a good morphologic identification of lymphoblasts as well as their phenotypic characterization in the blood and bone marrow. Disease subtypes are clinically and biologically relevant.

Usually, the diagnosis of ALL begins with clinical suspicion when the patient presents clinical features as mentioned above. The suspicion of ALL leads to a complete blood count (CBC) and the blood smear analysis. Bone marrow aspirates and/or biopsy is performed to confirm the diagnosis. Bone marrow aspirates undergo multiple analyses, including morphology, immunophenotype by flow cytometry or immunohistochemistry, cytogenetic as well as molecular studies. These analyses are performed not only to discriminate ALL from other leukemia types like AML, but also to distinguish different subtypes within the disease pattern of ALL and to allow surveillance of remission in follow-up examinations.

The morphologic diagnosis of leukemia enables the identification of the leukemia cells and the stage of cell differentiation. This diagnosis is based on the microscopic features of leukemic blasts using May–Grünewald–Giemsa-stained smears of bone marrow aspirates or peripheral blood (PB) smears. For the morphologic classification of ALL, the French-American-British (FAB) classification introduced in 1976, is applied ⁴⁰. The morphologic diagnosis is used for the initial detection of ALL ⁴¹, but it does not play a significant role in subclassification ⁴² and therefore, further tests need to be done.

The immunophenotyping of leukemia blast cells is carried out by flow cytometry and rapidly provides results. The immunophenotypic analysis is clinically relevant since it allows the establishment of leukemic cell lineage as well as the identification of the maturation stage of blast cells ⁴³. This is very important since the treatment of ALL depends on the lineage. This technique applies antibodies, which are highly lineage and subgroup specific. For instance, B-cell ALL (B-ALL) can well be discriminated from T-cell ALL (T-ALL). Further markers are used for the subtype classification (**Table 1**). With multi-channel flow cytometry (MFC), immunophenotyping has become the standard procedure for ALL diagnosis and subclassification. Together with PCR and next generation sequencing (NGS) methods, MFC represents a sensitive tool to detect and monitor minimal residual disease (MRD), a powerful predictor of the overall response to treatment in pediatric ALL ⁴⁴.

Table 1: Immunophenotype of B- and T-ALL and their subtypes.B lineage and T lineage ALL are classified according to the phenotypic profile of the blasts (WHO, EGIL). Adapted from ^{43,45,46}.

Lineage	Subtype	CD19	CD22	cCD79	CD10	CIgM	TdT	Slg or k or \(\lambda \)
	B-I (Pro-B) ALL	+	±	+	-	-	+	-
B-ALL	B-II (Common) ALL	+	+	+	+	-	+	-
	B-III (Pre-B) ALL	+	+	+	\pm	+	+	-
	B-IV (Mature B) ALL	+	+	+	-	-	-	+
	_	cCD3	CD7	CD2	CD5	CD8	CD1a	sCD3
	T-I (Pro-T) ALL	+	+	-	-	±	-	-
T-ALL	T-II (Pre-T) ALL	+	+	+	+	±	-	-
	T-III (Cortical T) ALL	+	+	+	+	±	+	±
	T-IV (Mature T) ALL	+	+	+	+	±	-	+

cIgM: Cytoplasmic IgM, c: cytoplasmic, s: surface, TdT: Terminal deoxynucleotidyl transferase, k/ λ: kappa or lambda-chain.

Cytogenetic is the investigation of a cell's chromosomes and provides information about structural and numerical aberrations. Translocations, change in ploidy, large deletions, insertions or inversions can be revealed ^{47,48}. Tests such as fluorescence *in situ* hybridization (FISH) and karyotyping are used to establish cytogenetic features. Nowadays, it is known that several genetic abnormalities can affect multiple pathways and contribute to leukemogenesis, including proliferation, cell cycle, apoptosis, and/or differentiation. For instance, inherited genetic variants increases the risk to develop ALL²⁸. Genetic abnormalities provide information about the prognosis of the disease as shown in **Table 2**. They allow the classification of ALL into different risk subgroups: good or poor prognosis groups. High hyperdiploidy with more than 50 chromosomes and t(12;21) (p13;q22) is classified into good-risk subgroup, while t(9;22)(q34;q11) represents a poor-risk subgroup.

1.1.3.1 Classification of childhood acute lymphoblastic leukemia

ALL was classified in 1976 according to a scheme proposed by a group of French, American and British hematologists (French-American-British (FAB) Co-operative Group) ⁴⁹. The original FAB classification was arbitrarily using a cut-off of 30% bone marrow blasts as criterion for ALL ⁴⁰. The FAB system was based largely on morphologic criteria (cell size, chromatin, nuclear shape, nucleoli and the degree of basophilia) ⁵⁰. The FAB system divides ALL into 3 subtypes (L1 to L3) ⁵¹. Using the FAB classification, clinical symptoms, prognosis, and genetic abnormalities could not differentiate between the L1 and L2 subtypes. In 1997, the WHO therefore proposed a revised classification of ALL, in which immunophenotypic features were included in this classification. The L3 type is classified as Burkitt's leukemia/lymphoma. The recent WHO classification in 2017 classified ALL together with lymphoblastic lymphomas as lymphoid precursor lymphoid neoplasms of B- or T-cell type. The diagnosis is ALL if blasts exceed 25% in the bone marrow ⁵², even if there are extra-medullary lesions. The disease is classified as lymphoblastic lymphoma (LBL) when the bone marrow blast rate is lower than 25% and the patient has extra-medullary lesions.

Table 2: 2016 World Health Organization classification of B- and T-acute lymphoblastic leukemia/lymphoma ¹¹.

B-lymphoblastic leukemia/lymphoma

B-lymphoblastic leukemia/lymphoma, not otherwise specified (NOS)

B-lymphoblastic leukemia/lymphoma with recurrent genetic abnormalities

B-lymphoblastic leukemia/lymphoma with t(9;22) (q34.1; q11.2); BCR-ABL1

B-lymphoblastic leukemia/lymphoma with t(v;11q23.3); MLL1 (KMT2A) rearranged

B-lymphoblastic leukemia/lymphoma with t(12;21) (p13.2; q22.1); *TEL-AML1* (*ETV6-RUNX1*)

B-lymphoblastic leukemia/lymphoma with hyperdiploidy

B-lymphoblastic leukemia/lymphoma with hypodiploidy

B-lymphoblastic leukemia/lymphoma with t(5;14) (q31.1; q32.3); *IL3-IGH*

B-lymphoblastic leukemia/lymphoma with t(1;19) (q23;p13.3); E2A-PBX1 (TCF3-PBXI)

Provisional entity: B-lymphoblastic leukemia/lymphoma, BCR-ABL1-like

Provisional entity: B-lymphoblastic leukemia/lymphoma with iAMP21

T-lymphoblastic leukemia/lymphoma

Provisional entity: Early T-cell precursor lymphoblastic leukemia

1.1.3.2 Prognostic factors in ALL

Survival outcomes of children with ALL have been significantly improved in recent years. The survival rate is approximately 90% at 5 years in many high-income countries ⁵³. Despite treatment advance in pediatric ALL, there remain several factors that can affect the chance of recovery and treatment options. These include immunophenotype, genetics, patient age, leukocyte count and treatment response, which are summarized in **Table 3** according to the quality of the outcome.

Children with ALL are often classified as low risk, high risk or very high risk according to these risk factors.

Table 3: Risk factors in pediatric acute lymphoblastic leukemia 54.

	Poorer outcome	Better outcome
Patients and clinical factor	s	
Age at diagnosis:	<1 or ≥10 years	1-9 years old
Initial leucocyte count:	• ≥50,000 cells/mm ³	 <50,000 cells/mm³
ALL-subtype:	• T-ALL	B-ALL
Sex:	• Male	• Female
Cytogenetic & genetics		
Diploidy:	 Hypoploidy 	Hyperdiploidy
	(<46 chromosomes)	(>50 chromosomes or DNA
		index >1.16)
	 BCR-ABL1 t(9;22) 	• ETV6-RUNX1 t(12;21)
Translocations and others:	 TCF3-HLF t(17;19) 	 TCF3-PBX1 t(1;19)
	• MLL, BCL2 or MYC	 NUMT1 rearrangement
	gene rearrangement	
	• iAMP21	
Response to initial treatme	nt	
	High risk: MRD level	Standard risk (low risk):
Minimal residual disease	>10 ⁻³ at day 78	Negative MRD at day 33
(MRD):	 Very high risk: 	with a sensitivity of at least
	positive MRD	10 ⁻⁴
	assessment at week 22	

1.2 Non-coding RNAs

Almost 70% of the human genome is transcribed into RNA, but only 2% of the transcribed RNA code for proteins ⁵⁵. This mirror demonstrates the presence of a high abundance of so-called non-coding RNAs in the human transcriptome, which code for RNAs that are not translated into protein. Until recently, many of these RNA transcripts were considered to be junk. However, with the advent of NGS and broad transcriptome analyses, a better understanding of the human gene expression was achieved and several species of non-coding RNAs were discovered. Non-coding RNAs (ncRNAs) are classified into two groups, namely housekeeping ncRNAs and regulatory ncRNAs ⁵⁶.

Housekeeping RNAs include ribosomal RNAs (rRNAs), transfer RNAs (tRNAs), small nucleolar RNAs (snRNAs) and small nuclear RNAs (snoRNAs) ⁵⁶. According to the

structure of the transcript, regulatory RNAs can be categorized in linear or circular RNAs (circRNAs). Linear transcripts consist of small non-coding RNAs (shorter than 200 nucleotides) and long non-coding RNAs (larger than 200 nucleotides). Small ncRNAs comprise micro RNAs (miRNAs), PIWI-interacting RNAs (piRNAs), small interfering RNAs (siRNAs), while long non-coding RNAs (lncRNAs) include sense, antisense, intronic, intergenic and enhancer-associated RNAs (eRNAs). Nowadays, many studies reported that non-coding RNAs play a crucial role in the regulation of gene expression at its different levels such as transcription, translation and epigenetic ^{57,58}.

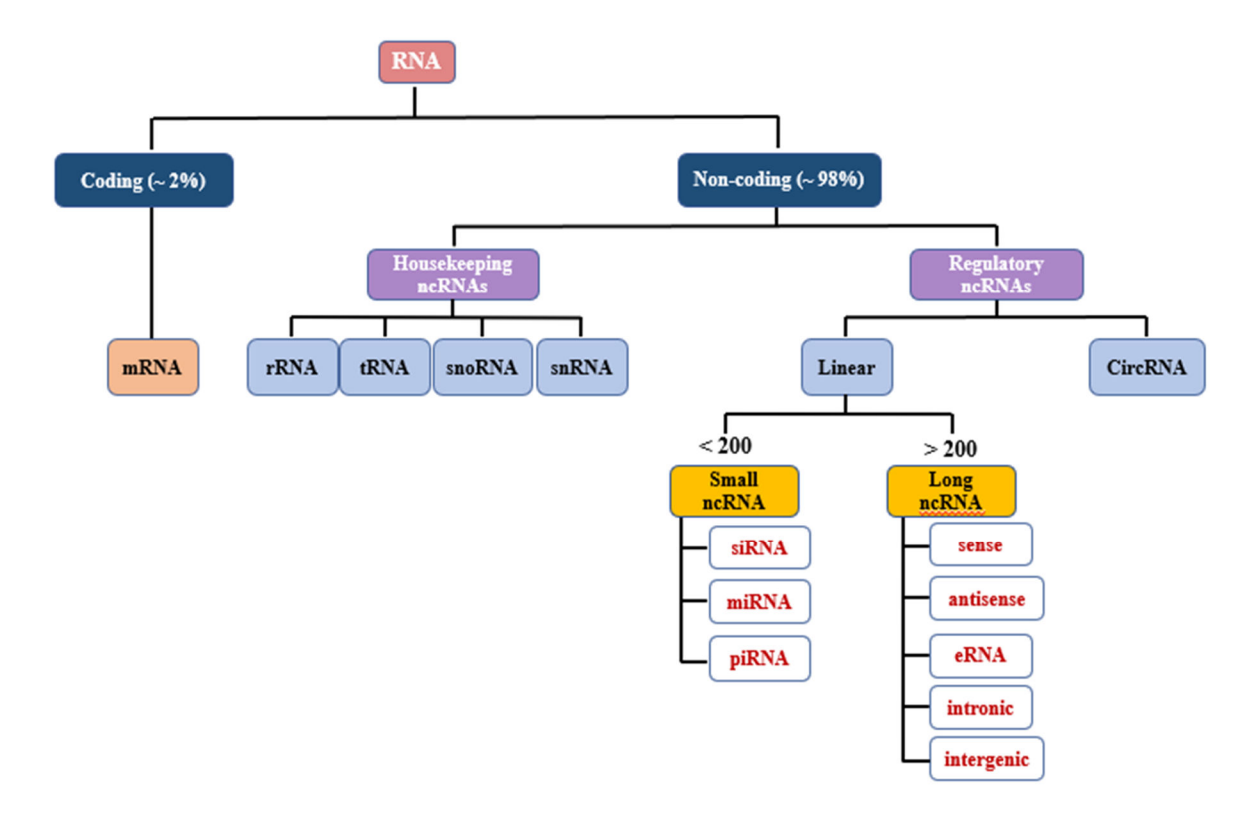


Figure 3: Classification of non-coding RNAs.

Almost 70% of the human genome is actively transcribed into RNA and only approximately 2% of them code for a protein (messenger RNAs = mRNAs). The remaining part of RNAs does not encode proteins (non-coding RNA). Non-coding RNA are separated into two classes: housekeeping and regulatory RNAs. This figure is adapted from ^{59,60}

1.2.1 Discovery of circular RNAs (circRNAs)

As the name implies, circRNAs are a class of endogenous RNAs, which unlike linear RNAs, have a circular shape. CircRNAs were first observed more than 40 years ago by Sanger and colleagues when studying the viroid in 1976 ⁶¹. circRNAs have been overlooked for a long time, because they were thought to be the result of splicing errors ^{62,63}. Also, most sequencing algorithms are designed to select for reads that display the linear order of the reference

genome. In 1980, circRNAs were discovered in yeast mitochondria ⁶⁴, and later on in the hepatitis delta virus ⁶⁵. In mammalian cells, they were detected in 1991, but reported as scrambled transcripts ⁶⁶ and considered to be the by-products of canonical splicing because of their low expression ⁶⁷. Recent advances in RNA sequencing (RNA-seq) techniques, together with specialized computational pipelines or tools enabling the identification of thousands of human circRNAs, greatly accelerated circRNA research ^{68,69}.

1.2.2 Properties of circRNAs

Not all active genes express circRNAs. High-throughput RNA seq revealed that only 20% of them do ⁷⁰. CircRNAs are covalently closed single stranded RNAs, which derived from pre-mRNA by the event called back-splicing ⁷¹. Contrary to linear RNAs, circRNAs display neither 5'to 3'polarity nor polyadenylated tail ^{72,73}. The lack of 5'and 3' orientation protects them from degradation by exoribonucleases such as RNase R. circRNAs are expected to be more stable than most linear RNAs. Exoribonucleases are enzymes that attack RNA molecules at their ends. RNase R is one of these enzymes with 3'to 5' exonuclease activity that is commonly used to enrich circRNAs. Furthermore, circRNAs are evolutionary conserved and tissue-specific ⁷⁴.

Depending on how circRNAs are generated, they are classified into three types: exonic circRNAs (EcircRNAs), intronic circRNAs (IcircRNA), and exonic-intronic circRNAs (EIciRNAs) ⁷³ (**Figure 4**). EcircRNAs exclusively contain exons and account for ~80% of known circRNAs ⁷⁵. They are the best investigated of the described circRNAs and most of them are localized to the cytoplasm ⁷⁶. EIciRNAs contain both introns and exons, and are abundant in the nucleus ⁷³.

1.2.3 Biogenesis of circRNAs

Canonical splicing is a post-transcriptional process, which is catalyzed by the spliceosomal machinery. During this process, introns are removed from the pre-mRNA and exons are joined together. Numerous studies have revealed the biogenesis of circRNAs through backsplicing mechanism. During the post-transcriptional modification of most human genes, the canonical splicing mechanism is in competition with the backsplicing mechanism ⁷⁷. Backsplicing is a mode of inverse splicing compared to canonical splicing event. This phenomenon occurs when a downstream splice-donor site joins an upstream splice-acceptor

site, leading to the formation of the covalently closed continuous loop ⁷⁷. Even though the mechanism of circRNA biogenesis is not yet fully understood, previous research revealed that the backsplicing is catalyzed by the canonical spliceosome machinery, since the mutagenesis of the canonical spliceosome as well as its inhibition using isoginkgetin showed the reduction of circRNA levels ^{78,79}. So far, three paths of circRNA formation have been proposed **Figure 4**:

Intron pairing-driven circularization occurs by the directly base-pairing of intronic motifs, such as ALU repeats (reverse complementary sequences) that flank the potential circRNA, thus enabling the formation of EcircRNAs as well as the production of EIciRNAs by intron retention ⁷⁷.

Lariat-driven circularization is a process in which exon-containing lariat is first generated from a precursor RNA. This leads to the formation of lariat, linear mRNA and EcircRNAs when the introns are spliced completely or EIciRNA in some cases of intron retention ^{77,80}.

RNA-binding proteins (RBPs) such as muscleblind (MBL) and quaking (QKI) have been reported to regulate circRNA production. It can bridge two flanking introns close together 80,81

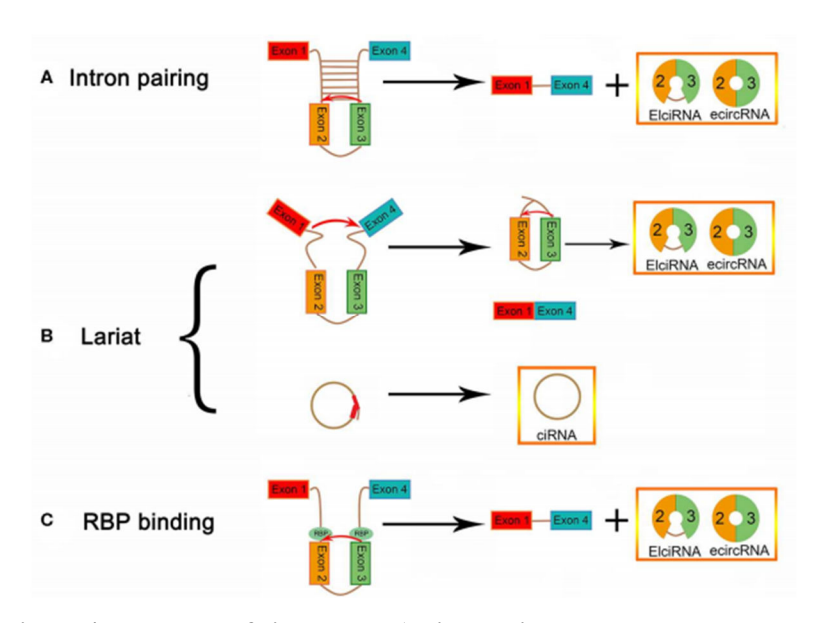


Figure 4: Pathways of circular RNA biogenesis

(A): Intron pairing-driven circularization: This model is mediated by the base-pairing of intronic motifs, such as ALU elements, which support the formation of ecircRNAs or EIciRNAs in the case of intron retention, (B): Lariat-driven circularization: This supports the production of lariats, EIciRNAs, ecircRNAs and linear mRNA (C): EIciRNA and ecircRNA biogenesis via RBP-associated pairing-driven circularization. Modified from ⁸⁰

1.2.4 Biological relevance of circRNAs

Despite an explosion in circRNA study, the molecular and cellular roles of the vast majority of circRNAs remain undefined. However, numerous studies reported that circRNAs can modulate gene expression through various mechanisms, such as sponging miRNAs. This can be illustrated for example by circRNA CDR1as (Cerebellar Degeneration Related 1 antisense RNA) also known as ciRS-7, which positively regulates miR-7 targets by acting as miRNA sponge of miR-7 ⁸². The circRNA CDR1as, also known as ciRS-7, harbors more than 70 binding sites for miR-7.

CircRNAs can also interact with RBPs (RNA-binding proteins). This is the case for circPABPN1 (circular RNA Poly(A) Binding Protein Nuclear 1) that contains *PABPN1* (*Poly(A) Binding Protein Nuclear 1*) translation avoiding the interaction between the RBP HuR/ELAVL1 (ELAV Like RNA Binding Protein 1) and its linear counterpart *PABPN1* ⁸³. Most circRNAs are located and enriched in cytoplasm. EcircRNAs (exonic circRNAs) are predominantly expressed in this part of the cell.

Various studies have shown that circRNAs located in the cytoplasm play important regulatory roles by interaction with miRNAs or proteins in the cytoplasm. These include for example CDR1as, SRY (Sex-determining region Y protein) and circHIPK3 (circular RNA homeodomain-interacting protein kinase 3), which were found to act as miRNA sponges ^{82,84,85}. Some circRNAs such as circFOXO3 (circular RNA forkhead box O3) have been shown to interact with proteins by regulating gene expression ⁸⁶.

In the nucleus, circRNAs such as circANRIL ((antisense non-coding RNA in the INK4 locus) regulate the processing and maturation of rRNA by preventing for example the interaction between the pre-rRNA and the protein named Pescadillo homologue 1 (PES1) ⁸⁷. Other circRNAs like circEIF3J (circular RNA Eukaryotic translation initiation factor 3 subunit J) and circPAIP2 (Poly(A) Binding Protein Interacting Protein 2) that are localized in the nucleus have been reported to promote the expression of their counterpart gene by recruiting factors such as snRNP ⁸⁸.

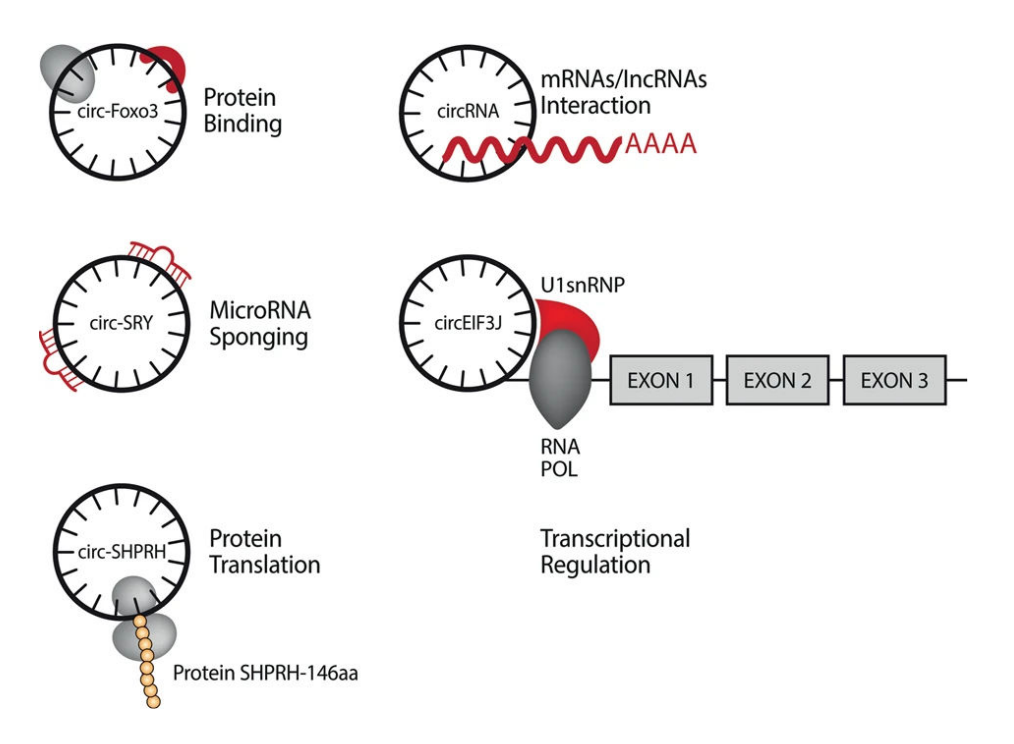


Figure 5: CircRNA functions 89

CircRNAs can interact with proteins and other RNAs like mRNAs, lncRNAs and miRNAs. MiRNA sponge effect is the well-described circRNA function, which is exerted by circRNAs such as circSRY. Other circRNAs like CircEIF3J regulate the expression of their parental genes by interaction with U1 snRNA. Furthermore, circRNAs can also be translated in Proteins. This is the case of CircSHPRH which translates to SHPRH146aa using an overlapping genetic code.

1.2.5 Role of circRNAs in cancers

Several studies showed that circRNAs are associated with human diseases, including cancers. CircRNAs are implicated in the regulation of cancer hallmarks, including self-sustenance in growth signaling, proliferation, angiogenesis, resistance to apoptosis, unlimited replicative potential and metastasis ^{90,90,91}. Thus, their expression may vary within different cancers, depending on how they are required for cancer survival. CircRNAs can have oncogenic or tumor-suppressive properties. It has been reported that circNRIP1(circular RNA nuclear Receptor Interacting Protein 1) promotes gastric cancer progression via AKT1 (AKT Serine/Threonine Kinase 1)/mTOR (Mechanistic Target Of Rapamycin Kinase) pathway by sponging miR-149-5p ⁹². Hu et al. revealed that circASAP1 promotes cell proliferation and invasion in hepatocellular carcinoma (HCC) cells by sponging miR-326 and miR-532-5-p, which regulates MAPK1 (Mitogen-activated protein kinase 1)/CSF-1 (colony stimulating factor 1) signaling ⁹³. circZNF292 (circular RNA Zinc Finger Protein 292) may be induced by hypoxia and exhibits pro-angiogenic activities. Here the molecular mechanism is not yet understood ⁹⁴. CircPVT1 (Pvt1 Oncogene) contributes to ALL progression by regulating let-7 and miR-125 expression ^{95 91}.

1.3 Autophagy

The term autophagy derives from the greek words *auto* (self) and *phagein* (eating or devouring). Literally, this term means self-eating of a cell and was coined by Christian de Duve in 1963, based on his discovery of the functions of lysosomes ⁹⁶. Autophagy is an intracellular catabolic process, in which the cytoplasmic components are delivered to lysosomes for degradation ⁹⁷. Autophagy is an intracellular recycling mechanism in eukaryotic cells, essential for maintaining cellular homeostasis. It degrades long-lived or aggregated proteins and cellular organelles ^{98,99}. It is an important process that helps cells to overcome various stressful stimuli, including hypoxia, DNA damage, endoplasmic reticulum (ER) stress and pathogen infections ¹⁰⁰. Autophagy is an evolutionary conserved homoeostatic process that promotes cell survival by eliminating superfluous or unwanted materials. Furthermore, autophagy takes part in various cellular processes such as inflammation, innate and acquired immunity as well as oxidative stress, which are relevant for the development of diseases, including malignant diseases like cancer ¹⁰¹.

There are three major forms of autophagy in eukaryotes: Microautophagy, Chaperone-mediated autophagy (CMA), Macroautophagy.

Microautophagy

Microautophagy is a non-selective lysosomal degradative process, in which autophagic cargos are directly engulfed by lysosomes ¹⁰².

> Chaperone-mediated autophagy

Chaperone-mediated autophagy (CMA) is responsible for the degradation of at least 30% of cytosolic proteins and presents a secondary response to nutrient starvation¹⁰³. Specifically, cytoplasmic protein targets with a KFERQ motif are selectively recognized by chaperone heat shock 70 kDa protein 8 (HSPA8/HSC70) and then bind to the LAMP-2A, which works as a receptor for proteins substrates at the lysosomal membrane ^{102,104}.

> Macroautophagy

Macroautophagy, hereafter referred to as autophagy, is the most common type of autophagy process, the most efficient autophagic clearance mechanism and the most extensively studied autophagy in yeast and mammalian that mediates the degradation of cytoplasmic long-lived proteins and organelles within lysosomes.

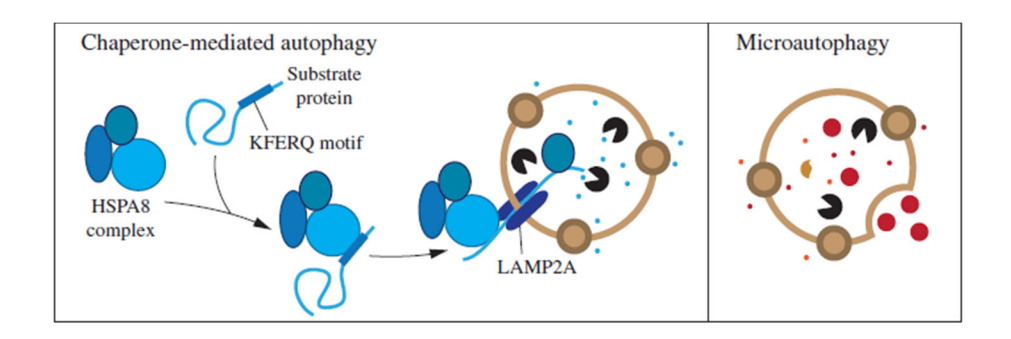


Figure 6: Schematic illustration of microautophagy and chaperone-mediated autophagy in mammalian, Image modified from ¹⁰⁵.

1.3.1 The autophagy machinery and regulation of autophagy in mammalian cells

To maintain homeostasis, basal autophagy occurs in most cases permanently at a low level within many mammalian cells. However, autophagy can be rapidly induced under conditions of starvation or stress.

Autophagy is initiated by the formation of membrane structures called phagophores. This membrane expands and encapsulates cytoplasmic contents (cargos) within maturated double-membrane vesicles called autophagosomes. Subsequently, the autophagosomes fuse with lysosomes to form autolysosomes, where the entrapped cytosolic contents (long-lived proteins and damaged organelles) are degraded by lysosomal enzymes. Finally, degraded products are recycled into new macromolecules ¹⁰⁶.

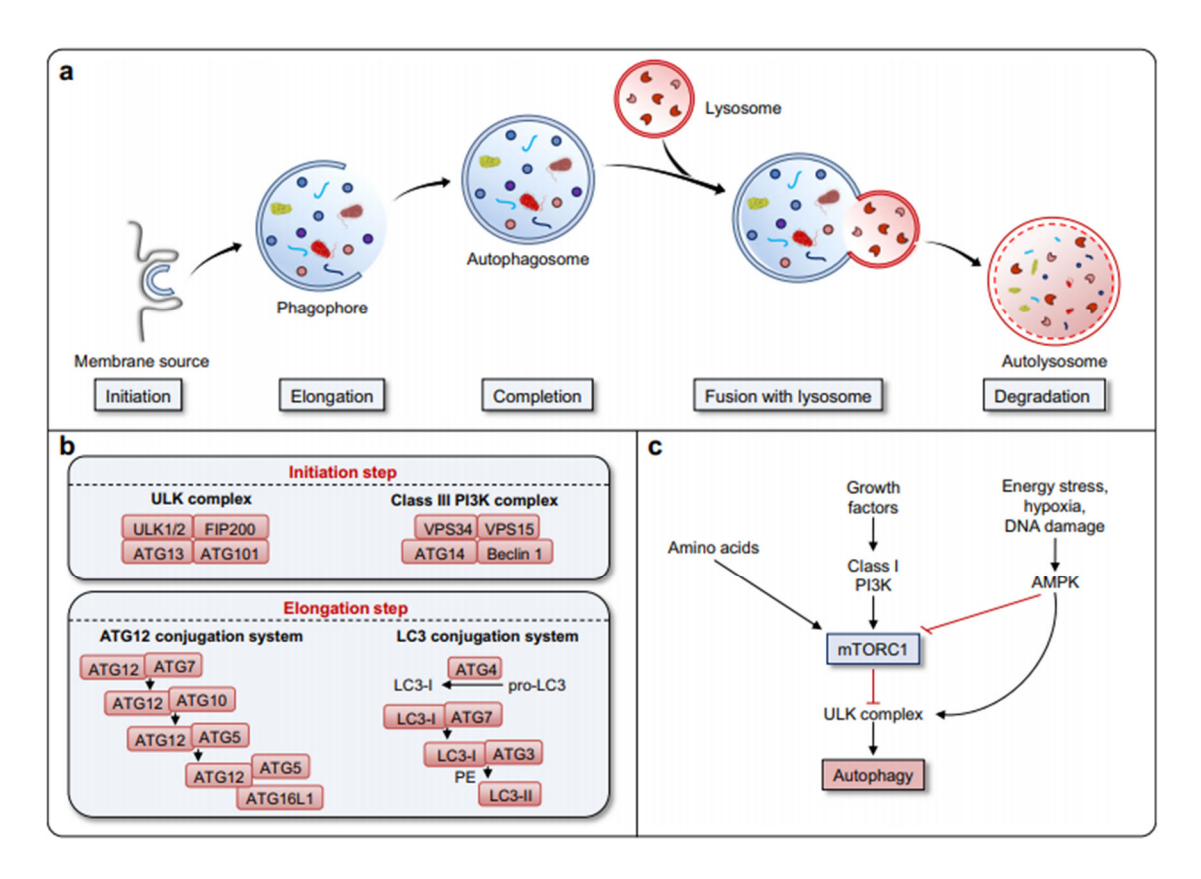


Figure 7: Mammalian autophagy pathway. Image taken from ¹⁰⁷.

a Autophagy is divided in several steps: Initiation with the formation of a phagophore (also called isolation membrane); elongation of the phagophore, which leads to formation of the autophagosomes engulfing the autophagic cargos; after autophagosome completion, autophagosomes fuse with the lysosomes, where the encapsulated cargos are degraded inside the autolysosome. b Activation of the ULK1/2 complex is crucial for nucleation of the phagophore. Elongation of phagophore occurs with the help of ATG12–ATG5-ATG16L1 complex, the class III PtdIns3K complex, LC3-II, and ATG9. c mTORC1 is an important element in the regulation of autophagy. Sufficient amounts of amino acids as well as growth factors reduce autophagy activity due to the inactivation of ULK complex by mTORC1 activity, while cellular stress such as energy deprivation, DNA damage, and hypoxia inhibit mTORC1 activity, leading to the activation of ULK complex, which enables the initiation of autophagosome formation ¹⁰⁷. There are various autophagy-related proteins (ATGs) and non-ATGs that regulate autophagy pathways.

Initiation of autophagy requires the unc-51-like kinase 1 (ULK1) kinase complex, which is tightly controlled by 5'-AMP-activated protein kinase (AMPK) and by mammalian target of rapamycin complex 1 (mTORC1). The ULK1 protein kinase complex consists of the Ser/Thr kinase ULK1, autophagy-related protein 13 (ATG13), ATG101 and focal adhesion kinase family interacting protein of 200 kDa (FIP200) ¹⁰⁸. AMPK and mTORC1 are two opposing regulatory kinases that modulate autophagy induction depending on nutrient availability. AMPK is activated via the increased ratio of AMP (adenosine monophosphate)/ ATP (adenosine triphosphate) ¹⁰⁹ under energy-low conditions, whereas mTORC1 is activated under growth conditions (non-starvation conditions or in the presence of amino acid availability). Under these conditions, mTORC1 can repress autophagy initiation by phosphorylating ULK1 and ATG13 (Autophagy-Related Protein 13) ¹¹⁰. In contrast, mTORC1 is inhibited in the absence of amino acids and by growth factor withdrawal ¹¹¹,

allowing the fast dephosphorylation of ULK1 and ATG13, and thus the activation of the ULK1 complex. Importantly, AMKP can activate ULK1 by phosphorylation at Ser555, thereby inducing autophagy signaling ^{112,112}. The ULK1 complex translocates to autophagy initiation sites and modulates the recruitment of a second kinase complex, the class III PI3K complex, containing Vps34 (vacuolar sorting protein 34)/PIK3C3 (Phosphatidylinositol 3-Kinase Catalytic Subunit Type 3), Beclin-1, p150 and ATG14 (Autophagy-Related Protein 14). This complex converts phosphoinositide into the endoplasmic reticulum to phosphatidylinositol 3-phosphate (PI3P) at the site of forming phagophore, which is required for the recruitment of WIPI2B (WD Repeat Domain, Phosphoinositide Interacting 2) and DFCP1 (Double FYVE-Containing Protein1). Once these proteins are recruited, it is followed by the recruitment of the protein complex ATG12 (Autophagy-Related Protein 12)-ATG5 (Autophagy-Related Protein 5)-ATG16L1 (Autophagy Related 16 Like 1), which acts as a ubiquitin E3-ligase by catalyzing the conjugation of the ubiquitin-like ATG8 members (LC3A, B and C, GABARAP (GABA Type A Receptor-Associated Protein), GABARAPL1 (GABA Type A Receptor Associated Protein Like 1) and GABARAPL2 (GABA Type A Receptor Associated Protein Like 1) 107. ATG5 plays an important role in the expansion of the phagophore.

1.3.2 Role of autophagy in cancer

The role of autophagy in cancer is context dependent: it may support the degradation of potentially oncogenic molecules (dysfunctional proteins and organelles) at the early stages of tumor development, or it may promote the survival of tumor cells in more advanced stages of tumor ^{113,114}.

During cancer initiation, autophagy hinders DNA damage, maintains genome integrity, and digests damaged mitochondria to avoid reactive oxygen species (ROS) accumulation ^{115,116}. Playing the role in diverse cellular functions such as proliferation, metastasis, invasion, the expression of autophagy is an important element in tumor cells. Polak et al. demonstrated that the negative regulation of autophagy in *ETV6-RUNX1* gene positive B-ALL decreases cell proliferation and cell survival ^{117,118}.

In contrast, there is growing evidence supporting the role of autophagy in tumor growth. In advanced stages of cancer development, autophagy may help cells to survive in nutrient-limited environments ¹¹³. Cancer cells activate autophagy to reorganize their metabolism in order to satisfy the demands of proliferation, cell growth and long-term maintenance ¹¹⁹.

Furthermore, the basal level of autophagy is increased in hypoxic regions of tumor cells, favoring the survival of cells that overcome apoptosis ¹²⁰.

The regulation of autophagy can also be mediated by circRNAs, promoting, or inhibiting cancer progression in various cancers. circ-DNMT1 for example stimulates autophagy to promote cancer progression ¹²¹.

The influence of autophagy on the effectiveness of anticancer therapy has already been reported ¹²². Increasing evidence showed that the inhibition of autophagy may improve anticancer therapy ¹²². It was reported that the proliferation as well as survival of leukemic blast of BCP-ALL can be negatively influenced by autophagy inhibitors such as hydroxychloroquine (HQC) ¹¹⁸.

1.3.3 Role of ATG5

The autophagy-related gene 5 (ATG5) is a protein, which in humans is encoded by the *ATG5* gene. It is located on the chromosome 6 on the long arm q. ATG5 is a protein with multiple functions. Exploring its function in autophagy, ATG5 is a crucial gene for autophagic vesicle formation¹²³. It forms a complex with ATG12 and ATG16L, which is generated through the ubiquitin-like pathway by ATG7 and ATG10 that covalently links ATG5 and ATG12. Hence, this complex mediates LC3 lipidation and is involved in the elongation ¹²⁴ and maturation of autophagosome.

Autophagy is a cellular process, which according to the context can promote cell survival or cell death. Yousoufi and colleagues found that ATG5 sensitized cells to different apoptotic stimuli ¹²⁵. Apoptosis occurs when ATG5 is cleaved by calpain. The cleaved ATG5 translocates from the cytosol to mitochondria, where its interaction with anti-apoptotic molecules BCL-X_L triggers the activation of caspase as well as cytochrome c release. Here, the interaction between ATG5 and ATG12 is not required. Furthermore, the group observed both *in vitro* as well as *in vivo* that cells that overexpress ATG5, are more sensitive to anticancer therapies than those where ATG5 expression was silenced ¹²⁵. This could be relevant for clinical anticancer therapies.

Additionally, ATG5 is required for the survival of B cells during their development¹²⁶. In T-cells also, it has been reported that it supports cell survival and proliferation¹²⁷.

ATG5 is essential for cellular immunity to eliminate or to withstand against intracellular pathogens by autophagosome independent processes^{128,129}.

The knockout of ATG5 in mice is associated with an early postnatal lethality¹³⁰. Depending on the context, the upregulation of ATG5 is associated with an improvement of lifespan in the mice¹³¹ or it suppresses tumorigenesis like melanoma by inducing cell senescence¹³².

2 Aim of the thesis

The recent advance in RNA sequencing (RNAseq) and the development of specialized computational pipelines or tools enabled the identification of thousands of human circRNAs. Nowadays, it is known that circRNAs are involved in the regulation of gene expression and their expression signatures are deregulated in most human cancers. Moreover, circRNAs can contribute to cancer development and progression in various types of human cancers including childhood acute lymphoblastic leukemia, by inhibition or activation of autophagy. Autophagy, for its parts, is considered as a double-edged sword since it can prevent the development of cancer or promote its progression, as well its role in cancer therapy has already been demonstrated.

In this thesis, a circRNA derived from exons 4 and 5 of *ATG5* gene was investigated. The circBase (http://www.circbase.org/) and circInteractome ID of the circRNA candidate is hsa_circ_0077535 and was called circATG5 4-5 in this work. So far, this is the first study about circATG5 4-5.

The aim of this study was to elucidate the functional role of cirATG5 4-5 in *TCF3*-rearranged ALL according to following strategies:

- 1- Detection and validation of circATG5 4-5 expression in difference B-ALL lines
- 2- Determination of the subcellular localization of circATG5 4-5
- 3- Investigation of the effect of the modulation of circATG5 4-5 expression on *ATG5* and its consequences in autophagy signaling pathways
- 4- Characterization of the consequence of the modulation of circATG5 4-5 expression in B-ALL

3 Materials and Methods

3.1 Materials

3.1.1 Human cell lines

Three cell lines (HAL-01, 697 and HEK293) were examined in this thesis. All cell lines were purchased from the German Collection of Microorganisms and Cell Cultures (DSMZ, Brunswick, Germany). (www.dsmz.de).

3.1.2 Media and cell culture supplements

Culture media and supplements used in this thesis are listed in the Table 4.

Table 4: Media and cell culture supplements

Name	Company	Order No.
Bafilomycin A ₁ from Streptomyces	Sigma-Aldrich, St. Louis, USA	B1793-2UG
griseus		
Blasticidin S Ready Made Solution	Sigma-Aldrich, St. Louis, USA	SBR00022-1ML
DMEM GlutaMAX ^{TM-} I	Thermo Fischer, Waltham,	31966-021
	Massachusetts, USA	
Dimethylsulfoxide (DMSO)	Sigma-Aldrich, St. Louis, USA	D2650-100ML
Dulbecco's PBS	Sigma-Aldrich, St. Louis, USA	D8535-100 ML
Fetal Bovine Serum (FBS)	Sigma-Aldrich, St. Louis, USA	F9665-500ML
EBSS, Earle's Balanced Salt Solution	Thermo Fischer, Waltham,	24010-043
(1X)	Massachusetts, USA	
G 418 disulfate salt solution	Sigma-Aldrich, St. Louis, USA	G8168-100ML
LB-Agar	Roth, Karlsruhe, Germany	X965.2
LB-Medium	Roth, Karlsruhe, Germany	X964.3
Opti-MEM TM I Reduced Serum	Thermo Fischer, Waltham,	31985-062
Medium	Massachusetts, USA	
Penicillin-Streptomycin	Sigma-Aldrich, St. Louis, USA	P4333-100ML
RPMI 1640 Medium, GlutaMAX	Thermo Fischer, Waltham,	61870-010
	Massachusetts, USA	
Trypsin-EDTA 0.05%	Thermo Fischer, Waltham,	25300-054
	Massachusetts, USA	

3.1.3 Reagents and chemicals

Reagents and chemicals used in this thesis are listed in Table 5.

Table 5: Reagents and chemicals

Name	Company	Order No.
Dithiothreitol (DTT)	Roth, Karlsruhe, Germany	6908.3
4–20% Mini-PROTEAN® TGX™ Precast	Bio-Rad, Hercules, USA	4561094
Protein Gels		
8–16% Mini-PROTEAN® TGX TM Precast	Bio-Rad, Hercules, USA	4561105
Protein Gels		
20X SSC Solution	Invitrogen, Carlsbad, CA, USA	AM9763
Actinomycin D	Sigma-Aldrich, St. Louis, USA	A1410-2MG
Albumin Fraktion V	Roth, Karlsruhe, Germany	8076.3
Ampicillin	Sigma-Aldrich, St. Louis, USA	A9518-5G
Ammoniumpersulfat (APS)	Merck, Darmstadt, Germany	7727-54-0
Attractene Transfection Reagent	Qiagen, Hilden, Germany	301005
Biozym LE Agarose	Biozym, Hessisch Oldendorf,	840004
Biozyiii LE Agaiose	Germany	
Bio-Rad Protein Assay Dye Reagent	Bio-Rad, Hercules, USA	5000006
Concentrate		
Bromophenol blue	Sigma-Aldrich, St. Louis, USA	B-8026
CalFectin TM Mammalian DNA Transfection	SignaGEN Laboratories,	SL100478
Reagent	Rockville, MD, US	
Complete, EDTA-free Protease Inhibitor	Roche Diagnostics, Mannheim,	11873580001
Cocktail Tablets	Germany	
Chloroform	Merck, Darmstadt, Germany	67-66-3
Dextran sulfate	VWR, Langenfeld, Germany	9011-18-1
dNTP Mix, 10 mM, 200 ul	Promega, Madison, USA	U1511
EDTA	Sigma-Aldrich, St. Louis, USA	E5134
Ethanol	VWR, Langenfeld, Germany	20821.330
Formamide deionized	Invitrogen	AM9342
Formaldehyde	VWR, Langenfeld, Germany	1.04002.2500
Glycerin	Roth, Karlsruhe, Germany	3783.1
Glycoblue	Invitrogen	AM9515
GoTaq® RT-qPCR Master Mix	Promega, Madison, USA	A6002

Hi-Di™ Formamide	Applied Biosystems, Waltham, USA	4311320
Lenti-X-TM Concentration	TAKARA Bio, Mountain View,	631231
	CA, USA	
Lipofectamine TM RNAiMAX Transfection	Invitrogen, Carlsbad, CA, USA	13778150
Reagent		
Methanol ≥99.8%	VWR, Langenfeld, Germany	20847.320
Midori Green Advance	Biozym, Hessisch Oldendorf,	617004
Midori Green Advance	Germany	
Isopropanol	VWR, Langenfeld, Germany	20842.330
Phos-Stop	Roche Diagnostics, Mannheim,	4906837001
	Germany	
Propidium Iodide 1.0 mg/ml solution in	Invitrogen, Carlsbad, CA, USA	1001298
water		
Sodium chloride	Sigma-Aldrich, St. Louis, USA	1064045000
Sodium fluoride	Sigma-Aldrich, St. Louis, USA	S7920-100G
Sodiumdodecylsulfate (SDS) Pellets	Roth, Karlsruhe, Germany	CN30.4
TE, pH 8.0	Invitrogen, Carlsbad, CA, USA	AM9849
TEMED	Bio-Rad, München, Germany	110-18-9
Tris Base	Sigma-Aldrich, St. Louis, USA	T1503-1KG
Tri-Sodium citrate dihydrate	VWR, Langenfeld, Germany	27833294
Trizol Reagent	Thermo Fisher Scientific,	15596026
Titzoi Keageiii	Bremen, Germany	
Triton X 100	Roth, Karlsruhe, Germany	6683.1
Tween® 20	Merck, Darmstadt, Germany	8.221.840.500
VECTASHIELD® HardSet™ Mounting	Vector Laboratories, Eching,	H-1400
Medium	Germany	
QIAZOL Lysis Reagent	Qiagen, Hilden, Germany	79306

3.1 Kits and ladders

Kits and ladders used in this thesis are listed in Table 6.

Table 6: Kits and ladders

Name	Company	Order No.
6x Purple Loading Dye	New England Biolabs,	B70245
	Frankfurt/Main, Germany	
Amaxa Nucleofector Kit V	Lonza, Basel Switzerland	VCA-1003
Autophagy LC3 HiBiT Reporter Assay	Promega, Madison, USA	GA2550
Celltiter Glo Luminescent Cell Viability	Promega, Madison, USA	G7570
Assay		
DyeEx® 2.0 Spin Kit	Promega, Madison, USA	63206
GeneRuler 100 bp DNA Ladder	Thermo Fisher Scientific,	SM0321
	Bremen, Germany	
GeneRuler 1 kb Plus DNA Ladder	Thermo Fisher Scientific,	SM1334
	Bremen, Germany	
miRNeasy Mini Kit	Promega, Madison, USA	217004
Monarch DNA Gel Extraction Kit	New England Biolabs,	T1020L
	Frankfurt/Main, Germany	
Monarch® Plasmid Miniprep Kit	New England Biolabs,	T1010L
	Frankfurt/Main, Germany	
MystiCq® microRNA cDNA Synthesis Mix	Sigma-Aldrich, St. Louis, USA	MIRRT-
		25RXN
NucleoBond Xtra Maxi Plus kit for	Macherey-Nagel, Düren,	740416.50
transfection-grade plasmid DNA	Germany	
PageRuler TM Prestained Protein Ladder, 10 to	Thermo Fisher Scientific,	26616
180 kDa	Bremen, Germany	
Rapid DNA Ligation Kit	Sigma-Aldrich, St. Louis, USA	11635379001
RNA Clean & Concentrator-5	ZYMO RESEARCH, Irvine,	R1013
	California, USA	
QIAquick PCR Purification Kit	Qiagen, Hilden, Germany	28106

3.1.1 Oligonucleotides

Oligonucleotides used in this thesis are listed in Table 7 and

Table 8.

Table 7: Commercially available oligonucleotides

Name	Company	Product No.
Random primers	Promega, Madison, USA	C1181
Hs_CDK6_1_SG	Qiagen, Hilden, Germany	QT00019985
Hs_ATG5_1_SG	Qiagen, Hilden, Germany	QT00073325
Hs_ATG7_1_SG	Qiagen, Hilden, Germany	QT00008974
Hs_STAT3_1_SG	Qiagen, Hilden, Germany	QT00068754
hsa-miR-557	Sigma-Aldrich, St. Louis, USA	MIRAP00542250
hsa-miR-507	Sigma-Aldrich, St. Louis, USA	MIRAP00454250
hsa-miR-1261	Sigma-Aldrich, St. Louis, USA	MIRAP00771-250
hsa-miR-892a	Sigma-Aldrich, St. Louis, USA	MIRAP00705-250
hsa-miR-556-5p	Sigma-Aldrich, St. Louis, USA	MIRAP00540-250
hsa-miR-324-5p	Sigma-Aldrich, St. Louis, USA	MIRAP00314-250
hsa-miR-485-3p	Sigma-Aldrich, St. Louis, USA	MIRAP00419-250
hsa-miR-1299	Sigma-Aldrich, St. Louis, USA	MIRAP00808-250
Universal PCR primer	Sigma-Aldrich, St. Louis, USA	MIRUP-500
RNU6-1 (RT-qPCR Control Primer)	Sigma-Aldrich, St. Louis, USA	MIRCP00001250

Table 8: Oligonucleotides

Name	Company	Length (nt)	Sequence 5' to 3'
ß-Actin RT-qPCR	MWG, Ebersberg,	20	AGAGCTACGAGCTGCCTGAC
fwd	Germany		
ß-Actin RT-qPCR	Eurofins	20	AGCACTGTGTTGGCGTACAG
rev	Genomics		
qRT_GAPDH fwd	MWG, Ebersberg,	24	
	Germany		ACCACTTTGTCAAGCTCATTTCCT
qRT_GAPDH rev	MWG, Ebersberg,	23	
	Germany		GTTGCTGTAGCCAAATTCGTTGT

BGH Reverse	Invitrogen,	18	TAGAAGGCACAGTCGAGG
	Carlsbad, CA,		
	USA		
CMV fwd	Invitrogen,	21	CGCAAATGGGCGTAGGCGTG
	Carlsbad, CA,		
	USA		
CircATG5 4-5 fwd	MWG, Ebersberg,	21	AGACCTTCTGCACTGTCCATC
	Germany		
CircATG5 4-5 rev	MWG, Ebersberg,	26	AATTGGATAATGCCATTTTGCAAT
	Germany		CC
EcoRV_circATG5	MWG, Ebersberg,	33	TAAGCAGATATCGCATTATCCAAT
4-5 fwd	Germany		TGGTTTGCT
SacII_circATG5 4-	MWG, Ebersberg,	33	TGCTTACCGCGGCATTTTGCAATC
5 rev	Germany		CCATCCAGA

3.1.2 RNA FISH probes

RNA FISH probes used in this thesis are listed in **Table 9**.

Table 9: RNA FISH probes

Name	Company	Length (nt)	Sequence 5' to 3'or product No.
ATG5 4-5 Probe	MWG,	20	TTG GAT AAT GCC ATT TTG CA
	Ebersberg,		[FITC]
	Germany		
hGAPDH w/Q570	Biosearch		SMF-2026-1
	Technologies		

3.1.3 Small interfering RNAs (siRNAs)

siRNAs used in this thesis are listed in Table 10.

Table 10: siRNAs

Name	Company	Length (nt)	Sequence (sense 5' to 3')
si_ATG5 4-5	MWG, Ebersberg,	27	GAUUGCAAAAUGGCAUUAUCC
	Germany		AAUUGG

Scrambled RNA	OriGene, Rockville,	27	rCrGrUrUrArArUrCrGrCrGrUrArUr
SR30004	USA		ArArUrArCrGrCrGrUAT

3.1.4 Plasmids and plasmid cards

Plasmids used in this thesis are listed in **Table 11**.

Table 11: Plasmids

Name	Company	Product number
Autophagy LC3 HiBiT Reporter Vector	Promega, Madison, USA	9PIGA255
LeGO-IG2	Adgene, Watertown, USA	27341133
pcDNA3.1(+) CircRNA Mini Vector	Addgene, Watertown, USA	60648 134
pLKO.1 - TRC cloning vector	Addgene, Watertown, USA	10878 135
psiCHECKTM-2 Vector	Promega, Fitchburg, WI, USA	C8021

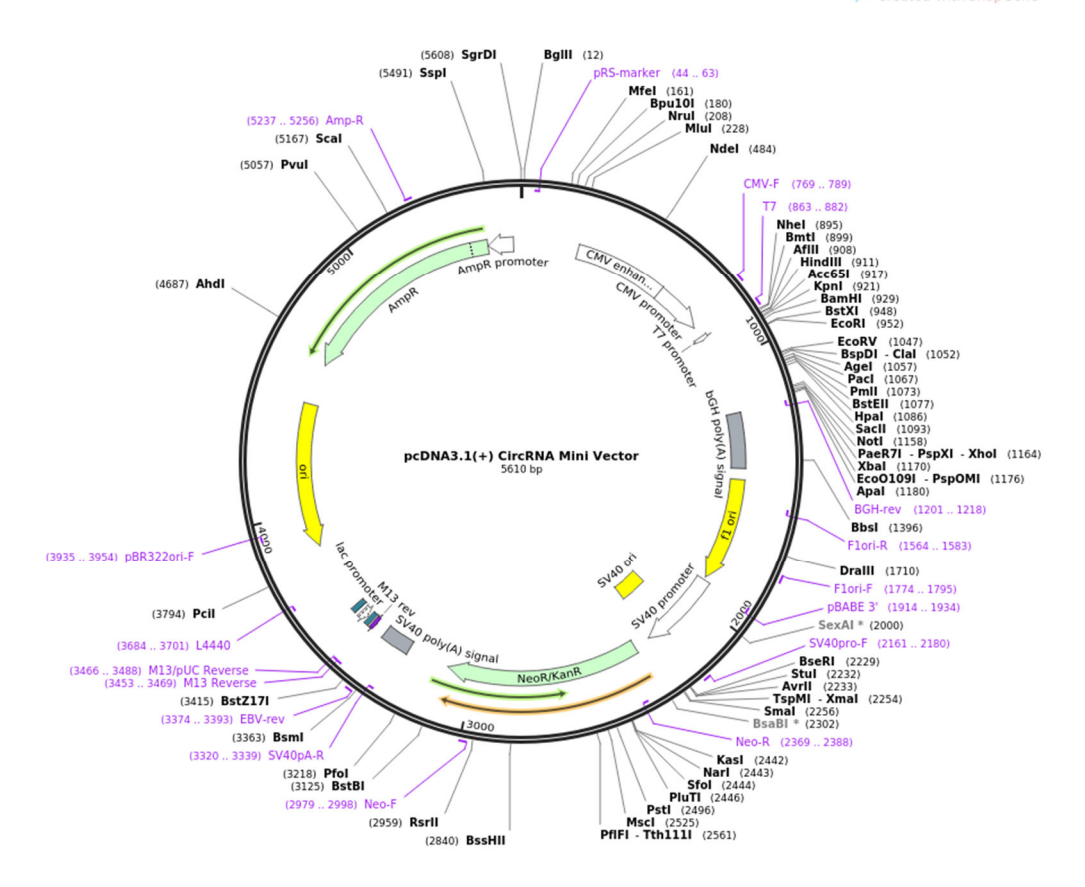


Figure 8: pcDNA3.1(+) CircRNA Mini Vector card.

pcDNA3.1(+) CircRNA Mini Vector was a gift from Jeremy Wilusz (Addgene plasmid # 60648) ¹³⁴. AmpR: Gene for ampicillin resistance; M13: Bacteriophage M13; NeoR/KanR: Neomycin/kanamycin resistance gene; CMV promoter: human cytomegalovirus immediate early promoter; f1 ori: bacteriophage origin of replication; SV40 ori: Simian Virus 40 origin of replication; SV40 poly (A) signal: Simian Virus 40 polyadenylation signal; Ori: High-copy number origin of replication, T7 promoter: Promoter for Bacteriophage T7 RNA polymerase, BGH poly (A) signal: Bovine growth hormone polyadenylation signal. Available under http://n2t.net/addgene:60648

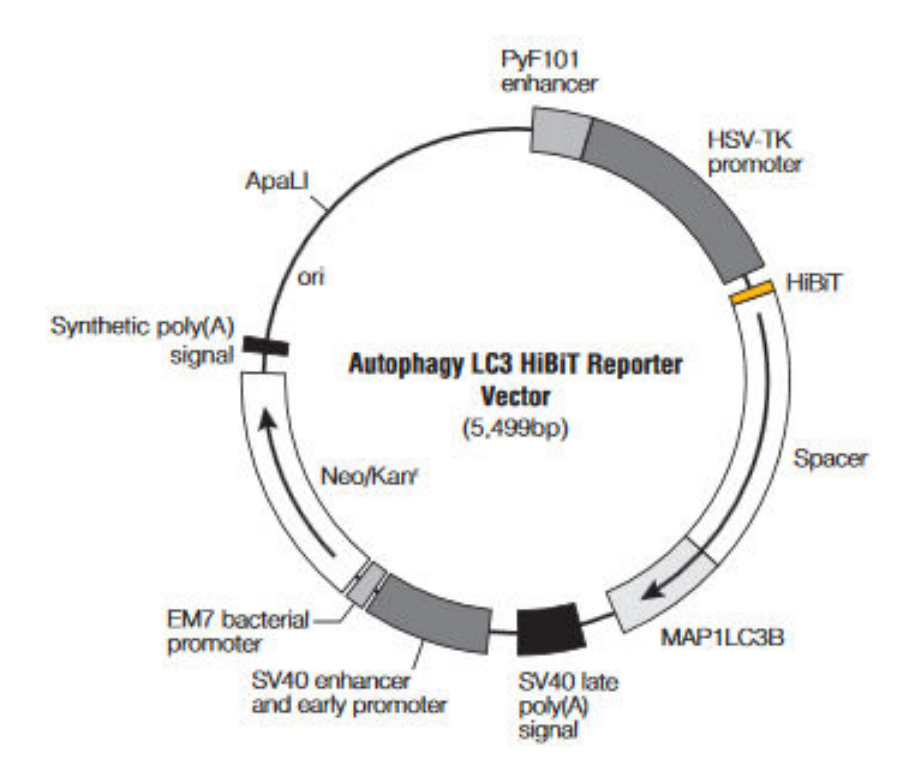


Figure 9: Autophagy LC3 HiBiT Reporter vector card from Promega

HSV-TK promoter; NeoR: eukaryotic selection marker; KanR: prokaryotic selection marker; HiBiT; Spacer; MAP1LC3B; EM7: synthetic modification of T7 promoter; Synthetic polyadenylation signal sequence; ColE1-derived plasmid replication origin; SV40 late polyadenylation signal; PyF101 enhancer; 2752SV40 enhancer and early promoter.



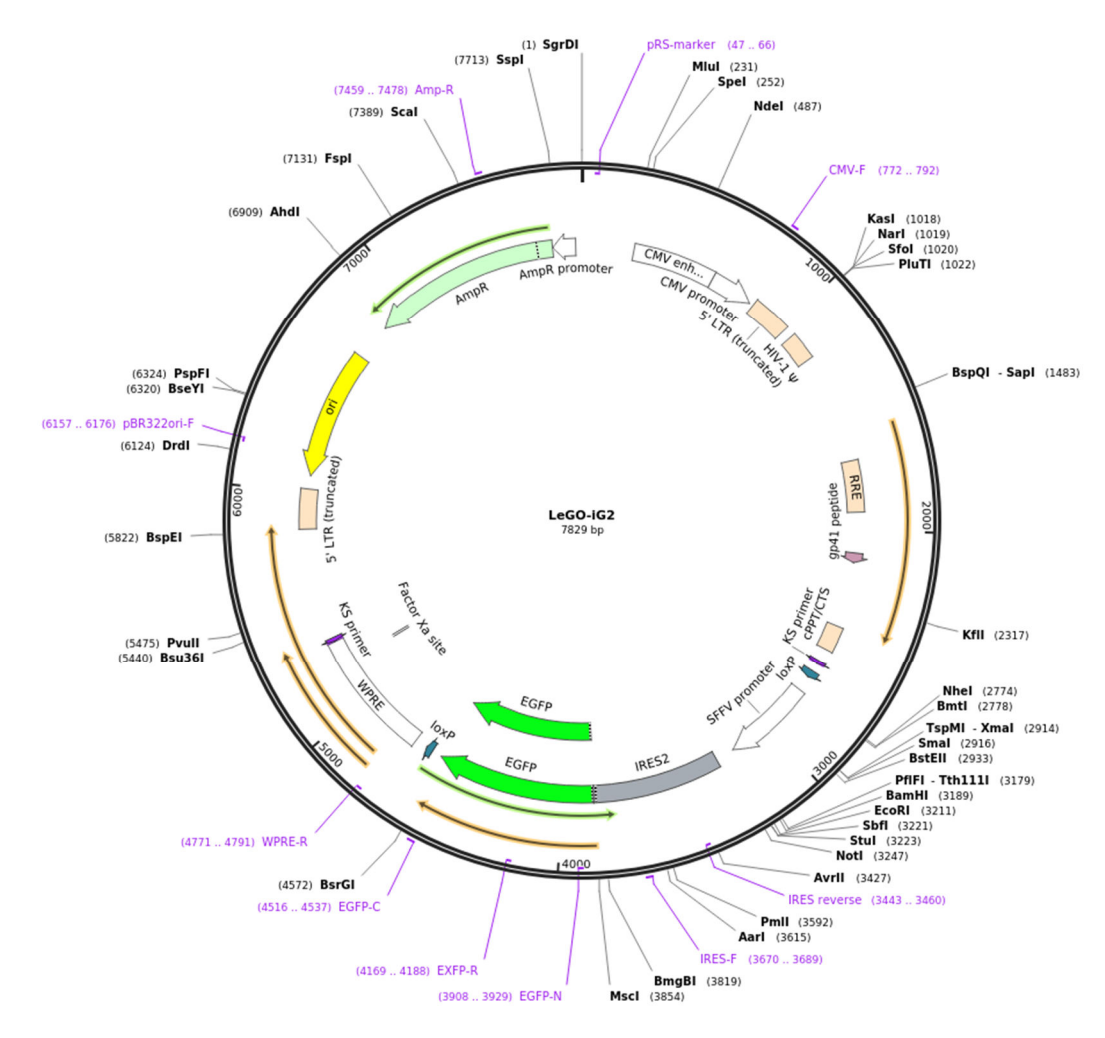


Figure 10: LeGO-IG2, mammalian expression, lentiviral

LeGO-iG2 was a gift from Boris Fehse (Addgene plasmid # 27341) 133

AmpR: Gene for ampicillin resistance; Ori: High-copy number origin of replication; CMV promoter: Cytomegalovirus; SFFV promoter; IRES-eGFP; HIV-1 Ψ : Packaging signal of HIV-1; 5'LTR (truncated): Truncated 5'long terminal repeat from HIV-1. Available under http://n2t.net/addgene:27341

3.1.5 Antibodies

Antibodies used in this thesis are listed in **Table 12**.

Table 12: Antibodies

Name	Company	Product No.
Anti-mouse IgG, HRP-linked Antibody	Cell Signaling Technology,	7076S
	Cambridge, UK	
Anti-rabbit IgG, HRP-linked Antibody	Cell Signaling Technology,	7074
	Cambridge, UK	
Anti-Atg5 pAb	Medical & Biological	PM050
	Laboratories (MBL), Nagoya,	
	Japan	
Atg7 (D12B11) Rabbit mAb	Cell Signaling Technology,	8558S
	Cambridge, UK	
ATG5 Antibody, Rabbit Polyclonal	Proteintech, Rosemont, USA	10181-2-AP
CDK6 (D4S8S) Rabbit mAb	Cell Signaling Technology,	13331S
	Cambridge, UK	
GAPDH Rabbit	Cell Signaling Technology,	14C10
	Cambridge, UK	
SQSTM1/p62 Antibody	Cell Signaling Technology,	5114S
	Cambridge, UK	

3.2 Enzymes

Enzymes used in this thesis are listed in Table 13.

Table 13: Enzymes

Name	Company	Product No.
BigDye Terminator v1.1 Cycle	Applied Biosystems,	4337450
	Waltham, USA	
DNase I	Qiagen, Hilden, Germany	79254
FastDigest ECORI	Thermo Fisher Scientific,	FD0274
	Bremen, Germany	
EcoRI-HF	New England Biolabs	R3101S
	Frankfurt/Main, Germany	

EcoRV-HF	New England Biolabs, R3195S			
	Frankfurt/Main, Germany			
GoTaq® RT-qPCR	Promega, Madison, USA	A6002s		
M-MLV Reverse Transcriptase	Promega, Madison, USA	M1701		
MystiCq® microRNA® SYBR® Green	Sigma-Aldrich, St. Louis,	MIRRM03-100RXN		
RT-qPCR ReadyMix TM	USA			
FootDisset NotI	Thermo Fisher Scientific,	Thermo Fisher Scientific,		
FastDigest NotI	Bremen, Germany	FD0594		
N4LUE	New England Biolabs,	R3189S		
NotI-HF	Frankfurt/Main, Germany			
Phusion HR PCR Master Mix	New England Biolabs,	M0531		
	Frankfurt/Main, Germany			
Recombinant RNasin(R) RNase Inhibitor	Promega, Madison, USA	N2511		
Ribonuclease R 20 U/μl	Epicentre, Madison, WI, US	RNR07250		
SacII	New England Biolabs,	R0157S		
	Frankfurt/Main, Germany			

3.3 Other consumables

Other consumables used in this thesis are listed in Table 14.

Table 14: Other consumables

Name	Supplier	Product
		number
Amersham Protran Supported 0.45 NC	GE Healthcare Life Sciences,	10600007
200 mmx4m 1 roll	Pittsburgh, PA, USA	
Cell culture flasks 25 cm2	Greiner Bio-One, Solingen,	690175
	Germany	
Cell culture flasks 75 cm2	Greiner Bio-One, Solingen,	657185
	Germany	
Falcon tubes 15 ml	Greiner Bio-One, Solingen,	188271
Falcon tubes 50 ml	Greiner Bio-One, Solingen,	227261
Hard-Shell PCR plates 96-well, thin	Bio-Rad, München, Germany	HSP9601
wall		
Microseal 'B' seal	Bio-Rad, München, Germany	MSB1001

3.4 Software

Software used in this thesis are listed in **Table 15**.

Table 15: Software

Name	Company/ available at
ApE – A Plasmid Editor	https://jorgensen.biology.utah.edu/wayned/ape/
Bio-Rad CFX Manager	Bio-Rad, Hercules, USA
circBase	http://www.circbase.org/
Circular RNA Interactome	https://circinteractome.nia.nih.gov/
CytoExpert	Beckman Coulter, Krefeld, Germany
D300(e)Control	Tecan, Männedorf, Switzerland
GraphPad Prism 5.03	GraphPad Software, San Diego, US
Inkscape 0.92.3	https://inkscape.org/de/
MirBase	http://www.mirbase.org/index.shtml
NEB Tools	https://international.neb.com/tools-and-resources/interactive-tools
ZEN 2.3 (blue edition)	https://www.zeiss.com/microscopy/int/products/microscope-
	software/axiovision.html

3.5 Hardware

Hardware used in this thesis are listed in **Table 15**.

Table 16: Hardware

Name	Company	
Agilent 2100 Bioanalyzer	ABI, Carlsbad, CA, USA	
Axiovert 200 Microscope	Zeiss, Oberkochen, Germany	
Axio Observer Z1 Microscope	Zeiss, Oberkochen, Germany	
ApoTome.2	Zeiss, Oberkochen, Germany	
BioPhotometer	Eppendorf, Hamburg, Germany	
Centrifuge 5403	Eppendorf, Hamburg, Germany	
Centrifuge 5417R	Eppendorf, Hamburg, Germany	
CFX384 Touch™ Real-Time	Bio-Rad, Hercules, USA	
CO2 incubator for cell culture (HERA cell)	Heraeus, Hanau, Germany	
CytoFLEX	Beckman Coulter, Krefeld, Germany	
D300(e) Digital Dispenser	Tecan, Männedorf, Switzerland	

HeroLab UVT 2035 UV lamp HeroLab, Wiesloch, Germany

Intas UV lamp Intas, Göttingen, Germany

LAS-3000 mini 2UV Transilluminator Fujifilm, Düsseldorf, Germany

Milli-Q Integral 15 Merck, Darmstadt, Germany Nanodrop 1000 Peqlab, Erlangen, Germany

NucleofectorTM 2b Device Lonza, Basel Switzerland

3130 Genetic Analyzer Applied Biosystems, Waltham, USA

P25 Powerpack Biometra, Göttingen, Germany

GeneAmp® PCR System 2700 Applied Biosystems, Waltham, USA

Thermomixer Comfort Eppendorf, Hamburg, Germany UVT 2035

Beckmann Coulter, Krefeld, Germany Vi-cell XR Cell Viability Analyzer

Herolab, Wiesloch, Germany

Vortex2 Genie Scientific Industries, NY, USA

4 Methods

4.1 Cell culture techniques

4.1.1 Cultivation of human cell lines

The suspension cell lines HAL-01 and 697 were grown in RPMI 1640 medium supplemented with 10% fetal bovine serum (FBS) and 1% Penicillin-Streptomycin. Cells were splitted twice a week in a 1:3 ratio and incubated at 37 °C in a 5% CO₂ enriched atmosphere.

The adherent cell lines HEK293 were maintained as monolayer culture in DMEM supplemented with 10% FBS and 1% Penicillin-Streptomycin. Cells were splitted twice a week in a 1:10 ratio and incubated at 37 °C in a 5% CO2 enriched atmosphere. The medium of stably transfected HEK293 cells was supplemented with 800 μ g/ml G418, while stably transfected HAL-01 and 697 were selected with 1 μ g/ml Puromycin.

The Vi-cell XR Cell Viability Analyzer from Beckman Coulter was used to regularly determine the total number of viable cells.

4.1.2 Cryopreservation and thawing of human cell lines

Cells were removed from the culture flask. For adherent cells, Trypsin-EDTA was used to detach the cells from the flask. Following, cells were transferred in a conical tube and pelleted for 5 min at 200 times gravity (xg). Approximately 5x10⁶ cells were resuspended in 1 ml freezing medium consisting of 70% growth medium, 20% FBS and 10% DMSO and transferred into cryotubes. The cryotubes were then placed into a cryo-freezing container containing 2-isopropanol in order to reduce the temperature at approximately 1 °C per minute. Cells were stored at -80 °C for short-term storage. For long-term storage, cells were kept in the gas phase of liquid nitrogen.

For thawing, cells in a cryotube were thawed in a water bath at 37 °C and transferred into prewarmed complete growth medium. Freezing medium was taken away by centrifugation of cells at 200 xg for 5 min, and finally resuspended in fresh culture medium. After 24 h of thawing, the medium was replaced to remove any residual DMSO.

4.1.3 RNA isolation

Total RNA extraction was performed by using TRIzol or by using the miRNeasy Mini Kit according to the manufacturers' protocol. The concentration of extracted RNA was measured by NanoDrop 1000 spectrophotometer.

4.1.4 RNase R treatment

Ten (10) μg of total RNA were digested with 1 μl of 20 U/μl RNase R. The reaction is summarized in **Table 17**. The mix was incubated at 37 °C for 2 h, followed by RNA purification with RNA Clean & Concentrator-5. The concentration of purified RNA was measured by NanoDrop 1000 spectrophotometer.

Table 17: RNase R treatment

Component	Amount
Ribonuclease R 20 U/µl	1 μ1
RNase 10X reaction buffer	2 μ1
Total RNA	10 μg
RNase-free water	Up to 20 μ l

4.1.5 RNA sequencing

Total RNA was isolated from HEK293, 697 and HAL-01 cells stably overexpressing circATG5 4-5 and control cells (empty vector). For this, the miRNA easy Kit for RNA extraction was used. All cell lines were cultivated in DMEM and HEK293 were additionally incubated in EBSS overnight. RNA samples from HEK293 were analyzed in the Genomics and Transcriptomics Laboratory, BMFZ, University of Düsseldorf, while the RNA samples from 697 and HAL-01 were analyzed at the DKFZ. All samples were measured in triplicate.

4.1.6 cDNA synthesis

As circRNAs lack poly (A) tails, the first strand cDNA was synthetized using random hexamer primers. As reverse transcriptase, Moloney Murine Leukemia Virus Reverse Transcriptase (M-MLV RT) was used. The reaction is summarized in the following table:

Table 18: cDNA Synthesis using M-MLV reverse transcriptase.

Step1: Mix I	Amount	
RNA	2 μg	
Random primer	1 μ1	
RNase-free water	Το 17.25 μl	

Mix I was incubated at **70 °C for 5 min** and immediately put on ice afterwards.

Step2: Mix II	
Mix I	17.25 μl
M-MLV 5X Reaction Buffer	5 μL
dNTPs (10 mM each)	1.25 μl
M-MLV RT	1 μ1
RNase inhibitor	0.5 μl
Total	25 μ1

Mix I was supplemented with mix II and then incubated for 60 min at 37 °C.

4.1.7 Quantitative real-time PCR (RT-qPCR)

The quantitative real-time PCR was performed with GoTaq® RT-qPCR Master Mix (Promega). **Table 19** and **Table 20** show the compositions and conditions for the RT-qPCR.

Table 19: RT-qPCR compositions

Components	Volume in µl
GoTaq® RT-qPCR Master Mix	12.5
10 μM Forward Primer	1.5
10 μM Reverse Primer	1.5
cDNA	1
Nuclease-free Water	To 25

The RT-qPCR reaction was performed on a Bio-Rad CFX Real-Time PCR System using Hard-Shell® 96-Well PCR Plates covered with a Microseal® 'B' PCR Plate Sealing Film (Biorad).

Table 20: RT-qPCR conditions (GoTaq®)

Step	Temperature [°C]	Time	Cycles
Activation of Hot Start Polymerase	95	2 min	
Denaturation	95	15 sec	
			40
Combined annealing/extension	60	1 min	
Melt curve	65 to 95		
Increment	0.5	0.05 sec	

Samples were run in triplicates and normalized to endogenous GAPDH and β -actin. All sequences for reverse and forward primers used are listed in

Table 8. Data were evaluated using the $2^{-\Delta\Delta Ct}$ method with and normalized to control sample.

4.1.8 MicroRNA quantification system

cDNA synthesis for microRNA quantification can be summarized in two steps as follows: First, a polyadenylation of microRNAs by poly (A) polymerase, which is followed by the synthesis of the first-strand cDNA using reverse transcriptase and an oligo-dT adapter primer. Synthetized cDNAs were utilized to amplify the microRNAs of interest by RT-qPCR using a microRNA specific primer and a universal primer. The universal primer (reverse primer) binds to the adapter sequence and a forward primer was used for the amplification of the miRNA of interest.

Table 21: Polyadenylation, first-strand synthesis, and RT-qPCR of miRNAs

Component	Volume in µl	Step
Poly (A) Tailing Buffer 5X	2	
1 μg total RNA	Up to 7	
		Polyadenylation
Poly (A) Polymerase	1	
Nuclease-free water	To 10	

Samples were gently vortexed, briefly centrifuged and then incubated for 60 min at 37 $^{\circ}$ C and 5 min at 70 $^{\circ}$ C.

Poly (A) Tailing Reaction (from step above)	10		
MystiCq microRNA cDNA Reaction Mix	9	First-strand	cDNA
Ready Script Reverse Transcriptase	1	synthesis	
Nuclease-free water	To 20		

Samples were incubated 20 min at 45 $^{\circ}\text{C}$ and followed by 5 min at 85 $^{\circ}\text{C}$

MystiCq microRNA SYBR Green RT-qPCR	12.5	1
Ready Mix (2X)		
microRNA specific primer or microRNA RT-	1	
qPCR Control Primer		Real-Time SYBR Green
Universal PCR Primer (10 µM)	1	RT-qPCR amplification
Undiluted microRNA cDNA (from step above)	1	
Nuclease-free water	To 25	

The samples were run in triplicates and normalized to endogenous RNU6-1.

4.1.9 Standard PCR

Standard PCR was performed using Phusion HF PCR Master Mix (NEB). **Table 22** and **Table 23** show the compositions and conditions for the standard PCR.

Table 22: PCR reaction using Phusion HF (High Fidelity)

Component	Reaction in µl
2X Phusion Master Mix	25 μL
10 μM Forward Primer	2.5 μL
10 μM Reverse Primer	2.5 μL
DNA/cDNA	2 μL
Nuclease-free Water	To $50~\mu L$

Table 23: PCR conditions

Step	Temperature	Time	Cycles
Initial denaturation	98 °C	30 sec	
Denaturation	98 °C	10 sec	
Annealing	3 °C above the melting		
	temperature (Tm) of lower	10-30 sec	30-35
	Tm primer		
Extension	72 °C	15 sec/kb	
Final extension	72 °C	5 min	

The standard PCR was also used to add restriction sites at the ends of the DNA in order to insert it into a plasmid of interest.

4.1.10 Agarose gel electrophoresis

Nucleic acids were separated using agarose gel electrophoresis. Depending on the expected product size, the separation was done in a percentage of agarose gel ranging between 1% and 3% with 1:10 Midori Green Advance for 45 min at 120 V. The Intas UV lamp was applied for the visualization of the DNA bands and the size of the DNA fragments was determined using Gene Ruler 100 bp or 1 kbp plus ladder. If necessary, the expected band was excised, purified, and sequenced by Sanger sequencing.

4.1.11 Gel extraction

Excised PCR products were extracted from the gel fragment using Monarch DNA Gel Extraction Kit according to the manufacturer's instructions.

4.1.12 Sanger sequencing

For Sanger sequencing, 20 ng DNA or 200 ng plasmid DNA were used. The PCR reaction for Sanger sequencing is summarized in **Table 24** and PCR conditions in **Table 25**. The PCR product was purified with DyeEx 2.0 Kit (QIAGEN) according to the manufacturer's instructions in order to remove dye terminators and then 20 µl HiDi (Applied Biosystems) was added. Samples were transferred to a MicroAmp Optical 96-well plate (Applied Biosystems) and sequenced on a 3130 Genetic Analyzer. Sequencing data were analyzed by using the software ApE-A plasmid editor, created by Wayne Davis.

Table 24: PCR for Sanger sequencing

Component	Reaction
Big Dye Terminator (Applied Biosystems)	4 μl
DNA or plasmid DNA	20 ng or 200 ng
10 μM primer (forward or reverse)	0.5 μ1
Nuclease free water	Up to 20 μl

Table 25: PCR condition

Step	Temperature [°C]	Time	Cycles
Initial denaturation	96	1 min	
Denaturation	96	10 sec	
Annealing	55	30 sec	26
Extension	60	4 min	
Holding	4	∞	

4.1.13 DNA cloning

To study the function of circATG5 4-5, exons 4 and 5 of ATG5 were cloned into the pcDNA3.1 (+) CircRNA Mini Vector for non-viral gene delivery system and into LeGO-IG2

for viral gene delivery system. Both systems contain short intronic sequences, which facilitate circRNA production. To generate the exons 4 and 5 of ATG5, a PCR was performed with the forward and reverse primers containing EcoRV-HF and SacII sites for the non-viral vector and EcoRI-HF and NotI-HF sites for the lentiviral vector. After the purification of the PCR product with QIAquick PCR Purification Kit or with Monarch DNA Gel Extraction Kit according to the manufacturer's instructions, the plasmid, or the insert was double digested with corresponding enzymes for 15 min at 37 °C prior to doing the ligation.

Table 26: Composition of the double digestion mix

Component	Amount
DNA (Plasmid or PCR product)	1 μg
10X CutSmart Buffer	5 μL
Enzyme A	1 μL
Enzyme B	1 μL
Nuclease-free water	To 50 μL

Digested DNAs were separated with agarose gel as described in section **4.1.10** and purified using Monarch DNA Gel Extraction Kit according to the manufacturer's instructions. Subsequently, the plasmid DNA and the insert were ligated in a molar ratio of 3:1 using Rapid DNA Ligation Kit according to the manufacturer's instructions. The online tool NEBiocalculator from New England Biolabs. was applied for the calculation of the ratio, which is available under https://nebiocalculator.neb.com/#!/ligation.

4.1.14 Virus production

HEK293-T cells were seeded on 120 mm petri dishes one day prior to transfection so that they reached a confluence of approximately 75%. The next day, the medium was changed, and the transfection mix as described in **Table 27** was added to the cells 15 min after incubation.

Two days after the transfection, the lentiviral containing medium was collected and filtered through a $0.45~\mu l$ filter. The lentiviral solution was treated with Lenti-X for viral concentration according to the manufacturer's protocol. The virus pellet was resuspended in

the medium. Target cells were transduced with the virus solution, or the virus solution was stored at -80 $^{\circ}$ C.

Table 27: Composition of transfection mix

Components	Amount
Serum-free media	500 μl
LeGO-IG2_circATG5 4-5 or empty LeGO-IG2	10 μg
pMDLg/pRRE	5 μg
pRSV-Rev	3 μg
pMD2.G	2 μg
CalFectin	60µl

LeGO-IG2_circATG5 4-5 contains the gene of interest (GOI) circATG5 4-5 and the LeGO-IG2 is an empty plasmid that is used as mock control.

pMDLg/pRRE (Addgene #12251) and pRSV-Rev (Addgene #12253) are a third-generation packaging plasmids, which require pMD2.G (Addgene #12259), an envelope expressing plasmid. pMDLg/pRRE contains HIV1 Gag and Pol, pRSV-Rev contains Rev and an pMD2.G has a VSV-G envelope expressing plasmid.

4.1.15 Transformation

The chemically competent *Escherichia coli* (*E. coli*) was thawed on ice. Up to 1/10 of the volume of the ligation reaction mix or 1-100 ng of plasmid DNA was added to 40 µl of competent cells. Cells were incubated on ice for 30 min followed by the heat shock at 42 °C for 1 min and the recovery on ice for 2 min. Subsequently, 900 µl of pre-warmed LB medium without antibiotics were added to the cells and incubated at 37 °C for 45 min while shaking at 350 rpm to allow the expression of the antibiotic resistance gene. Afterwards, 50 µl bacterial suspension was spread on a LB agar plate containing an appropriate selective antibiotic (100 µg/ml ampicillin) and incubated overnight at 37 °C.

4.1.16 Plasmid purification

E. coli colonies were picked from LB agar plates and cultivated in 3 ml LB medium supplemented with an appropriate selective antibiotic (100 μg/ml ampicillin) overnight at 37 °C and 450 rpm in a Certomat BS-T incubator shaker (Braun Biotech). The plasmids

were isolated using Monarch Plasmid Miniprep Kit (NEB) according to the manufacturer's instructions. When a large amount of plasmid DNA was required, bacteria grown in 3 ml LB medium were transferred into 250 ml LB medium containing 100 μg/ml ampicillin antibiotics. Bacteria were incubated at 37 °C and 450 rpm overnight. The plasmids were subsequently extracted using the NucleoBond Xtra Maxi Plus kit (Macherey-Nagel) according to the manufacturer's instructions.

4.1.17 Transfection of plasmid DNA

This transfection reagent was used for adherent cells. Cells were seeded out into a 24-well, 12-well or 6-well plate one day prior to the transfection. The size of wells depended on the analysis that had to be done further. The next day, cells were transfected according to the manufacturer's instructions. Cells were incubated with the plasmid for 1–3 days at 37 °C in a 5% CO₂ enriched atmosphere. For stable transfection, the appropriate antibiotic was added onto the cells 2 days after transfection. Transfected cells were applied for the investigation of the role of cicATG5 4-5.

4.1.18 RNA interference using small interfering RNA (siRNA)

HEK293 cells were seeded into a 24-well or 6-well plate one day prior to the transfection. The following day, siPOOL transfection was performed using Lipofectamin® RNAiMAX Reagent according to the manufacturer's instructions. Transfected cells were used for diverse analyses such as autophagy assay, cell proliferation, or stability of ATG5 by circATG5 4-5.

4.1.19 RNA fluorescence in situ hybridization (FISH)

To localize circATG5 4-5 in the cell compartment, RNA FISH was performed with a single fluorescently labeled probe spanning the circATG5 4-5 backsplice junction. The RNA FISH assay was carried out based on Stellaris® RNA FISH protocol. This experiment was performed in HEK293 cells. First, 4×10^5 cells were fixed in 4% formaldehyde at RT for 10 min and then permeabilized in 70% ethanol at 4 °C for 1 h, followed by the hybridization with FITC-labeled circATG5 4-5 or with AF555-labeled *GAPDH* in hybridization buffer (10% formamide, 10% dextran sulfate, 2x saline sodium citrate) at 37 °C overnight. Nuclei were counterstained with DAPI. Images were acquired using a wide field fluorescence

microscope Axio Observer.Z1 (Zeiss) with an ApoTome 2 (Zeiss) attachment. *GAPDH* was used as a control for cytoplasm.

4.1.20 mRNA stability assay using transcription inhibition by Actinomycin D

To assess whether the expression of circATG5 4-5 has a protective effect on its host gene ATG5, the expression of circATG5 4-5 was altered through the overexpression or knockdown in HEK293 cells, followed by the treatment of the cells with 8 μ g/ml Actinomycin D. This drug has the ability to inhibit the *de novo* mRNA synthesis (transcription).

Experimentally, $1x10^5$ HEK293 cells transfected with circATG5 4-5 or with empty vector were seeded into a 12-well plate. The next day, 8 µg/ml Actinomycin D was added to the medium and cells were harvested at different time points after compound addition (1 h, 4 h, 6 h, 8 h and 24 h).

For knockdown, $1x10^5$ HEK293 cells were seeded into a 12-well plate one day prior to the transfection. The next day, cells were transfected with 30 pmol siRNA against circATG5 4-5 or scrambled siRNAs as non-targeted control. Forty-eight hours after transfection, Actinomycin D (8 μ g/ml) was added to the medium and cells were harvested at different time points after compound addition (1 h, 4 h, 6 h, 8 h and 24 h). Additionally, cells were harvested before the addition of the compound (0 h).

4.1.21 Cell based assays

4.1.21.1 Cell viability

Cell viability was determined using the CellTiter-Glo® Luminescent Cell Viability Assay according to the manufacturer's instructions. The CellTiter-Glo® Reagent was diluted with PBS (1:2, v/v).

4.1.21.2 Autophagy assay

The autophagy assay used in this study is based on autophagy LC3 HiBit reporter assay system. This system uses a plasmid which bears a HiBit tag and contains a sequence encoding the *MAP1LC3B* gene. This construct can be transiently expressed in cells or stably expressed in the cells by selecting positive clones with culture medium containing geneticin (G418). Like the endogenous LC3, when autophagy is induced, LC3 HiBit Reporter proteins expressed in the cells are targeted to phagophores. Subsequently, the reporter molecule is captured within autophagosome and then degraded after the fusion with lysosome. For the detection of autophagy, cells are lysed with a lytic reagent, which provides the LgBiT protein and furimazine substrate crucial for luminescence. HiBit is an 11 amino acid peptide tag that binds to LgBiT to produce a luminescent signal, which is directly proportional to the level of autophagy reporter present. Autophagy inhibitors like Chloroquine and Bafilomycin A₁ can be used to block autophagosome degradation. **Figure 11** shows an example of the result of this system so that it is easier to understand how it works.

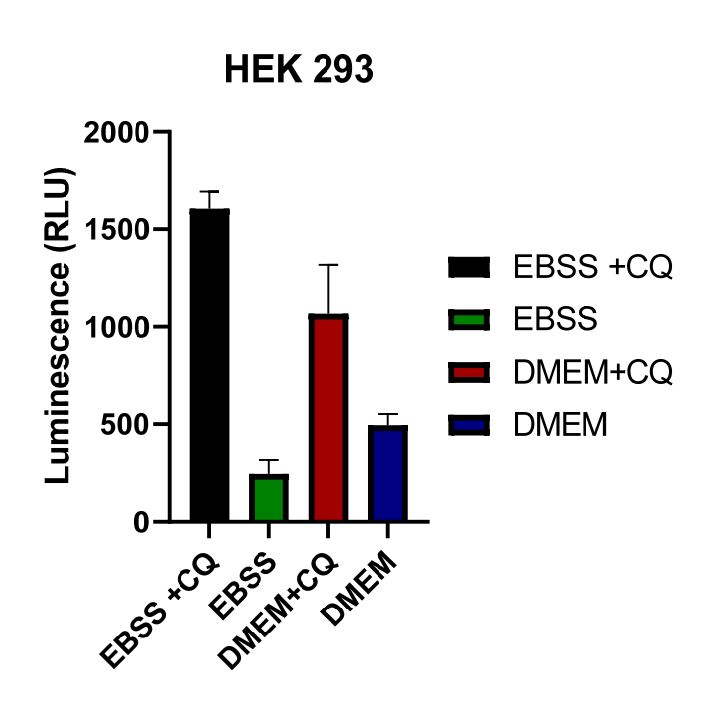


Figure 11: Autophagy LC3 HiBiT Reporter Assay system (Promega)

Black bar: Autophagy was induced by using EBSS medium and the degradation of autophagosomes was inhibited by using chloroquine (CQ). As consequence, there is an accumulation of the reporter, which is indicated by an increase in luminescent signal. In green: Autophagy was induced by using EBSS in absence of the inhibitor of autophagosome degradation. This results in increased autophagy flux, which accelerates the degradation of the autophagy reporter, thus a decreased luminescent signal. In red: Cells were cultured in a complete growth medium in presence of chloroquine to prevent the degradation of the autophagosome. As consequence, there is a moderate accumulation of reporter associated with a normal increased in luminescence signal. In blue: Like in red, cells were here cultured in complete growth medium but without chloroquine. There is a moderate ("physiological") degradation of autophagy reporter, which is not accumulated. Thus, a decreased luminescent signal. This example was done in HEK cells.

In order to study the effect of circATG5 4-5 on autophagy flux, the Autophagy LC3 HiBiT Reporter Assay System from Promega was used according to the manufacturer's instructions. For this, the effect of both overexpression and knockdown of circATG5 4-5 was analyzed. For the overexpression, $5x10^3$ HEK293 cells, which stably co-express the Autophagy LC3 HiBiT Reporter vector and circATG5 4-5 or the Autophagy LC3 HiBiT Reporter vector and the empty vector were seeded in 96-well plates. The next day, cells were incubated in culture medium (DMEM) or starvation medium (EBSS) in the presence or in absence of 50 μ M chloroquine for 5 h at 37 °C.

For the knockdown, $3x10^5$ HEK293 cells that stably express the Autophagy LC3 HiBiT Reporter vector were seeded in a 6-well plate one day prior to the transfection. The next day, cells were transfected with siRNA against circATG5 4-5 or with scrambled siRNA and $5x10^3$ from the transfected cells were transferred into a 96-well plate. After 48 h, cells were incubated in culture medium (DMEM) or starvation medium (EBSS) in the presence or absence of 50 μ M chloroquine for 5 h at 37 °C.

After incubation, cells were lysed with 100 µl HiBiT lytic reagent, shaken at 400 rpm for 2 min, and then incubated for at least 10 min. The luminescence signal was measured using TECAN. The HiBiT lytic reagent was diluted 1:2 with PBS.

4.1.21.3 CFSE

To measure the influence of circATG5 4-5 on cell proliferation *in vitro*, cells were labeled with Carboxyfluorescein succinimidyl ester (CFSE). CFSE is cell permeable and covalently couples to intracellular proteins containing lysine or other amine residues. Basically, proliferating cells halve the CFSE fluorescence upon each cell division because this dye is equally distributed to the daughter cells.

For the assay, $10x10^7$ cells were transferred to a 15 ml conical tube and washed three times with PBS by centrifugation at 200 xg for 5 min. For the staining, the cell pellet was resuspended 1 ml PBS containing CFSE (final concentration of 5 μ M). After incubation time of 15 min at 37 °C in the dark, 5 volumes of cold complete media were added to the cells and incubated for 5 min on ice. Cells were pelleted and washed twice with complete medium Subsequently, they were pelleted again, resuspended in the medium and the cell number was adjusted to $1x10^5$. Cells were then seeded into a 6-well plate containing complete medium. The day 0 is the day on which the cells were stained with CFSE. After staining HEK293

cells that stably expressed circATG5 4-5, the CFSE intensity was measured by flow cytometry on day 0, 1, 3 and 4. To achieve a knockdown, cells were transfected with siATG5 4-5 one day after staining cells with CFSE. Cells were analyzed by FACS.

4.1.22 Cell cycle analysis

For the analysis of the cell cycle, PI staining was performed. For this, cells were harvested by centrifugation and then resuspended in 100 μl PBS. The volume of 900 μl ice-cold 70% EtOH was added to the cells, which were then vortexed and fixed for 30 min at 4 °C or stored at –20 °C. Afterwards, cells were centrifuged for 5 min at 500 xg, washed with PBS and 4 °C and the cell pellet was resuspended in 50 μl RNase with the final concentration of 0.1 mg/ml. Additionally, 150 μl PI (50μg/ml) were added to the cells and the mix was incubated overnight at 4 °C, followed by the analysis of the cells by flow cytometry.

4.1.23 Proteomics

HEK293, 697 and HAL-01 cell lines that stably overexpress circATG5 4-5 and control cells (empty vector) were seeded into 6-well plates. HEK293 were harvested without Trypsin-EDTA. Cells were washed two times with ice-cold PBS. Afterwards, cells were resuspended in 1 ml PBS and transferred into a 2 ml Eppendorf tube of known weight. PBS was removed by centrifuging the cells at 800 xg for 5 min at 4 °C. After determining the weight of the pellet, cells were stored at -80 °C. Four replicates of test and control samples were sent to the Molecular Proteomics Laboratory, BMFZ, University of Düsseldorf for analysis by mass spectrometry.

4.1.24 Western blot

HEK293 cells overexpressing circATG5 4-5 were harvested without Trypsin-EDTA, washed with ice-cold PBS and lysed using RIPA buffer supplemented with protease inhibitor cocktail and PhosSTOP The protein concentration was determined using the Protein Assay Dye Reagent (BIO-RAD) and measured by using Eppendorf BioPhotometer. Twenty (20) µg protein per sample was separated by SDS polyacrylamide gel electrophoresis (SDS-PAGE, 30 mA/gel for about 1 h) and transferred onto a nitrocellulose membrane at 100 V for 1 h. The membrane was blocked for 1 h in 5% BSA in TBST at room temperature followed by the incubation with primary antibodies at 4 °C overnight. Protein bands were

detected by incubation with secondary antibodies conjugated to horseradish at room temperature for 1 h and visualized using the SuperSignal® West Femto Maximum Sensitivity Substrate. The device LAS 3000 Imaging System (Fujifilm) was used to detect the signal.

4.1.25 Statistical analysis

GraphPad Prism 8.0.2 was used to perform statistical analyses. All data are presented as mean \pm SEM of three independent experiments. Comparisons between groups were made using Student's t-test. The difference was statistically significant at p-values \leq 0.05.

5 Results

5.1 Detection of circATG5 4-5 in B cell acute lymphoblastic leukemia cell lines

A previous study conducted in our laboratory (Department of Pediatric Oncology, Hematology and Clinical Immunology, Heinrich Heine University Düsseldorf) aimed to identify circRNAs associated with B-ALL. For that study, the sequencing was carried out by Cai Chen and the data treatment was performed by Daniel Picard. In that study, the expression of circRNAs was determined by performing circRNome and whole transcriptome sequencing. For this, two cell lines with different genetic background and therapy responses were compared, namely 697 (TCF3-PBX1-positive and drug sensitive) and HAL-01 (TCF3-HLF-positive and drug resistant). For the analysis, RNA samples for both applications were depleted of ribosomal RNA and then samples for circRNome analysis were additionally digested with RNase R to enrich for circRNAs. Samples for whole transcriptome sequencing were left RNAse R untreated. After TruSeq stranded library preparation (Illumina), samples were sequenced on a HiSeq 2500 (Illumina). CircRNAs were detected employing the workflow reported by Salzman et al. Briefly, unaligned sequencing reads were trimmed using Partek Flow software (Partek Inc., St. Louis, Missouri, USA) to remove bases from the beginning to position 13 and from position 99 to the end. Next, Bowtie233 was used to align samples against the human reference database (hg19) and SAMtools34 was used to extract unmapped reads. The find circ.py script in Python2.7 was then used to detect circRNAs followed by the scorethresh.py script to filter gene list. Finally, BEDTools was used to annotate the circRNAs. Read pairs where one of the reads mapped to a backsplice site and the other read mapped to the same transcript were considered as supportive of circRNAs. The gene expression level and the coverage of circRNAs were determined.

Overall, a total of 5195 circRNAs were discovered (**Figure 12 A**). Out of these, 4094 have already been described in the circBase database (http://www.circbase.org/). Among the discovered circRNAs, 2703 were expressed in both cell lines (*TCF3-PBX1+* and *TCF3-HLF1+*). Of those, 308 were novel circRNAs, while 2395 were known circRNAs. There were more circRNAs detected, which are expressed exclusively in HAL-01 (449) or in 697 (344, **Figure 12 A**).

By looking for circRNAs derived from ATG5, I examined these sequencing data (unpublished data), and I found that among circATG5s which were expressed,

hsa_circ_0077535 (named circATG5 4-5 in this thesis) was the only one with the highest expression (**Figure 12 D**). In addition, some cirATG5s with circBase ID were not detected. CircATG5 4-5 was selected as a candidate for this study and further methods were applied to validate its presence and to study its function.

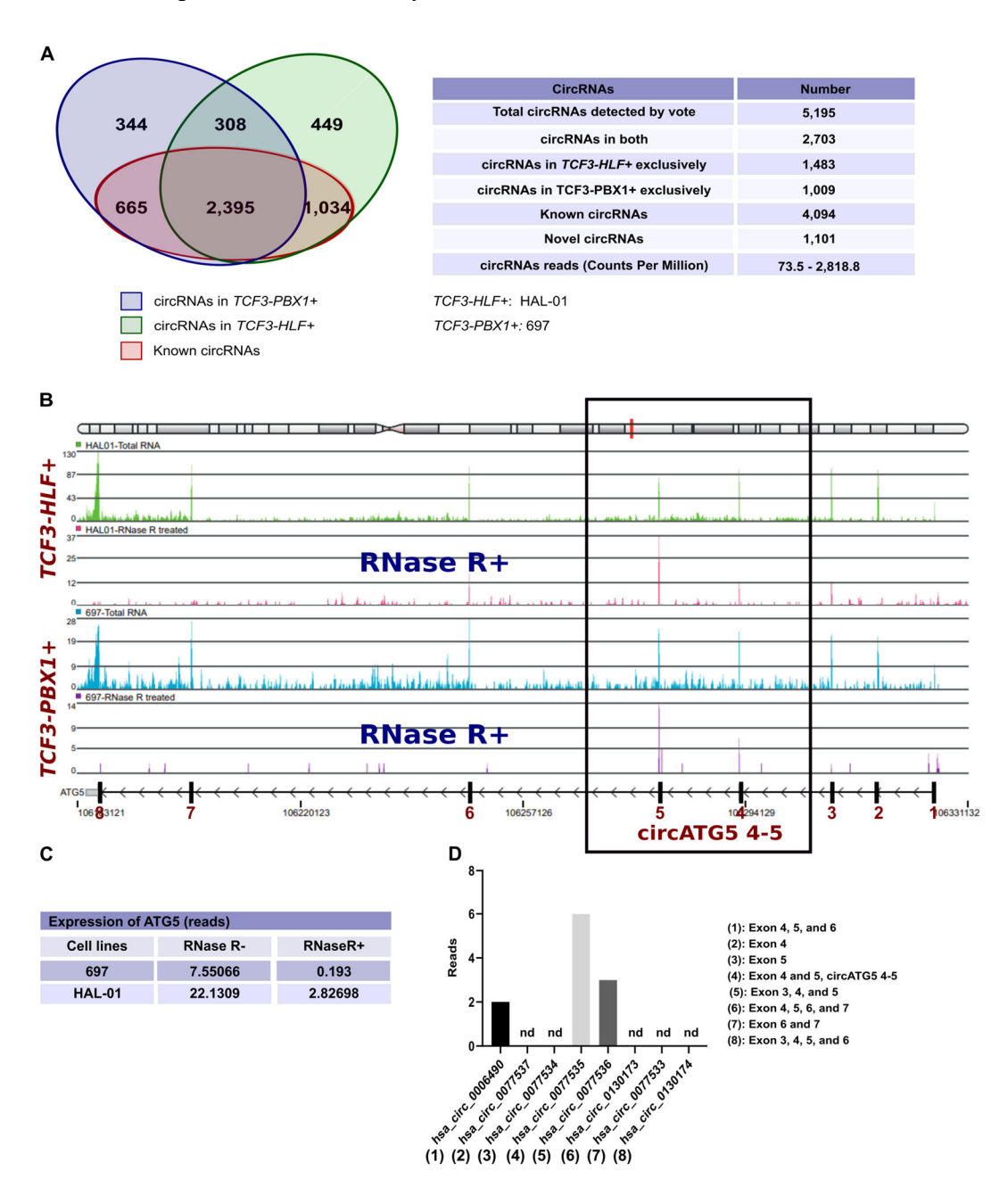


Figure 12: Identification of circATG5 4-5 in RNA seq data (Cai Chen and Daniel Picard)

(A) The Venn diagram represents the numbers of expressed circRNAs in the B-ALL cell lines 697 and HAL-01, taken from the accompanying table. (B) Presentation of the gene locus of *ATG5* on chromosome 6 and the coverage of the *ATG5* gene region by sequencing reads beneath. The region including exon 4 and 5 is marked by a black box (C) The table derived from (A) and shows only *ATG5* reads found by sequencing the cell lines 697 and HAL-01 following the treatment (RNase R+) or non-treatment (RNase R-) of total RNA with RNase R. (D) The bar diagram illustrates the expression of the exon combination of circRNAs derived from ATG5, identified in our RNAseq data. The Y-axis is scaled to Reads and the X-axis, contains circRNAs IDs taken from CircInteractome database ¹³⁶. Nd: non detected. In grey is circATG5, tha4-5 which presents more reads than the others detected circATG5. 1 to 8 indicate corresponding exon combinations of 1 to 8 on the X-axis of the bar diagram. CircATG5 4-5 encompasses the coding regions of exon 4 and 5 of *ATG5*.

5.2 Characterization of circATG5 4-5

The human *ATG5* gene is located on chromosome 6. According to the circInteractome database ¹³⁶, there are to date eight circRNAs known to derive from this gene. The ID of the circRNAs is provided by circInteractome. Exons were annotated using the Ensembl gene database ¹³⁷ and based on the mature sequence of circRNA available in circInteractome. Exons 1, 2 and 8 are not included in the formation of circATG5s, as depicted in **Figure 13**. CircRNAs derived from *ATG5* are all exonic.

CircATG5 4-5 is located on chromosome 6 q21:106727535-106740981. It is 242 (nt) in length, in its mature and spliced form. CircATG5 4-5 is generated by backsplicing of exon 4 and exon 5 of the *ATG5* precursor RNA. In the database circBase (http://www.circbase.org/) and circInteractome, circATG5 4-5 has the ID "hsa circ 0077535".

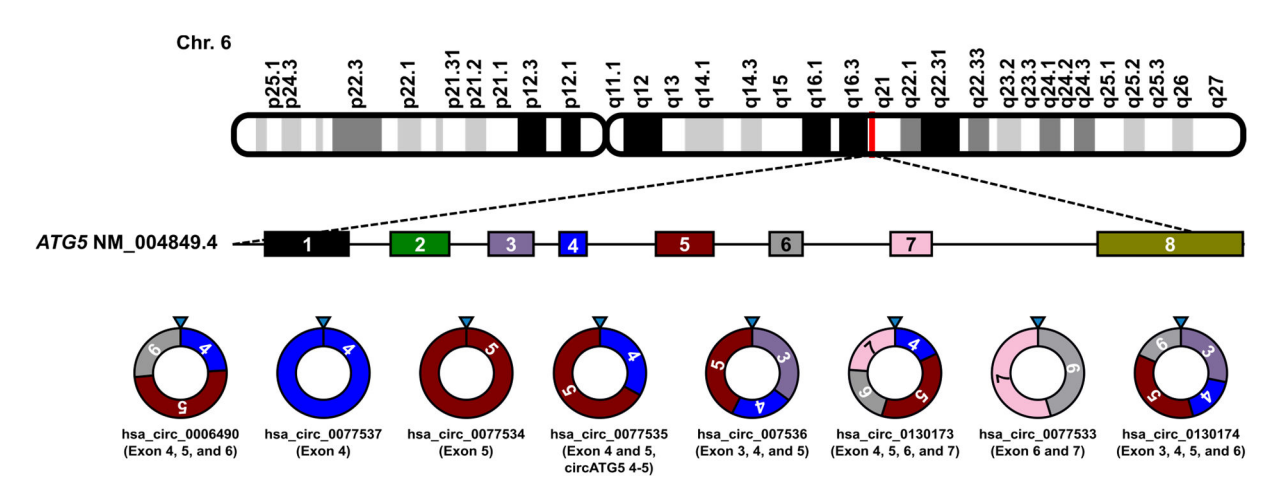


Figure 13: Schematic presentation of circRNAs derived from the human gene *ATG5*Eight circRNAs are known to derived from the gene *ATG5*, which is localized on chromosome 6q21. The ID of circRNAs was taken from CircInteractome ¹³⁶. Illustrated circRNAs are annotated according to mature sequences of circATG5s provided by CircInteractome where the exon annotation was done using Ensembl gene database ¹³⁷. The contribution of the exonic regions of *ATG5* to the linear consensus mRNA (transcript 1, NM 004849.4) and the circRNAs are presented.

5.3 CircATG5 4-5 can be detected and validated by RT-qPCR

CircRNAs are formed by non-canonical backsplice events where the 5' and 3' ends join by a covalent bond. The junction of the 5' and 3' ends is termed backsplice site or backsplice junction. This junction can be used for the validation of circRNAs, since it is a unique feature of this kind of RNA molecule.

Experimentally, divergent primers were designed to detect the backsplice junction (**Figure 14 A**). Applying this strategy, a band with the expected size (242 bp) as shown in **Figure 14 B** could be identified. The presence of the backsplice junctional sequence was validated by Sanger sequencing (**Figure 14 C**). Furthermore, the resistance of circATG5 4-5 towards RNase R has been tested, where total RNA extracted from HEK293 cells was treated with RNase R (**chapter 4.1.4**) and analyzed by RT-qPCR using divergent primers. RT-qPCR data showed a significant enrichment of circATG5 4-5 expression and a significant decrease in *ATG5* expression upon digestion (**Figure 14 D**). These findings indicate that there is the presence of a circular transcript.

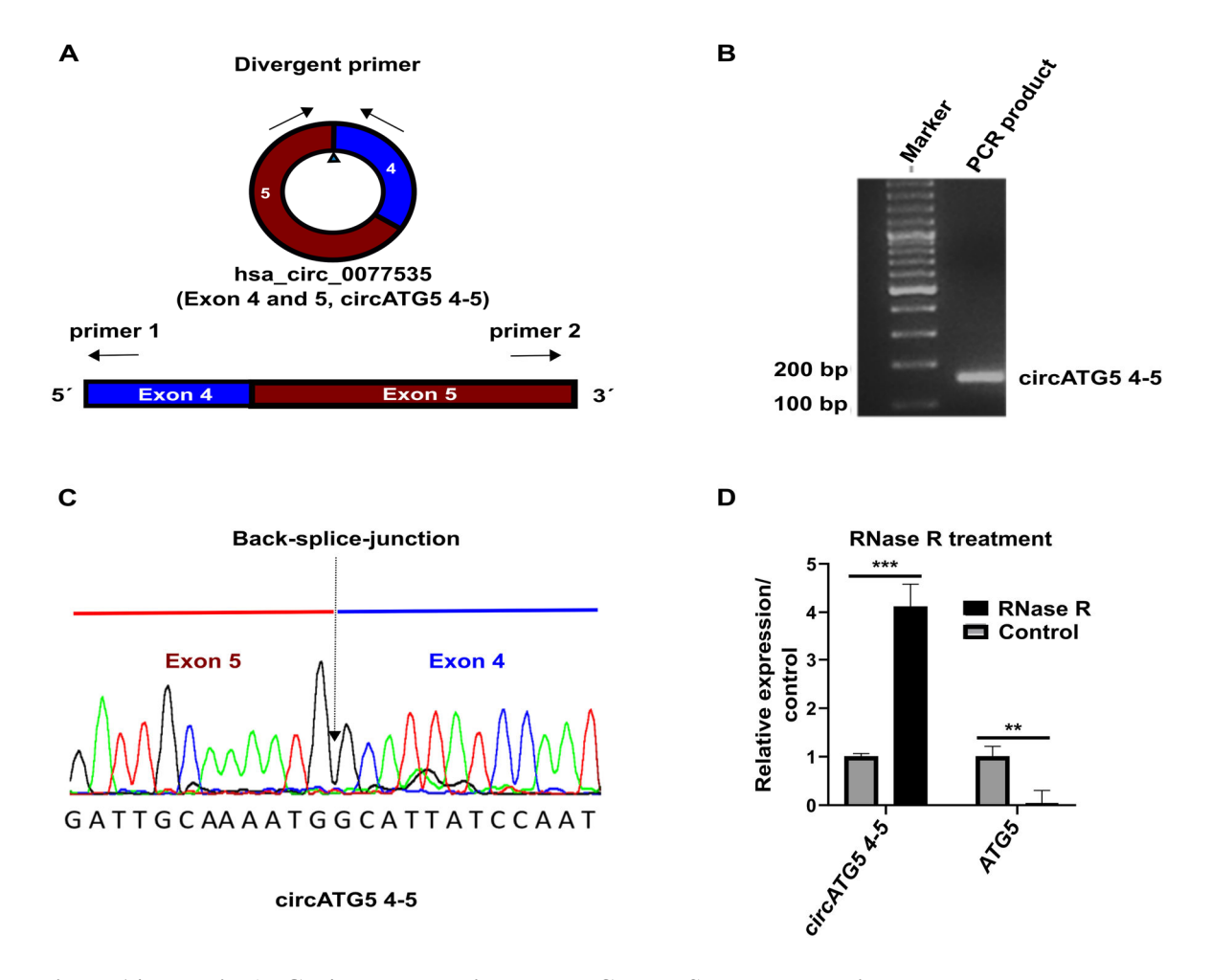


Figure 14: The circATG5 4-5 can be validated by PCR and Sanger sequencing

(A) Junction-spanning primers. (B) PCR products obtained using divergent primers and ran on 3% agarose gel. (C) The electropherogram shows the presence of the back-splice site joining exon 4 and exon 5 of circATG5 4-5, detected by Sanger sequencing using as well as divergent primers. (D) RT-qPCR following RNase R treatment from HEK293 RNAs. The black bars represent treated samples with 10 U/ μ l RNase R at 37 °C for 2h and grey bars are non-treated samples. This illustration shows an enrichment of circATG5 4-5 in the treated samples, while the expression of the ATG5 mRNA in this sample is negatively affected. This indicates in one hand the resistance of circular transcript to RNase R and in the other hand the degradation of ATG5 mRNA upon RNase R.

The RT-qPCR data were calculated using the $2^{-\Delta\Delta CT}$ method and normalized to the levels of non-treated control Values shown represent mean \pm SEM of three replicates. **p<0.01, ***p<0.001 (Student's t-test).

5.4 CircATG5 4-5 is expressed in B-ALL cell lines across different molecular subtypes.

The expression of circATG5 4-5 was investigated in B-ALL cell lines with different genetic backgrounds. RNA was isolated from these cells and RT-qPCR was carried out. The RT-qPCR data showed that circATG5 4-5 is expressed in all of these B-ALL cell lines. Notably, RS4 11 showed the highest expression of circATG5 4-5 among all tested cell lines. 697 and HAL-01, the cell lines that were analyzed by circRNome and whole transcriptome sequencing and are further elucidated in this thesis, show the lowest and an intermediate circATG5 4-5 expression, respectively. Moreover, the expression of circATG5 4-5 does not correlate with the genetic background.

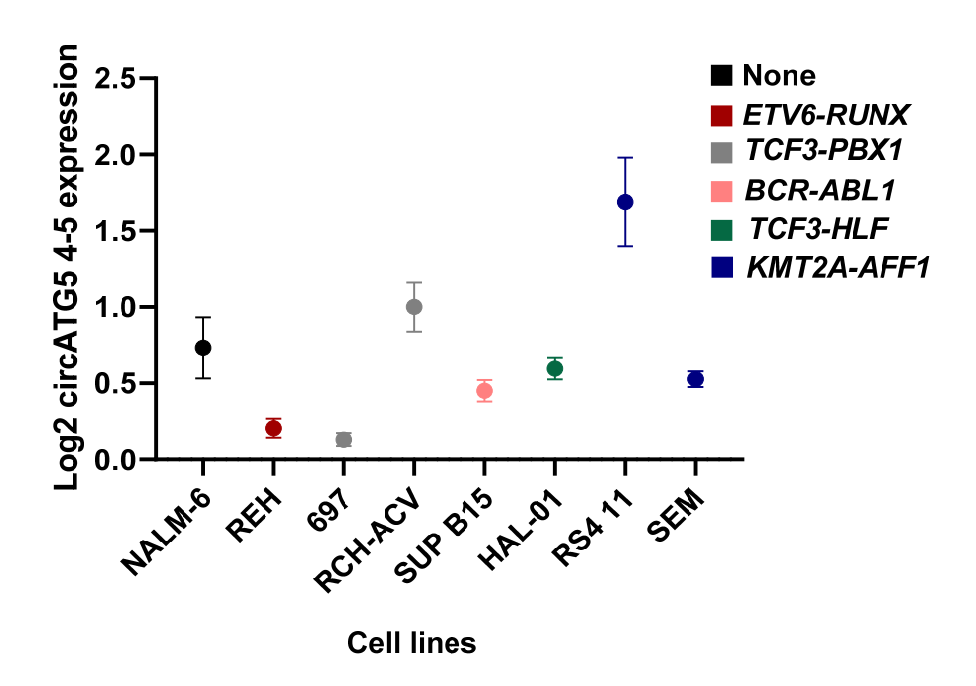


Figure 15: Expression of circATG5 4-5 in leukemia cell lines

The expression of circATG5 4-5 was derived from RT-qPCR data. Each color represents a molecular genetic feature of the cell line. The RT-qPCR data were normalized to GAPDH and are relative to RCH-ACV. Values shown represent the mean \pm SEM of three replicates.

5.5 CircATG5 4-5 can be detected in the cytoplasm

RNA FISH was conducted to assess the subcellular localization of circATG5 4-5 in HEK cells (**Figure 16**). Cells were incubated with 300 nM FITC-labeled RNA probes (250 nM) against the

backsplice junction of circATG5 4-5. An RNA probe hybridizing to *GAPDH* (Glycerinaldehyd-3-Phosphat-Dehydrogenase) (125 nM) was used as a positive control for cytoplasmic RNA. The circATG5 4-5 signal could be visualized using a Zeiss Observer Z.1 microscope equipped with the Zeiss ApoTome device. As illustrated in **Figure 16** (upper panels), circATG5 4-5 was clearly detected in the cytoplasm (indicated by green dots), whereas signals in the nucleus were sparse. As a control, *GAPDH*-RNA was stained and detected in the cytoplasm (**Figure 16**, **lower panels**, indicated by red dots).

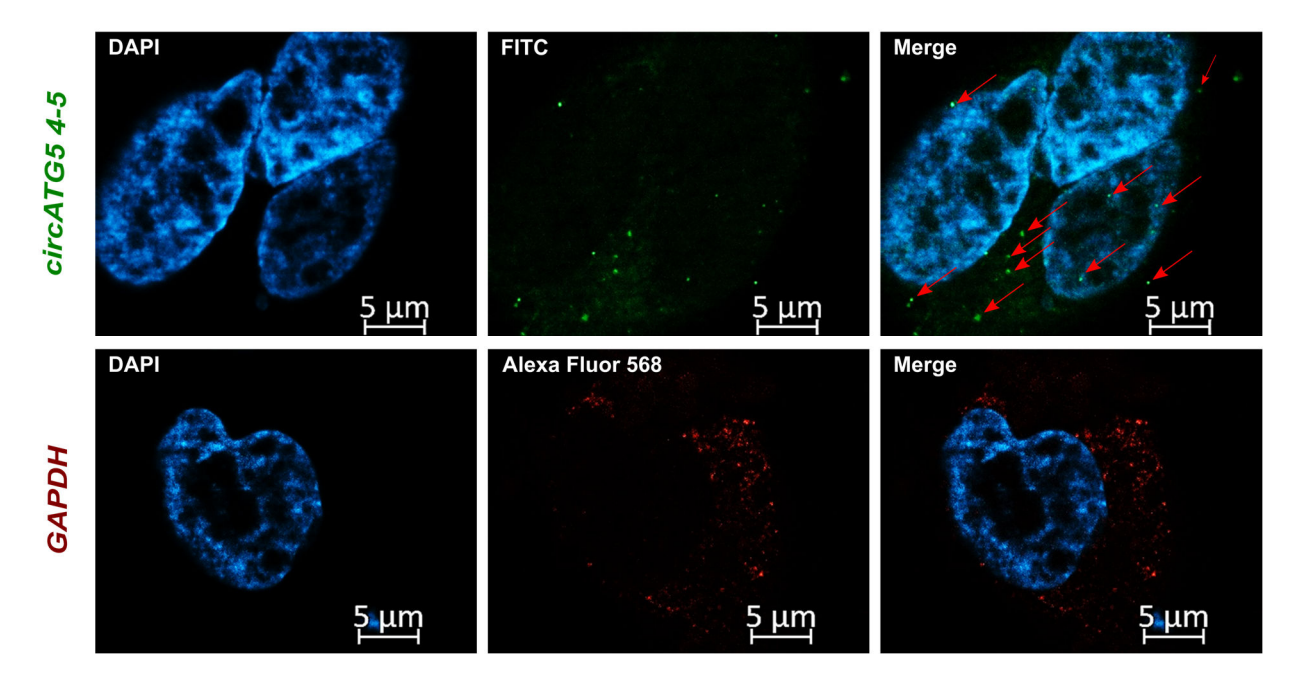


Figure 16: Analysis of the subcellular localization of circATG5 4-5 by RNA-FISH The subcellular distribution of circATG5 4-5 was identified by RNA-FISH using HEK cells (wild type). The green dots (FITC-labeled probe) indicate circATG5 4-5 and are marked by red arrows to better see them, the red dots or speckles (Quasar 570 dye labeled probe) are GAPDH, which was used as the cytoplasmic control. DAPI staining (blue) was used to stain the nucleus. This assay indicates that circATG5 4-5 can be detected in the cytoplasm.

5.6 Overexpression of circATG5 4-5

To generate the overexpression constructs, PCR products were digested with EcoRV and SacII sites to be integrated into the pcDNA3.1 (+) circ Mini vector or with EcoRI and NotI sites for the LeGO-IG2 lentiviral plasmid. Digested PCR products were purified and cloned into the corresponding plasmids. Those plasmids have been in general designed to be able to produce circRNAs when transfected into cells. The *in vitro* circularization of the insert is supported by the upstream intron sequence and the downstream intron sequence, which are complementary to each other. The insert (exon 4 and 5 of ATG5) is cloned in between the two complementary intron sequences as shown in **Figure 17**. Both plasmids contain the

same cassette for *in vitro* circularization of RNA, except that in pcDNA3.1 (+) CircRNA Mini vector this cassette is driven by the CMV promoter and in LeGo-IG2 by the SFFV promoter.



Figure 17: CircATG5 4-5 overexpression construct

For the *in vitro* circularization of the insert, the construct contains inverted repeat sequences (black) which are complementary at base pair level to each other (Up and Down), a splice acceptor (SA) and a splice donor (SD). The cDNA (Exon 4 and 5 of ATG5) is cloned between Up-SA and SD-Down. The expression of the gene is driven by the CMV pcDNA3.1 (+) CircRNA Mini vector or the SFFV (LeGo-IG2) promoter.

In order to functionally investigate the role of circATG5 4-5 in B-ALL, overexpression of circATG5 4-5 was performed in HEK293, HAL-01 and 697. Non-viral gene delivery system pcDNA3.1 (+) circRNA mini vector was used to transfect adherent cells (HEK293) and the lentiviral delivery system LeGo-IG2 was used for suspension cells (HAL-01 and 697).

The presence and correct sequence of the insert and the plasmid was controlled by Sanger sequencing. Since circRNAs are non-coding RNAs, the overexpression can be easily checked by RT-qPCR or PCR, but not by western blot. The plasmid pcDNA3.1 (+) circRNA mini vector construct was both transiently and stably transfected into the HEK293 cell line. The overexpression of circATG5 4-5 was then confirmed by RT-qPCR using junction-spanning primers as shown in **Figure 18**.

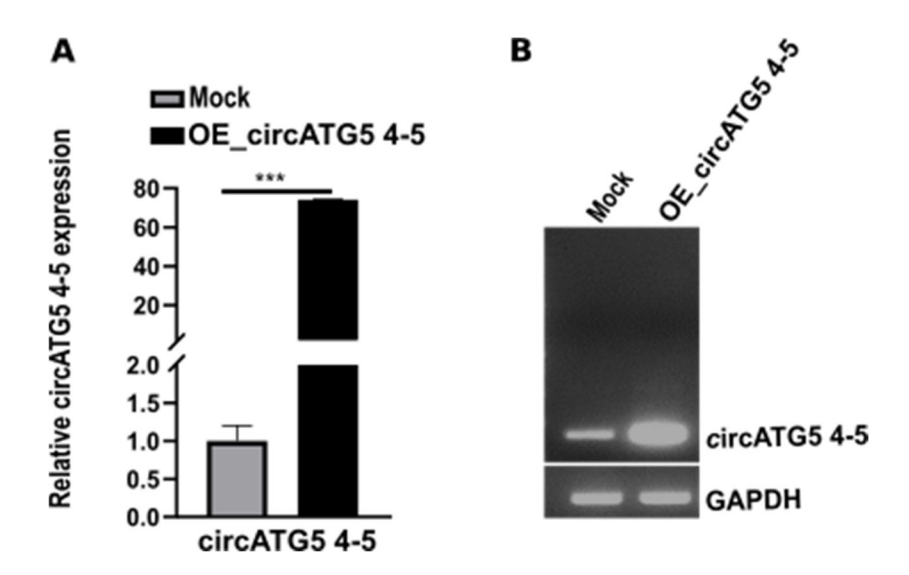


Figure 18: The expression of circATG5 4-5 can be upregulated (an example of a non-lentiviral vector pcDNA3.1 (+) circ Mini vector)

(A) RT-qPCR following the overexpression (stable) of circATG5 4-5 in HEK293. Divergent primers were applied, spanning the backsplice junction sequence of circATG5 4-5. Mock empty vector was used as control (B) The product of the RT-qPCR was run on a 3% agarose gel showing overexpression of circATG5 4-5 in transfected HEK293 cells compared to the mock transfected control (empty vector control). RT-qPCR data were calculated using the $2^{-\Delta\Delta CT}$ method and normalized by GAPDH expression. Values shown represent mean \pm SEM of three replicates. ***p<0.001 (Student's t-test).

To confirm that RNAs generated from our circRNA overexpressing system (**refer to chapter 5.6**) are circular, the resistance of the generated RNA against RNase R was tested. For this, RNA derived from circATG5 4-5 stably overexpressing cells was either treated or not treated with RNase R. Additionally, the expression of circATG5 4-5 was quantified by RT-qPCR. The data showed that the generated RNA is resistant to RNase R, since the treated RNA showed a resistance against RNase R. This observation is an indication of the presence of a circular transcript.

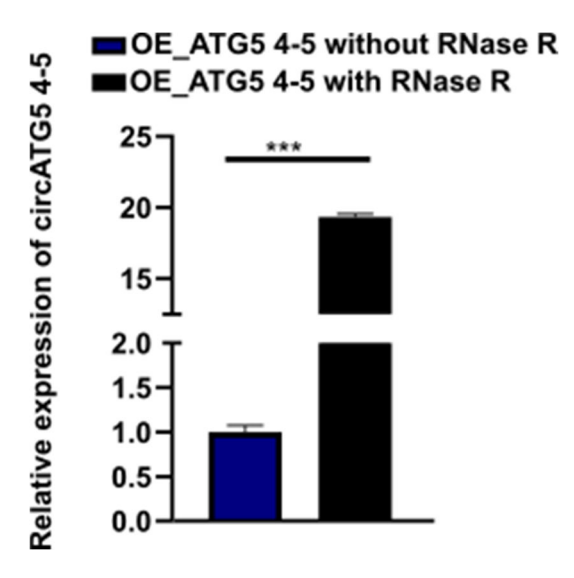


Figure 19: The generated circATG5 4-5 is resistant RNase R

RNA from stable cells that overexpress circATG5 4-5 was treated or not treated with RNase R. cDNA was synthetized and followed by RT-qPCR. According to RT-qPCR data, any negative influence of RNase R was seen in treated RNAs with RNase R. An enrichment of cirATG5 4-5 has been observed in those samples, indicating the presence of a circular transcript. The RT-qPCR data were calculated using the $2^{-\Delta\Delta CT}$ method and normalized to the levels of non-treated control. Black bar indicates the treated samples and blue the non-treated sample. Values shown represent mean \pm SEM of three replicates. ***p<0.001 (Student's t-test).

Stable cells expressing circATG5 4-5 were established by selecting transfected cells (HEK293) with geneticin (G418): The pcDNA3.1 (+) circRNA Mini vector contains Neomycin resistance gene.

Concerning 697 and HAL-01, they were transduced with the recombinant lentivirus bearing circATG5 4-5. Cells were sorted according to their GFP positive signal. RNAs from the GFP positive population were extracted, followed by the assessment of the overexpression by RT-qPCR. Data shown confirm a significant overexpression of circATG5 4-5 in 697 and HAL-01 (**Figure 20**).

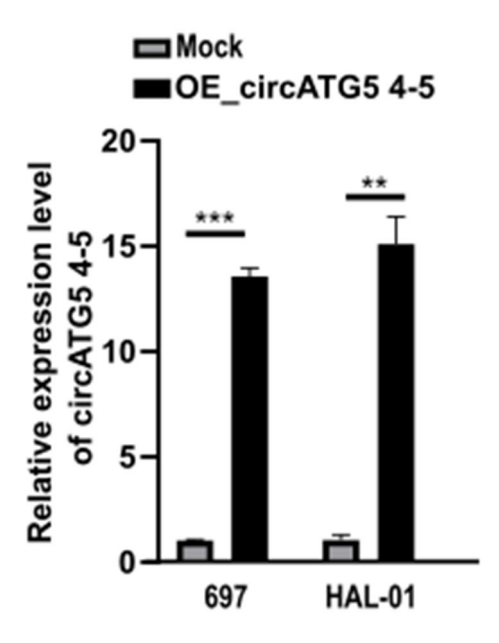


Figure 20: Overexpression of circATG5 4-5 using lentiviral vector

Real-Time PCR following the overexpression of circATG5 4-5 in both 697 and HAL-01. Divergent primers were used to detect the splice junction, thus the circular transcript. Values shown represent mean \pm SEM of three replicates. **p<0.01; ***p<0.001 (Student's t-test). This RT-qPCR was done before cells have been sorted.

5.7 circATG5 4-5 may correlate with ATG5

CircRNAs and their linear counterparts are expressed from the same host gene. It is known that circRNAs are also involved in the regulation of their parental genes. CircATG5 4-5 is derived from the *ATG5*. *ATG5* is involved in many cellular processes. In autophagy, it is necessary for the elongation of phagophores and autophagosome maturation ¹²³. To analyze the correlation between circATG5 4-5 and its linear counterpart *ATG5*, RT-qPCR and RNAseq from eight B-ALL cell lines has been performed.

Data generated showed that circATG5 4-5 and ATG5 move in the same direction. This positive correlation was observed in eight leukemia cell lines and was statistically not significant.

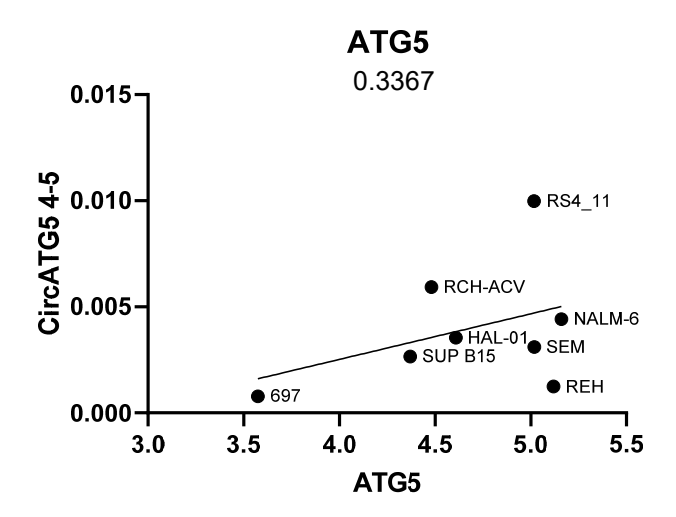


Figure 21: circATG5 4-5 and ATG5 mRNA tend to move in tandem cirATG5 4-5 data derived from RT-qPCR from eight B-ALL cell lines and *ATG5* data derived from RNAseq from the same RNA samples. This figure shows a positive correlation between circATG5 4-5 and *ATG5* mRNA, but not statistically significant. The X-axis label is in counts per million (CPM) and the Y-axis in log2 RT-qPCR fold change.

5.8 Overexpression of circATG5 4-5 increases ATG5 levels

Further experiments were conducted to check whether and how the circATG5 4-5 could influence the expression of ATG5. First, the overexpression of circATG5 4-5 was assessed in cells (HEK293, 697 and HAL-01) overexpressing circATG5 4-5. Cells expressing empty vectors were used as control. The expression of both circATG5 4-5 and *ATG5* was measured by RT-qPCR. In HEK293, the protein expression was also detected by Western blot.

In fact, a significant increase in ATG5 mRNA was observed in the three cell lines with circATG5 4-5 overexpression (**Figure 26 A, D-E**). In HEK293, also an increase in ATG5 protein expression was observed after circATG5 4-5 overexpression (**Figure 26 B and C**).

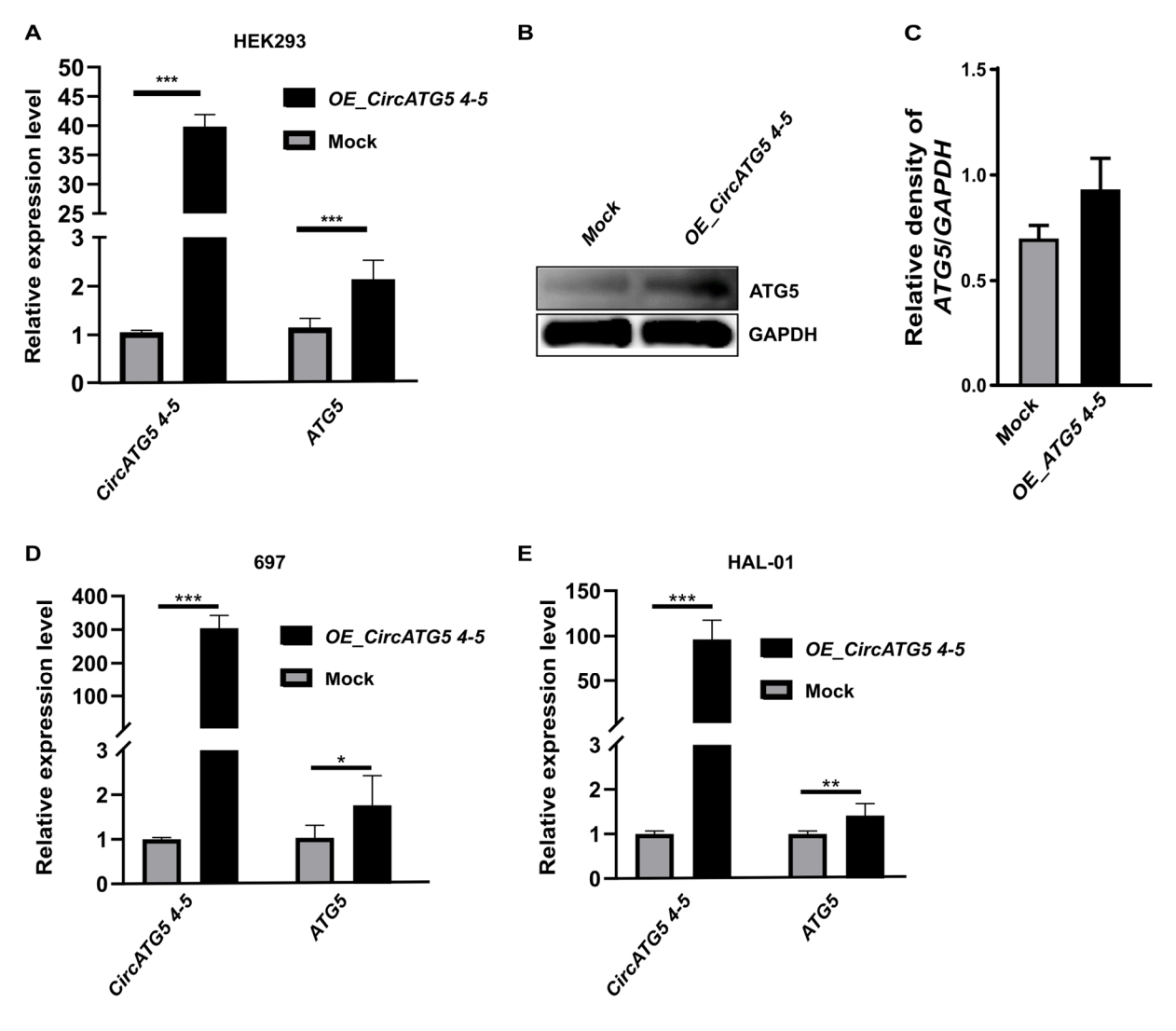


Figure 22: The overexpression of circATG5 4-5 positively influences ATG5 HEK293(A) cells were transfected with empty or with circATG5 4-5 and cultured in DMEM. RNA was isolated and subjected to RT-qPCR in order to quantify circATG5 4-5 and ATG5 expression. (B) and (C) HEK293 cells transfected with empty or circATG5 4-5 were cultured in DMEM. Protein lysate was applied for the detection of ATG5 by western blot. Densities of protein bands on immunoblots were quantified and normalized to GAPDH. 697(D) and HAL-01 (E) cells were transfected with empty or with circATG5 4-5 and in RPMI. RNA was isolated and subjected to RT-qPCR for quantification of circATG5 4-5 and ATG5 expression. The RT-qPCR data were calculated using the $2^{-\Delta\Delta CT}$ method and normalized by GAPDH. Values shown represent mean \pm SEM of at least three replicates. *p<0.05; **p<0.01; ***p<0.001 (Student's t-test).

Figure 22: The overexpression of circATG5 4-5 positively influences ATG5

5.9 Knockdown of circATG5 4-5 reduces ATG5 levels

In addition to circATG5 4-5 overexpression, it was also interesting to assess the effect of circATG5 4-5 on *ATG5* when downregulated. In HEK293, both a transient and a stable knockdown were tested, and in 697 as well as in HAL-01, only the transient knockdown was applied. To achieve the transient knockdown, cells were transfected with 30 pmol siRNA targeting the circular junction of circATG5 4-5. Cells were then harvested 48h after

transfection. For a stable system, CRISPR-Cas13 system against circATG5 4-5 was applied, which was driven by Tet-On inducible system. That means the knockdown was triggered in the presence of Doxycycline. Cas13 is an enzyme which acts on RNA level, but not on DNA level. The knockdown was induced by incubation of cells with 1.5 μ g/mL doxycycline for 5 days.

The RT-qPCR data revealed a significant decrease in the expression of *ATG5* in HEK293 when the expression of circATG5 4-5 is downregulated (**Figure 23A**). In the stable model, the same effect was seen, but not significant for the *ATG5* gene (**Figure 23B**). Indeed, the effect of circATG5 4-5 knockdown has not properly worked in 697 and HAL-01. Nevertheless, a downward trend of *ATG5* was observed (Figure 23C-D).

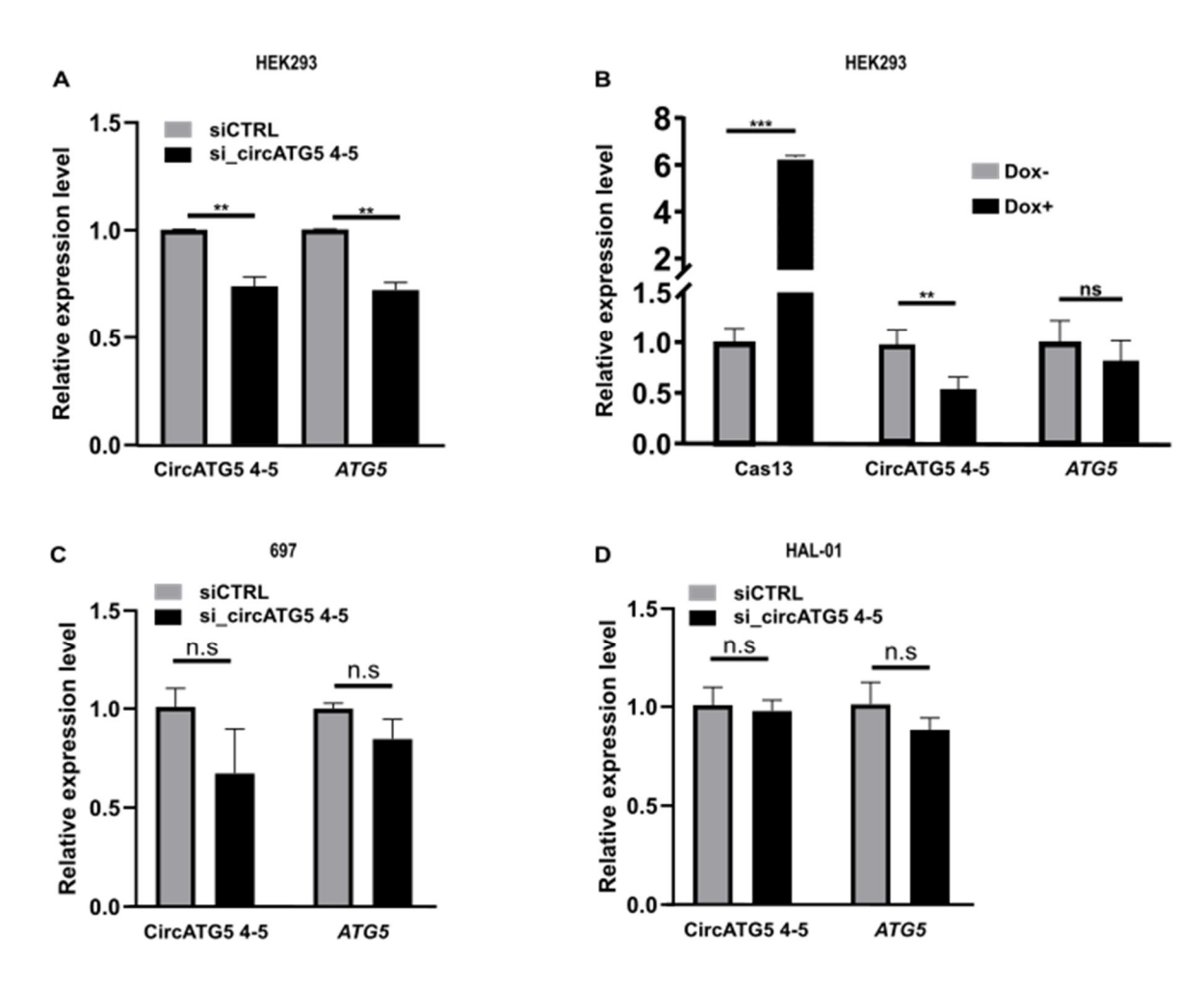


Figure 23: The circATG5 4-5 knockdown is associated with a downregulation of *ATG5* HEK293 (**A**) cells transfected with 30 pmol siRNA targeting circATG5 4-5 were incubated 48 h in appropriated growth medium. RNA was isolated, followed by RT-qPCR to measure circATG5 4-5 and *ATG5*. (**B**) HEK293 cells were stably transfected with CRISPR-Cas13 mediated knockdown of circATG5 4-5 and guide RNA and cultured in DMEM. To induce knockdown, cells were incubated with $1.5\mu g/ml$ Doxycycline for 5 days. RNA was then isolated, and RT-qPCR was run to measure circATG5 4-5 and *ATG5*. 697 (**C**) and HAL-01 (**D**) were carried out like described in (**A**). The RT-qPCR data were calculated using the $2^{-\Delta\Delta CT}$ method and normalized by *GAPDH*. Values shown represent mean ±SEM of at least three replicates. **p<0.01; ***p<0.001; ns: not significant (Student's t-test).

5.10 CircATG5 4-5 regulates the stability of ATG5 mRNA

It was hypothesized in this study that circATG5 4-5 could modulate ATG5 mRNA stability. To validate this hypothesis, the mRNA level of ATG5 was tested in HEK293 with overexpression or knockdown of circATG5 4-5. Cells were treated with actinomycin D in order to block the *de novo* transcription and quantified by RT-qPCR. RT-qPCR revealed that circATG5 4-5 overexpression enhanced the stability of ATG5, while circATG5 4-5 depletion in the cells increased the degradation of ATG5, as illustrated in **Figure 24**. The data would suggest that circularATG5 4-5 may have a protective effect on ATG5 mRNA when overexpressed.

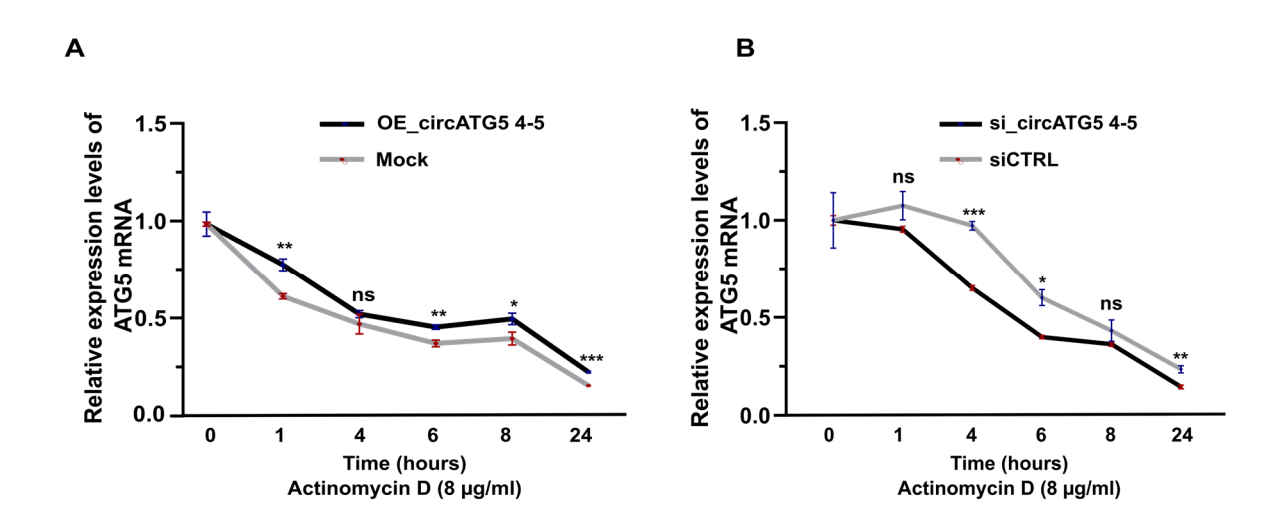


Figure 24: CircATG5 4-5 influences the stability of ATG5

(A) HEK293 overexpressing circATG5 4-5 were treated with 8 μ g/ml Actinomycin D and incubated for 24 h. Cells were harvested at different time points, followed by RT-qPCR for quantification of ATG5 mRNA (B) The time 0 is the time before adding the compound. (B) HEK293 cells were transfected with 30 pmol siRNA against circATG5 4-5 or scrambled siRNAs (siCTRL) as non-targeted control. 48 h after transfection, cells were incubated with 8 μ g/ml Actinomycin D for an additional 24 h. Cells were then harvested before addition of the compound (time zero) and at different time points after compound addition (1h, 2h, 4h, 6h, 8h and 24h). RNA was isolated, followed by the quantification of ATG5 mRNA using RT-qPCR.

The RT-qPCR data were calculated using the $2^{-\Delta\Delta CT}$ method and normalized by *GAPDH*. Values shown represent mean \pm SEM of at least three replicates. *p<0.05; **p<0.01; ***p<0.001 (Student's t-test), ns: non-significant.

5.11 Transcriptomic changes following circATG5 4-5 overexpression

In order to better understand the biological functions of circATG5 4-5, RNA sequencing (RNA-Seq) was performed following overexpression of circATG5 4-5 in HEK293, HAL-01 and 697 cells.

The criteria applied as cut-off for the selection of differentially expressed genes induced by circATG5 4-5 overexpression was a minimal fold change (OE_circATG5 4-5/mock) of ± 2 and a significance level of p ≤ 0.05 . **Table 28** gives an overview of significantly differentially expressed genes in the different cell lines used.

Table 28: Overview of significantly dysregulated genes upon circATG5 4-5 overexpression

Cell types or	Number of differentially	Number of	Number of
culture conditions	expressed genes	downregulated upregulated	
		genes	genes
HEK293 (DMEM)	317	141	176
HEK293 (EBSS)	329	192	137
697	51	21	29
HAL-01	85	39	46

These data confirm that the overexpression of circATG5 significantly increases the expression of *ATG5*, as demonstrated in **Figure 25 A –D (pointed by blue arrows)**. This observation was proven for all cell lines used as well as for different culture conditions of HEK293 (**Figure 25 A-B**). HEK293 cells were cultured in both DMEM and EBSS to induce autophagy.

The data showed that gene regulation through circATG5 4-5 overexpression is cell line specific. According to RNA-Seq data, there was one overlapping gene between the four cell lines investigated, namely *ATG5* (**Figure 25 E**). Between HAL-01 and 697, three genes were found to overlap, while five genes were found to overlap between HAL-01 and HEK293 incubated in EBSS. Between HEK293 cultured in DMEM and HEK293 incubated in EBSS, there were 168 overlapping genes.

Interestingly, in both 697 and HAL-01, there was a significant downregulation of *TLR4* induced by circATG5 4-5 overexpression (**Figure 25 F**).

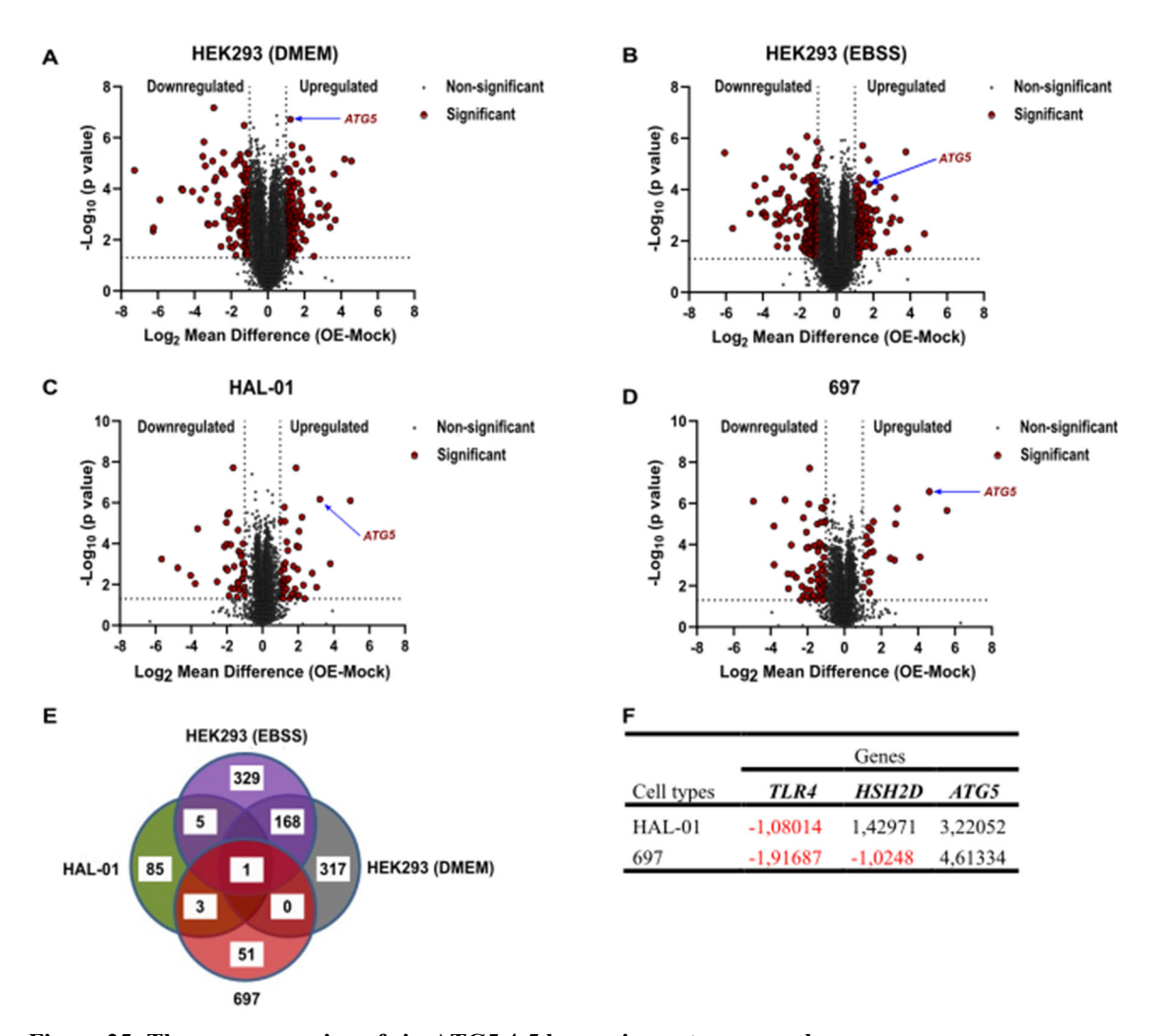


Figure 25: The overexpression of circATG5 4-5 has an impact on several genes

The volcano plots illustrate the distribution of statistical differentially expressed genes after the overexpression of circATG5 4-5, obtained through RNA-Seq. (A): HEK293 cells were cultured in DMEM, (B): HEK293 were incubated in EBSS overnight, (C): HAL-01 and (D): 697 were cultured in RPMI. The red dots indicate significantly differentially expressed genes and grey dots represent the non-significantly expressed genes. Genes with a fold change (OE_circATG5 4-5/mock) of ± 2 and a significance level of p ≤ 0.05 were considered significantly differentially expressed genes. The overexpression of circATG5 4-5 showed a positive influence on ATG5, which is pointed by the blue arrows. (E): Venn diagram showing the overlap of differentially regulated genes between the cells used. (F): Overlapping genes between HAL-01 and 697, whereby the downregulated genes are in red.

Unsupervised hierarchical clustering of the genes differentially following overexpression of circATG5 4-5 in all cell lines investigated was sufficient to subdivide the models into treatment groups (Figure 26).

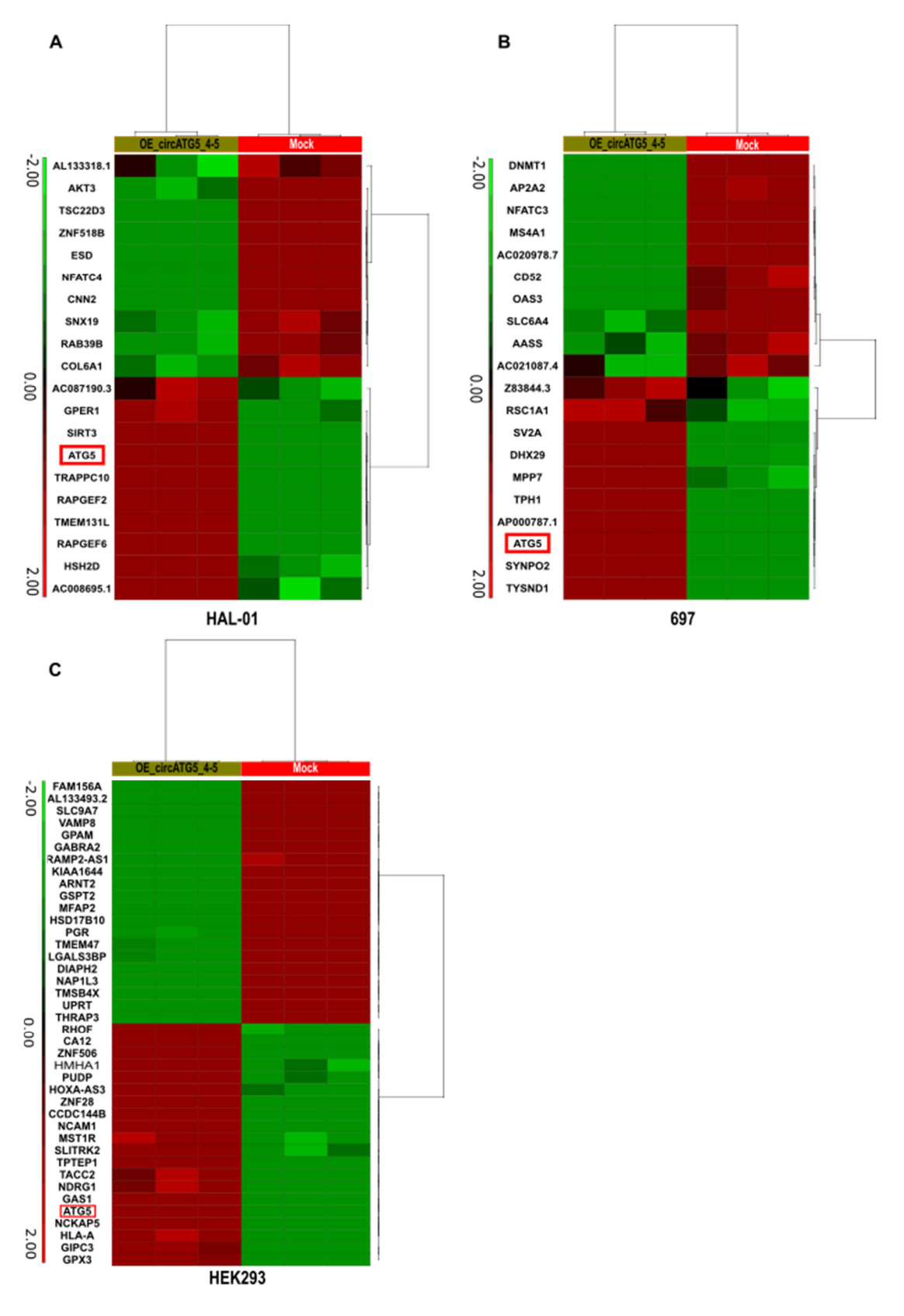


Figure 26: Top significantly dysregulated genes through circATG5 4-5 overexpression (RNA-Seq) The heatmap shows top significantly dysregulated genes following circATG5 4-5 overexpression where (A) represents HAL-01, (B) 697 and (C) HEK293. Each heatmap includes on the left three OE_circATG5 4-5 samples in triplicate and on the right three triplicates mock samples. Every band represents a single gene, and the color indicates the abundance of genes. Genes colored in red are highly expressed and in green lowly expressed.

5.12 Effect of circATG5 4-5 expression on autophagy flux

Since previous data generated in the scope of this work demonstrated that the expression of *ATG5* is affected by circATG5 4-5 and as ATG5 protein plays an important role in the autophagy pathway, particularly in the extension of the autophagosomes, it was therefore investigated, whether the alteration of circATG5 4-5 expression could have an impact on the autophagy pathway. To monitor that, Autophagy LC3 HiBiT Reporter Assay from Promega was used. The experiments were carried out in HEK293 cell lines. Both the effect of the overexpression and of knockdown of circATG5 4-5 have been investigated. If considering the bars of chloroquine-treated cells under starvation condition or not, current data revealed that the alteration of circATG5 4-5 expression significantly affects the autophagy flux, whereby the overexpression of circATG5 4-5 significantly increases the cellular autophagy activity. In contrast, the downregulation of circATG5 4-5 negatively influenced the autophagy activity. Chloroquine is a compound that prevents the degradation of autophagosomes by decreasing their fusion with lysosomes.

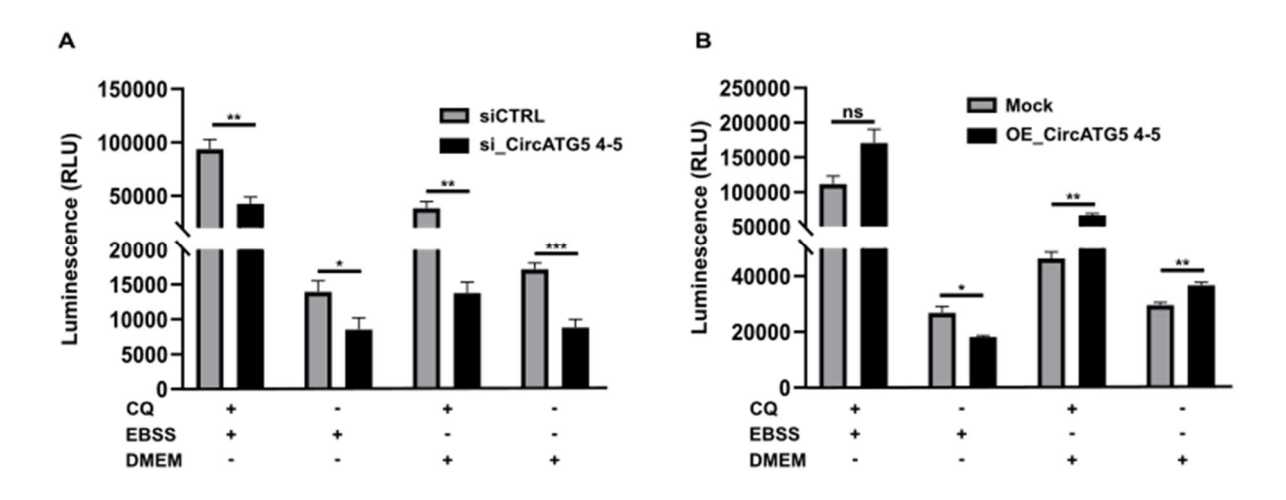


Figure 27: CircATG5 4-5 affects cellular autophagy activity

(A) HEK293 stably expressing the autophagy LC3 HiBiT Reporter vector were transfected with siRNA against circATG5 4-5 or with scrambled siRNA (siCTRL). 48h after transfection, cells were incubated in full medium (DMEM) or starvation medium (EBSS) in the presence or absence of 50 μ M chloroquine for 5 h. (B) HEK293 stably co-expressing the Autophagy LC3 HiBiT Reporter vector / circATG5 4-5 or Autophagy LC3 HiBiT Reporter vector / empty vector were incubated in full medium (DMEM) or starvation medium (EBSS) in the presence or absence of 50 μ M chloroquine for 5h. To monitor autophagy, cells were lysed with the HiBiT reagent from Promega, and the chemiluminescent signal was detected by TECAN. Values shown represent mean \pm SEM of three replicates. **p<0.05; **p<0.01; ***p<0.001 (Student's t-test).

5.13 MicroRNA prediction binding sites

In order to elucidate the mechanism by which *ATG5* is regulated by circATG5 4-5, potential circATG5 4-5-miRNA interactions were investigated.

Using the web tool CircInteractome (https://circinteractome.nia.nih.gov/) ¹³⁶, some predicted miRNAs which are supposed to interact with circATG5 4-5 have been identified. According to the web tool, ten miRNAs were supposed to interact with circATG5 4-5, as listed in **Figure 28 A**. All predicted miRNAs display each one binding site for circATG5 4-5. **Figure 28 B-C** illustrates the interaction between circATG5 4-5 and miR-1299 by displaying their binding site.

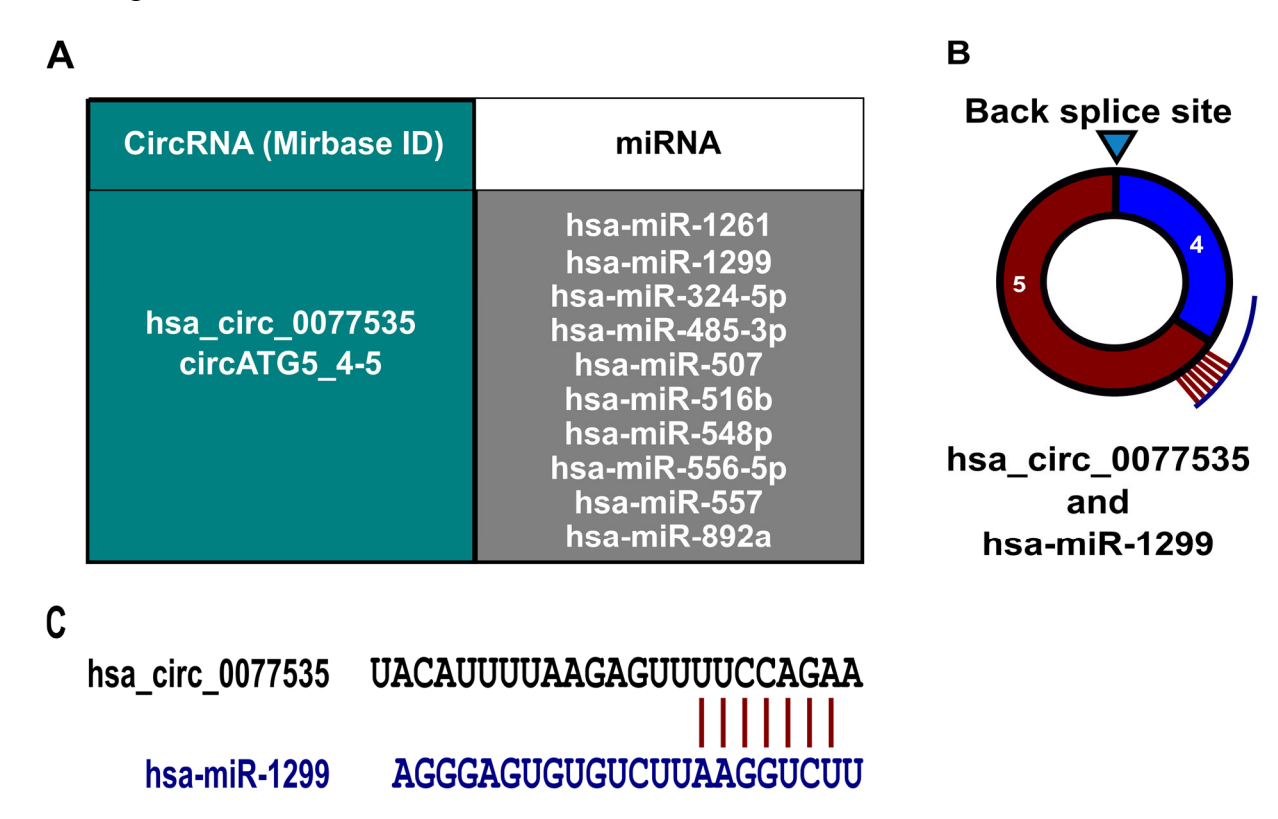


Figure 28: Potential circATG5 4-5-miRNA interactions

(A) Predicted miRNAs, which potentially target circATG5 4-5 (hsa_circ_0077535) taken from CircInteractome. **(B)** An example of circATG5 4-5- miRNA interaction using has-miR-1299. The biding site is in exon 5. **(C)** Illustration of circATG5 4-5-miRNA (has-miR-1299) interaction showing the binding sites.

5.14 Expression of predicted miRNA in HEK293, 697 and HAL-01 cell lines

Eight microRNAs from ten predicted were validated by RT-qPCR in HEK293, 697 and HAL-01. The RT-qPCR data showed that these miRNAs are highly expressed in 697 compared to HAL-01. Among analyzed cell lines, HEK293 showed the lowest levels of predicted microRNAs as it is shown in **Figure 29**.

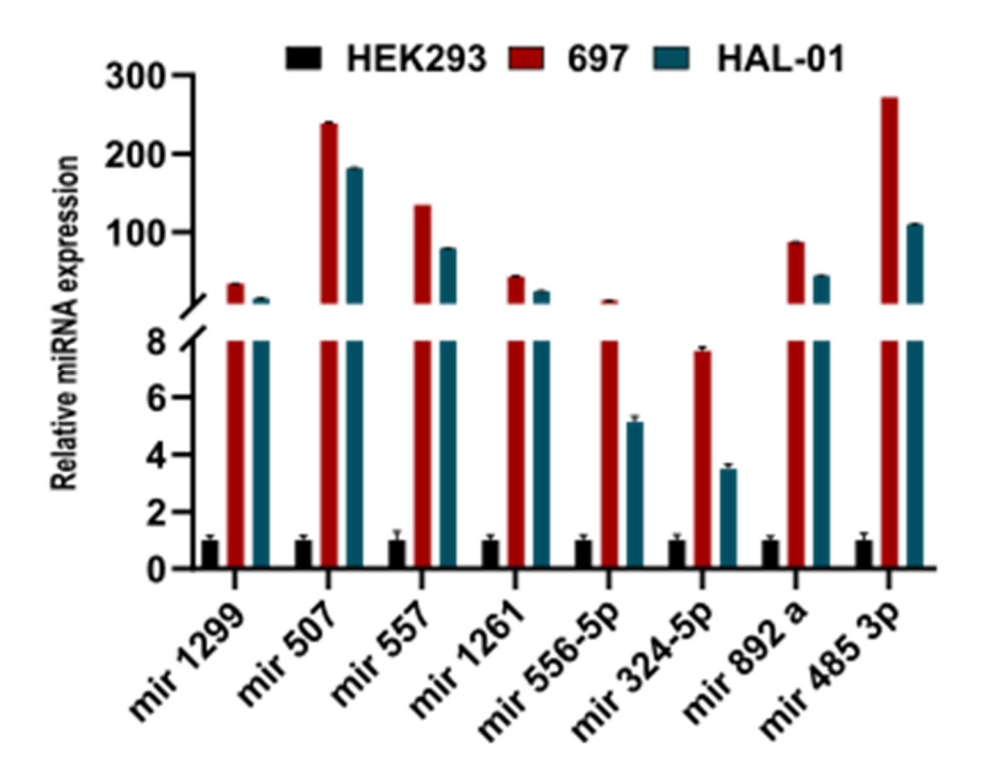


Figure 29: Expression of miRNAs in HEK293, 697 and HAL-01 cell lines

Total RNA was isolated from wild-type cell lines using Trizol, cDNA was synthetized followed by RT-qPCR.

RT-qPCR data were calculated using the 2^{-ΔΔCT}. method and normalized by RNU6-1.

5.15 Overexpression of circATG5 4-5 affects most predicted miRNAs

To assess the impact of circATG5 4-5 on the predicted microRNAs, RT-qPCR was performed in HAL-01, 697 and HEK293 following overexpression of circATG5 4-5. As indicated in **Figure 30A-H**, the expression of most predicted microRNAs decreases upon the overexpression of circATG5 4-5 in all cell lines analyzed.

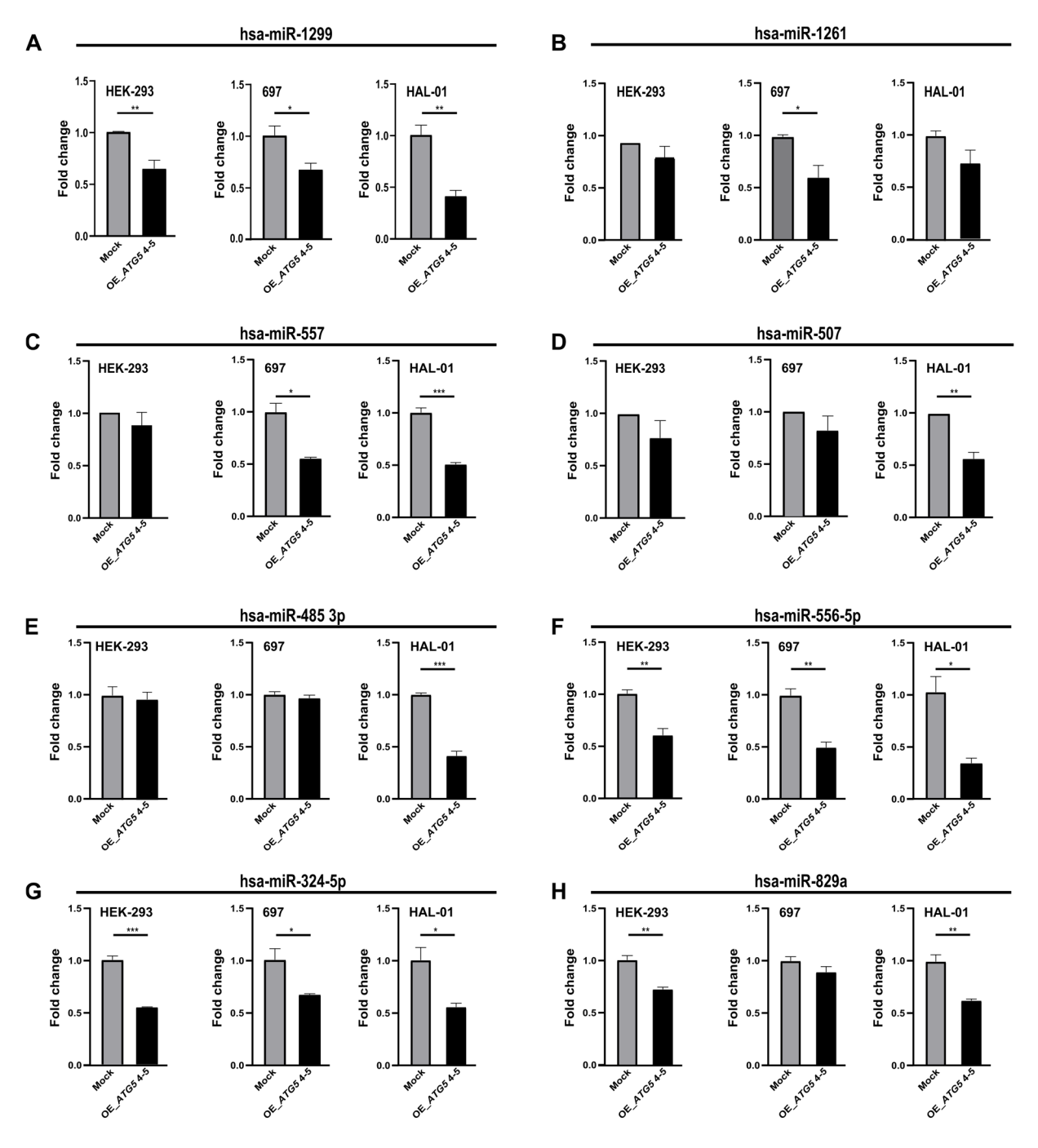


Figure 30: Impact of circATG5 4-5 on miRNA expression in HEK293, 697 and HAL-01 The effect of the overexpression of circATG5 4-5 on miRNAs. Each alphabet letter represents an expression of a given miRNA in cells overexpressing or not circATG5 4-5. RNA was isolated from transfected cells and miRNAs were quantified. RT-qPCR data were calculated using the $2^{-\Delta\Delta CT}$ method and normalized by RNU6-1. Values shown represent mean \pm SEM of three replicates. **p<0.05; **p<0.01; ***p<0.001 (Student's t-test).

5.16 circATG5 4-5 may regulate CDK6 upon affecting miRNA-1299 levels

It has been reported that miR-1299 plays an important role in the regulation of cell proliferation by targeting CDK6 ¹³⁸. Previous experiments in this study showed that the overexpression of circATG5 4-5 significantly reduces the expression levels of miR-1299 in

HEK293, 697 and in HAL-01. RNA from HEK293, 697 and HAL-01 overexpressing circATG5 4-5 or empty vector was extracted using Trizol, followed by the quantification of miR-199 as well as its target CDK6 by RT-qPCR. RT-qPCR data revealed a significant increase of CDK6 mRNA levels upon overexpression of circATG5 4-5 in both HEK293 and 697, and a significant decrease in miR-1299 levels in all cell lines investigated.

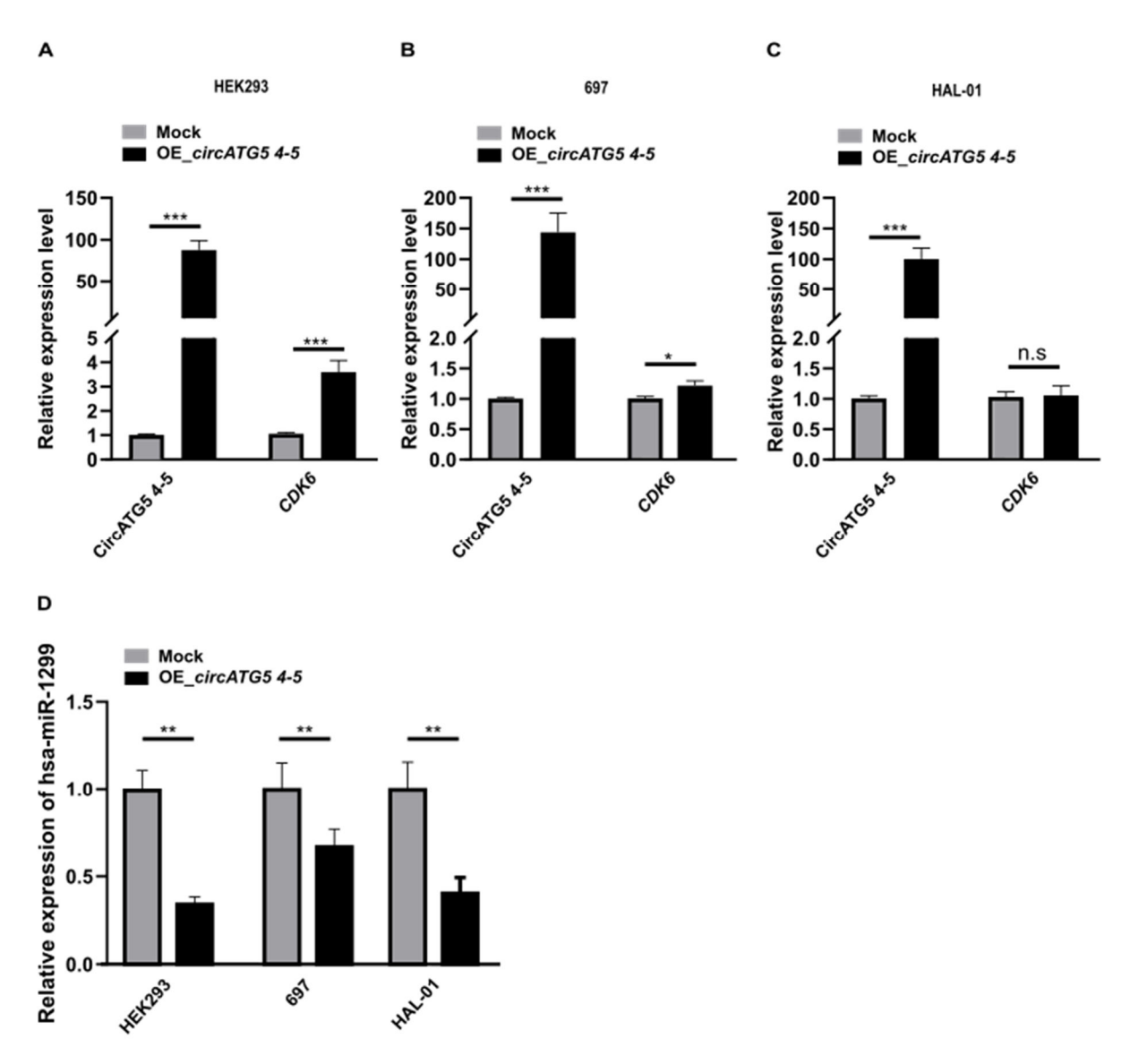


Figure 31: Overexpression of circATG5 4-5 is associated with increased CDK6 mRNA levels HEK293 (A), 697 (B) and HAL-01 (C) cell lines overexpressing circATG5 4-5 or empty vector were cultured in their appropriate growth media. Subsequently RNA was extracted, and RT-qPCR was performed to measure CDK6 mRNA levels (A, B and C) as well as the levels of microRNA hsa-miR-1299 (D). RT-qPCR data were calculated using the $2^{-\Delta\Delta CT}$ method and normalized by GAPDH for CDK6 and by RNU6-1 for miR-1299. *p<0.05; ***p<0.01, ***p<0.001 (Student's t-test), ns: non-significant.

5.17 circATG5 4-5 and ATG5 positively correlate with CDK6

The correlation analysis was additionally performed in non-treated cell lines in order to have a global view of how circATG5 4-5 and ATG5 mRNA can correlate with CDK6 in other cell lines than those used. For that assessment, RNA-seq as well as RT-qPCR data from eight B-ALL cell lines were used. The analysis showed that between circATG5 4-5 and CDK6, the correlation is tendentially positive but not significant and between ATG5 mRNA and CDK6, the correlation is positive and statistically significant (**Figure 32 A and B**).

Furthermore, it was also checked whether ATG5 mRNA and CDK6 also positively correlate in patient samples. The test could confirm that the correlation between ATG5 mRNA and CDK6 is positive and statistically significant **Figure 32 (C)**.

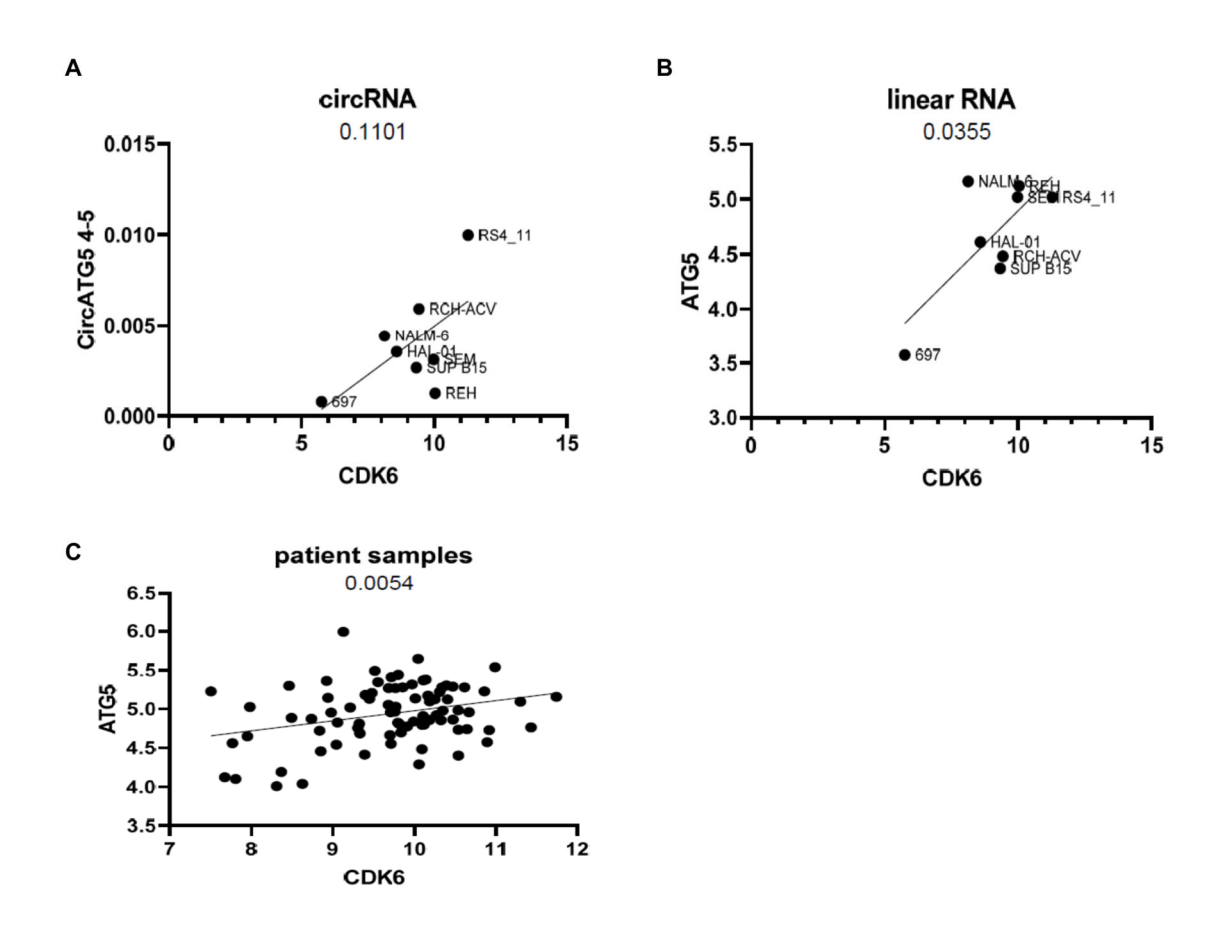


Figure 32: Correlation of circATG5 4-5 and ATG5 mRNA with CDK6(A) RT-qPCR was performed from eight B-ALL wild-type cell lines. Data was applied for correlation analysis. Between circATG5 4-5 and CDK6, the correlation is positive but not statistically significant.

(B) RNA-Seq was performed from the same RNA samples like in (A) and followed by the correlation analysis between ATG5 and CDK6, which was positive and statistically significant. (C) positive correlation between ATG5 and CDK6 from unselected cohort of diagnostic untreated B-ALL samples (inhouse generated unpublished data). Both axis labels in figures (A) and (C) are expressed in counts per million (CPM) and (B) in log2 RT-qPCR fold change

5.18 CircATG5 4-5 overexpression increases cell viability and proliferation

MiR-1299 has been largely investigated, particularly in cancers. It has tumor suppressor properties by regulating genes, which are involved in cell proliferation, migration, survival, and programed cell death ^{139,140}. I saw in the data that there are decreased miR-1299 levels in cells overexpressing circATG5 4-5, in comparison to mock control. This was a reason for checking if the dysregulation of circATG5 4-5 can affect cell viability and cellular proliferation. To prove this hypothesis, cells overexpressing circATG5 4-5 were incubated for 72h, then the cell viability was measured by using CellTiter-Glo. The assay showed that the overexpression of circATG5 4-5 significantly increased the cell viability compared to the mock control (empty control). This analysis is based on the detection of cellular ATP content. The transient overexpression of circATG5 4-5 was checked by RT-qPCR (Figure 33 A).

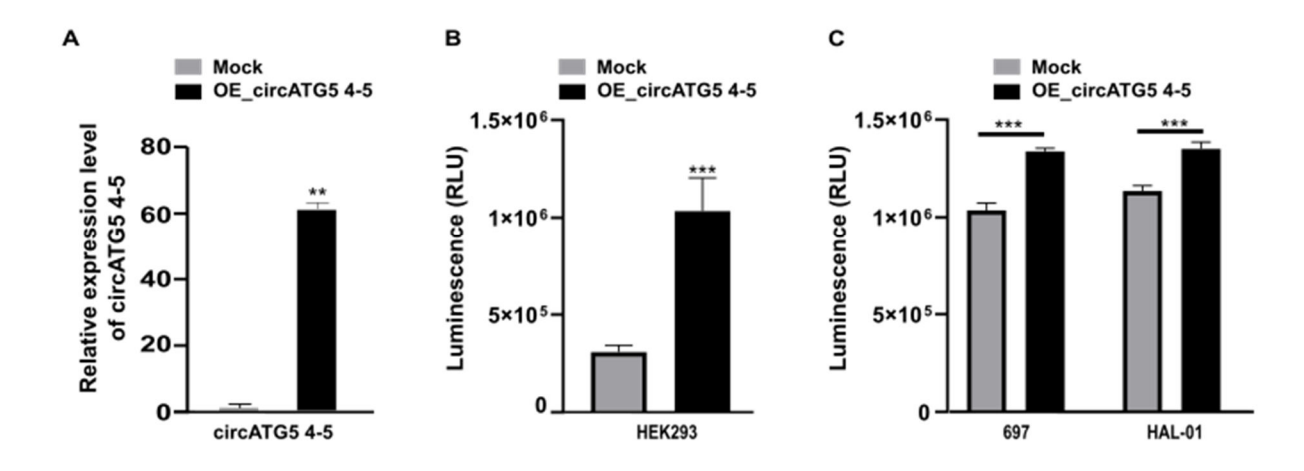


Figure 33: The overexpression of circATG5 4-5 promotes cell viability (A) The bar diagram represents 72 h post-transfection of circATG5 4-5 overexpression in HEK293. At 72 h post-transfection, ATP levels was measured using CellTiter-Glo. (C) Cells stably overexpressing circATG5 4-5 were seeded into 96 well plates and ATP content was measured 72h after seeding cells using CellTiter-Glo. Values shown represent mean ±SEM of three replicates. **p<0.01; ***p<0.001 (Student's t-test).

Furthermore, the impact of the overexpression of circATG5 4-5 on cell proliferation was also assessed. Since our ALL models, which stably overexpress circATG5 4-5 are GFP positive, the Carboxyfluorescein succinimidyl ester (CFSE) was not appropriate for these cells. CFSE has an identical excitation/emission spectrum to FITC as well as to GFP and the same channel is used for all three fluorescent dyes. Here, HEK293 cells that overexpress circATG5 4-5 were labeled with Carboxyfluorescein succinimidyl ester (CFSE). For knockdown, cells were first labeled with CFSE followed by the transient transfection of

HEK293 with siRNA against circATG5 4-5. Cells were measured by a flow cytometer device at different time points of CFSE treatment. Notably, the overexpression of circATG5 4-5 showed a significant increase in cell proliferation, while the knockdown showed a decrease in cell proliferation (**Figure 34 A-B**). As this dye is equally distributed into daughter cells, proliferating cells lose the intensity of the dye, which is indicated by the reduction in the bars; accordingly, short bars indicate high cell proliferation and high bars a low cell proliferation.

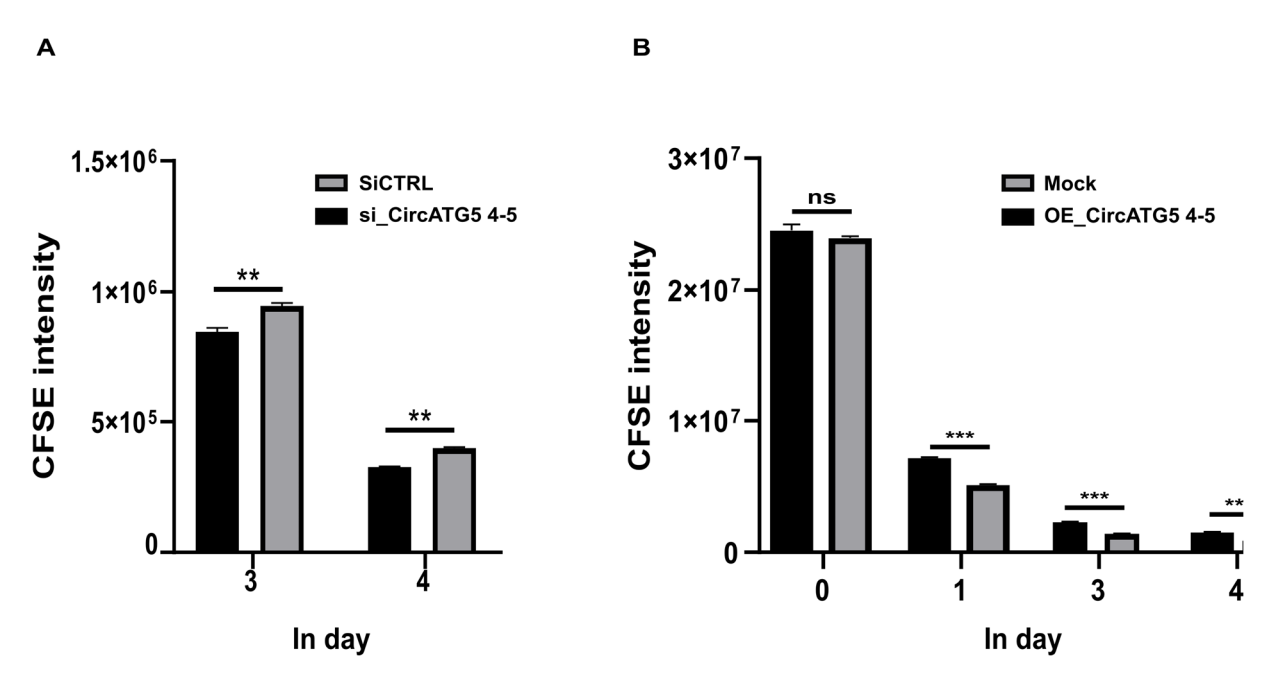


Figure 34: CircATG5 4-5 regulates cell proliferation

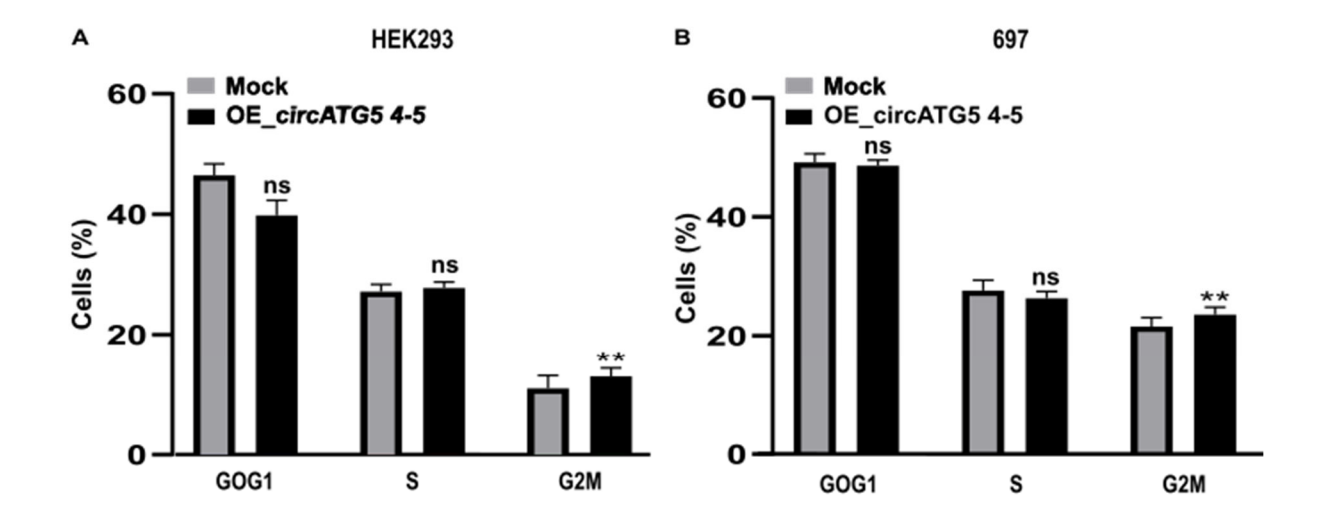
Cell proliferation is indicated by the loss of fluorescent intensity. The smaller the bar is, the faster cells grow. (A) Transient knockdown of circATG5 4-5 following CFSE labeling. Day 3 represents three days after staining cells, but two days after transfection and day 4 means four days after staining cells and 3 days after transfection. (B) Overexpression of circATG5 4-5 significantly promotes cell proliferation. Cells were labeled with CFSE and analyzed by flow cytometry. Day 0 indicates the day on which cells were stained, day 1 indicates the day after the staining, day 3, three days after staining and day 4 four days after the staining.

Hereby cells that stably express circATG5 4-5 were used. Values shown represent mean ±SEM of three

Hereby, cells that stably express circATG5 4-5 were used. Values shown represent mean \pm SEM of three replicates. **p<0.01; ***p<0.001 (Student's t-test).

5.19 Overexpression of circATG5 4-5 increases G2M cell fraction

To assess the effect of circATG5 4-5 overexpression on cell cycle state, HEK293, 697 and HAL-01 that overexpress circATG5 4-5, were used. Cells were fixed with alcohol, treated with RNase A, and stained with PI. Flow cytometer was used to measure distinct phases of the cell cycle. This assay showed a significant increase in the G2M fraction of cells following circATG5 4-5 overexpression in comparison with the mock control for all cell lines investigated, as illustrated in **Figure 35**.



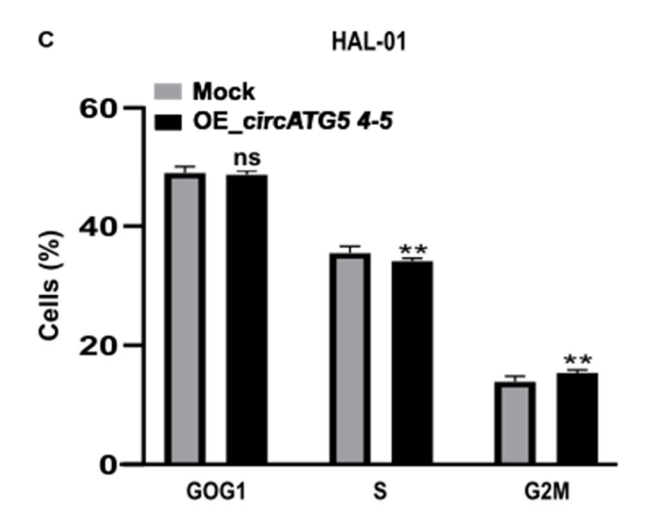


Figure 35: Overexpression of circATG5 4-5 leads to G2M Cell cycle profile of stable circATG5 4-5 overexpression in HEK293, 697 and in HAL-01 cell line. Cells were fixed with ethanol and stained with $50\mu g/ml$ propidium iodine (PI). Cells were analyzed by flow cytometer. Values shown represent mean $\pm SEM$ of three replicates. **p<0.01; Ns: not significant (Student's t-test).

6 Discussion

Growing evidence indicates that circRNAs act on biological processes through mechanisms, such as modulation of transcription or splicing, or acting as miRNA sponges or protein scaffolds. Several studies have shown that the dysregulation of circRNAs is implicated in a wide variety of diseases, including cancer ¹⁴¹. The emergence of their biological functions is changing our understanding of cell physiology and disease pathogenesis. However, despite the discovery of thousands of circRNAs so far, the specific function of most of them is still unknown.

In the current study, circRNAs were detected through analyzing RNA-seq data generated by whole transcriptomic and specific circular RNA sequencing of the B-ALL cell lines 697 and HAL-01. Given the fact that autophagy is an important process involved in maintaining cell viability ^{142,143}, but also impacts on the development of cancer, we screened the data for circRNA candidates derived from autophagy-related genes. We identified novel circRNAs encoded by the *ATG5* gene. Amongst them, hsa_circ_0077535 (circATG5 4-5) was the most abundantly expressed circRNA. CircATG5 4-5 expression was validated and profiled across B-ALL cell lines (n=8) using RT-qPCR. The data revealed that the expression of circATG5 4-5 varies between the different cell lines, whereby 697 cells showed the lowest and RS4_11 the highest expression of circATG5 4-5. Thus far, this is the first study about hsa_circ_0077535 (circATG5 4-5). In this work, two B-ALL cell lines were selected in addition to HEK293 as cell models for circATG5 4-5 overexpression, notably 697 (*TCF3-PBX1*-positive and drug sensitive) and HAL-01 (*TCF3-HLF*-positive and drug resistant). Since the knockdown efficiency of circATG5 4-5 was only moderate, further analyses were conducted in cells with transient downregulation expression of circATG5 4-5.

There is growing evidence that circRNAs do not only regulate the expression of other genes, but also of their parental genes. For example circ-PTEN, circ-AKT1 and circ-MAPK4 have been shown to regulate the expression of their parental genes, e.g. via inhibition of miRNAs ^{144–146}. We demonstrated in this study that circATG5 4-5 regulates the expression of its parental gene *ATG5*. To analyze this further, we first overexpressed circATG5 4-5 in HEK293 and in the B-ALL cell lines (HAL-01 and 697), subsequently the expression of circATG5 4-5 and *ATG5* was measured using RT-qPCR. Interestingly, we found that the parental *ATG5* mRNA was consistently upregulated in all circATG5 4-5 overexpressing cell lines. In line, the transient knockdown of circATG5 4-5 led to a significantly decreased

ATG5 expression in HEK293 cells as measured by RT-qPCR, but in suspension cells (697 and HAL-01), we could not observe any changes because the knockdown did not work properly. We first thought that this might be due to the fact that it is not easy to transfect suspension cells using a liposome-based transfection reagent. Then, looking for a solution to this issue, we applied the electroporation-based transfection method, unfortunately this did not improve the quality of transfection. On the contrary, many cells did not survive the electric shock.

Another interesting aspect was that a correlation of circATG5 4-5 with the expression of *ATG5* derived from RNAseq data showed a positive trend (not yet significant), indicating that circATG5 4-5 may play a role in regulating the expression of their parenteral gene.

Further evidence that circATG5 4-5 may regulate the expression of ATG5 is that we could show that circATG5 4-5 influences the stability of ATG5 mRNA. Here, the mRNA stability assay was performed to proof this hypothesis. HEK293 cells with overexpression or downregulation of circATG5 4-5 were used here, where cells were previously treated with the drug actinomycin D, which blocks de novo transcription. That assay revealed that the overexpression of circATG5 4-5 significantly enhanced the mRNA stability of the ATG5 compared to a mock control, whereas the knockdown of circATG5 4-5 significantly decreased ATG5 mRNA levels compared to a scrambled siRNA control. This indicates that the overexpression of circATG5 4-5 should protect ATG5 mRNA against a fast degradation, while the downregulation of circATG5 4-5 has an opposite effect on ATG5 mRNA. Recent studies also reported that circRNAs can affect mRNA stability to regulate their host gene expression. For instance, circ-CCND1 may stabilize CCND1 mRNA by interacting with the RNA binding protein HuR ¹⁴⁷. The transcript mRNA is an important molecule, serving as template for protein synthesis. Once synthetized, proteins exert a variety of functions. The transcript mRNA is essential for maintaining cellular homeostasis as being involved in the regulation of genes expression. Overall, the expression of mRNA can be modified in order to control the expression levels of specific proteins.

To regulate parental gene expression, circRNAs can occur in several ways. Some circRNAs interact in the nucleus with the transcriptional complex to regulate their parental gene expression ⁸⁸, other circRNAs interact in the cytoplasm with miRNAs ¹⁴⁵. Thus, to narrow down potential molecular functions of circATG5 4-5, RNA-FISH was carried out in HEK293 cells, which then showed a predominance of circATG5 4-5 expression in the

cytoplasm. This is in line with the fact that circATG5 4-5 is an exonic circRNA (EcircRNA) and the majority of exonic circRNAs are known to be localized in the cytoplasm ⁶⁹, while intronic circRNAs (IcircRNA) and exonic-intronic EIciRNAs are enriched in the nucleus ⁸⁸. CircATG5 4-5 could also be observed in the nucleus, which is likely due to its initial generation in the nucleus and subsequent export to the cytoplasm ^{148,149}.

Indeed, circRNAs enriched in the cytoplasm usually exert their function as miRNA sponges or interact with proteins. CircRNAs acting as miRNA sponges include e.g. CDR1as/ciRS-7, displaying more than 60 binding sites for miR-7 ¹⁵⁰, SRY sponging miR-138 and circHIPK3 targeting miR-124 ^{82,84}. CDR1as can also interact with the RNA binding protein *IGF2BP3* (insulin-like growth factor-2 mRNA-binding protein 3) to block metastasis ¹⁵¹. Circ-Foxo3 can bind to CDK2 (Cyclin-dependent kinase 2) and P21 to decrease cell cycle progression¹⁵². Moreover, being localized in cytoplasm, it would be very likely that circATG5 4-5 regulates its parental gene using one of the known molecular mechanisms by which cytoplasm-localized circRNAs regulate the expression of their parental genes, such as miRNA sponges. In this thesis, we have not found any potential miRNAs in RNAseq data conducted in our cell models, which can interact with circATG5 4-5 and *ATG5*. Further studies may be needed to uncover the molecular mechanism by which *ATG5* is regulated by circATG5 4-5.

Using the web tool circInteractome, we could identify miRNAs predicted to interact with circATG5 4-5. Ten miRNAs have been predicted to bind circATG5 4-5, each with only one potential binding site for circATG5 4-5. We validated the expression of eight of those by RT-qPCR in HEK293 cells and the B-ALL cell lines (697 and HAL-01). Interestingly, miR-1299, miR-557, miR-556-5p and miR-324-5p were significantly downregulated in circATG5 4-5 overexpressing B-ALL cell lines.

MiR-1299 and miR-557 are known to have a tumor suppressing properties ^{139,153}. MiR-1299 negatively influences proliferation, invasion and metastasis when upregulated ¹³⁹ by regulating the expression of genes, such as *CDK6* ¹³⁸, *STAT3* ¹⁵⁴ and *EGFR* ¹⁴⁰. Overexpression of miR-557 induces apoptosis and inhibits the cell migration, for instance, by down-regulating *LEF1* (Lymphoid Enhancer Binding Factor 1) in lung cancer cells ¹⁵³. In osteosarcoma cells, the up-modulation of miR-557 has a negative effect on the proliferation ¹⁵⁵. However, the role of miR-556-5p and miR-324-5p seem to depend on the type of cancer. In colorectal cancer and in breast cancer, miR-556-5p has a tumor suppressive effect since its downregulation enables the progression of cancer cells by promoting metastasis, cell invasion and migration ^{156,157}. MiR-556-5p has also been reported to promote

cell proliferation when upregulated, e.g. via downregulating *PPP2R2A* (Protein Phosphatase 2 Regulatory Subunit Balpha) in prostate cancer ¹⁵⁸. MiR-324-5p negatively impacts on cell invasion and metastasis in the hepatocellular cancer (HCC) when overexpressed, while in gastric cancer the downregulation of its expression suppresses cell proliferation, migration and invasion ¹⁵⁹ ¹⁶⁰.

The tumor suppressive properties of the miRNAs binding to circATG5 4-5 indicate a prosurvival, proliferative and potentially oncogenic function of circATG5 4-5. In line with this, B-ALL cell lines overexpressing circATG5 4-5 showed decreased miR-1299 expression and elevated levels of *CDK6*, a target of miR-1299 ¹³⁸. The expression of *CDK6* has recently been reported to be regulated by different circRNAs through hindering miR-1299. In osteosarcoma, circ_ARF3 supported pathogenesis through suppressing miR-1299 expression to maintain CDK6 expression ¹⁶¹. Liu and colleagues showed that overexpression of hsa_circ_0136666 promoted cell proliferation and increased G₂/M cell cycle arrest in breast cancer cells by positively regulating CDK6 via inhibition of miR-1299 ¹⁶². These findings corroborate the experimental data gained in this work showing that circATG5 4-5 overexpression in B-ALL enhances proliferation and cell viability and increases the fraction of cells blocked in the G₂/M cell cycle phase compared to mock controls. Interestingly, when analyzing expression data of a cohort of 200 unselected diagnostic B-ALL cases, we found a positive correlation (p= 0.0054) between *ATG5* and *CDK6* and a similar trend in the analyzed B-ALL cell lines (n=8, p= 0.0355).

In the current study, we demonstrated that *ATG5* is regulated by circATG5 4-5. *ATG5* is a well-characterized mediator of autophagy via the recruitment of ATG8 and essential for autophagosome formation and elongation ¹⁶³. *ATG5* is e.g. required for T-cell survival and proliferation ¹²⁷. In B-ALL, the inhibition of autophagy has a negative influence on cell proliferation and survival ¹¹⁸. To test if circATG5 4-5 also regulates autophagy, cells with altered circATG5 4- 5 expressions were treated with EBSS to induce autophagy or were left untreated. Subsequently autophagy flux was blocked using hydroxychloroquine. In this setting, the overexpression of circATG5 4-5 increased the cellular autophagy flux, while the knockdown showed the opposite effect.

Autophagy can promote the physiological hemostasis of tumor cells and enable cancer cells to maintain nutrient availability ¹⁶⁴. Autophagy also sustains cell viability of tumor cells with defects in apoptosis and protects from metabolite stress ¹⁶⁵. There is growing evidence demonstrating that the crosstalk between circRNAs and autophagy plays an important role

in tumor development ¹⁶⁶. For instance, circCDYL is known to promote breast cancer progression by increasing cellular autophagy ¹⁶⁷. Our study shows that elevated expression of circATG5 4-5 can contribute to the malignant phenotype of B-ALL cells by increasing autophagy, proliferation, cell cycle progression and viability. In line, the knockdown of circATG5 4-5 produces a reverse effect. In general, the results presented in this work support the role of circATG5 4-5 as a regulator of vital cellular functions.

Ectopic expression of circATG5 4-5 in B-ALL cell lines and HEK293 promoted a differential expression in several genes. Focusing on B-ALL cell lines, we detected by RNAseq after circATG5 4-5 overexpression a total of 85 dysregulated genes in HAL-01 cell line, of which 39 genes and 46 genes have been shown to be downregulated and upregulated, respectively. In 697 cell line, 86 genes were defined, of which 22 genes and 29 genes have been shown to be upregulated and downregulated, respectively. Interestingly, we found three genes, which have been shown to overlap between 697 and HAL-01, including *ATG5* that already has been described, Toll-like receptor 4 (*TLR4*) and Hematopoietic SH2 Domain Containing (*HSH2D*). *ATG5* was upregulated and *TLR4* downregulated in both cell lines, while *HSH2D* was upregulated in HAL-01 and downregulated in 697. The low number of overlapping genes between the two B-ALL cell lines could be due simply to the fact that both cells have distinct genetic backgrounds (refer to Figure 15).

TLR4 is one of the most studied TLRs. It is known to recognize exogenous molecules from pathogens, in particular Lipopolysaccharide (LPS) from gram-negative bacteria as a main Pathogen-associated molecular patterns (PAMPs) ¹⁶⁸. This is very important in the fight against invading microorganisms. TLR4 is expressed by many tumor cells, promoting their growth and immune evasion ^{169,170}. Da Cruz and colleagues published in 2021 that the expression of TLR4 is downregulated in glioblastoma, supporting thus immune evasion ¹⁷¹. In other words, the downregulation of TLR4 in glioblastoma is a mechanism by which glioblastoma cells protect themselves from recognition and elimination by the host immune response. We hypothesized that the downregulation of TLR4 expression observed in our in B-ALL cell models, overexpressing circATG5 4-5 may probably be involved in immune escape strategy, as mentioned for glioblastoma. This must be assessed experimentally in further studies.

The reason why *HSH2D* is up-regulated in HAL-01 and down regulated in 697 following the circATG5 4-5 is still unclear. what we know about this gene is that *HSH2D* may play a role in the activation of T cells and is also involved in drug resistance in T-cell acute

lymphoblastic leukemia ¹⁷². In HAL-01 the upregulation of *HSH2D* could perhaps support the drug resistance of this cell line.

Taking together, through this study we could functionally characterize circATG5 4-5. CircATG5 4-5 is a transcript that can be detected by RT-qPCR using divergent primers. It is resistant against RNase R and is expressed in various cell lines. Predominantly localized in the cytoplasm the transcript circATG5 4-5 has also been seen in the nucleus. We guess that it could be due to the fact that circRNAs are primo synthesized in nucleus and then, for those that would not stay in that location are subsequently transported elsewhere.

This thesis demonstrated that circATG5 4-5 significantly regulates the expression of their parental gene ATG5, whereby when it is upregulated, the mRNA level of ATG5 goes up, whereas, by using siRNA against circATG5 4-5, an opposite effect is observed. Additionally, circATG5 4-5 showed to slow down ATG5 degradation, when overexpressed. CircATG5 4-5 influences the autophagy pathway via the regulation of ATG5, whereby the overexpression of circATG5 4-5 has a positive effect on cellular autophagy. Furthermore, the in-silico microRNA binding prediction suggests that circATG5 4-5 might potentially interact with miR-1299 that is also targeting CDK6, STAT3 and EGFR. Experimentally, we could demonstrate that in circATG5 4-5 overexpressing cells, the expression of miR-1299 was constantly downregulated and the expression of CDK6 was upregulated. The impact of ectopic expression of circATG5 4-5 is not only limited on the regulation of abovementioned genes, but there are many more genes, which were differentially expressed after ATG5 4-5 overexpression as found by RNAseq. This makes this transcript very attractive and could be the subject of different studies. This study demonstrated that elevated expression of circATG5 4-5 is associated with a pro-survival, proliferative and potentially oncogenic function in experimental model system.

CircATG5 4-5 showed during this study that it is a very promising circRNA candidate. However, further investigations need to be done to strengthen the data generated here. In this study, we could prove that circATG5 4-5 regulates the expression of *ATG5*, nevertheless, we could not uncover the mechanism by which it occurs. Moreover, the overexpression of circATG5 4-5 has shown a negative impact on miR-1299, thus a positive effect on *CDK6*, which is the target of miR-1299. Experimentally, we could observe it several times by RT-qPCR, but it should be desirable to demonstrate a direct interaction between circATG5 4-5 -miR1299 and *CDK6* for instance, by using luciferase assay. This

requires a good strategy to achieve it. Finally, *ATG5* may produce several circATG5, which should be interesting to validate all of them and to investigate their cellular functions.

7 References

References

- 1. Erdmann F, Kaatsch P, Grabow D, Spix C. German Childhood Cancer Registry Annual Report 2019 (1980-2018) (Johannes Gutenberg University Mainz, 2020).
- 2. Sun, W., Gaynon, P. S., Sposto, R. & Wayne, A. S. Improving access to novel agents for childhood leukemia. *Cancer* **121**, 1927–1936; 10.1002/cncr.29267 (2015).
- 3. Gomes, A. C., Saraiva, M. & Gomes, M. S. The bone marrow hematopoietic niche and its adaptation to infection. *Seminars in cell & developmental biology* **112**, 37–48; 10.1016/j.semcdb.2020.05.014 (2021).
- 4. Passegué, E., Jamieson, C. H. M., Ailles, L. E. & Weissman, I. L. Normal and leukemic hematopoiesis: are leukemias a stem cell disorder or a reacquisition of stem cell characteristics? Proceedings of the National Academy of Sciences of the United States of America 100 Suppl 1, 11842–11849; 10.1073/pnas.2034201100 (2003).
- 5. Traver, D. et al. Development of CD8alpha-positive dendritic cells from a common myeloid progenitor. Science (New York, N.Y.) 290, 2152–2154; 10.1126/science.290.5499.2152 (2000).
- 6. Seita, J. & Weissman, I. L. Hematopoietic stem cell: self-renewal versus differentiation. *Wiley interdisciplinary reviews. Systems biology and medicine* **2**, 640–653; 10.1002/wsbm.86 (2010).
- Kennedy, J. A. & Barabé, F. Investigating human leukemogenesis: from cell lines to in vivo models of human leukemia. *Leukemia* 22, 2029–2040; 10.1038/leu.2008.206 (2008).
- 8. Bonnet, D. & Dick, J. E. Human acute myeloid leukemia is organized as a hierarchy that originates from a primitive hematopoietic cell. *Nature medicine* **3**, 730–737; 10.1038/nm0797-730 (1997).
- 9. Marchand, T. & Pinho, S. Leukemic Stem Cells: From Leukemic Niche Biology to Treatment Opportunities. *Frontiers in immunology* **12**, 775128; 10.3389/fimmu.2021.775128 (2021).
- 10. Sun, T. (ed.). Atlas of Hematologic Neoplasms. 1st ed. (Springer US, New York, NY, 2009).
- 11. Arber, D. A. *et al.* The 2016 revision to the World Health Organization classification of myeloid neoplasms and acute leukemia. *Blood* **127**, 2391–2405; 10.1182/blood-2016-03-643544 (2016).
- Cacciotti, C., Fleming, A. & Ramaswamy, V. Advances in the molecular classification of pediatric brain tumors: a guide to the galaxy. *The Journal of pathology* 251, 249–261; 10.1002/path.5457 (2020).
- 13. Hunger, S. P., Teachey, D. T., Grupp, S. & Aplenc, R. Childhood Leukemia. In *Abeloff's Clinical Oncology* (Elsevier2020), 1748-1764.e4.

- 14. Hunger, S. P. & Mullighan, C. G. Acute Lymphoblastic Leukemia in Children. *The New England journal of medicine* **373**, 1541–1552; 10.1056/NEJMra1400972 (2015).
- 15. Vijayakrishnan, J. *et al.* Identification of four novel associations for B-cell acute lymphoblastic leukaemia risk. *Nature communications* **10**, 5348; 10.1038/s41467-019-13069-6 (2019).
- 16. Steimlé, T. *et al.* Clinico-biological features of T-cell acute lymphoblastic leukemia with fusion proteins. *Blood cancer journal* **12**, 14; 10.1038/s41408-022-00613-9 (2022).
- 17. Greaves, M. A causal mechanism for childhood acute lymphoblastic leukaemia. *Nature reviews. Cancer* **18**, 471–484; 10.1038/s41568-018-0015-6 (2018).
- Hein, D., Borkhardt, A. & Fischer, U. Insights into the prenatal origin of childhood acute lymphoblastic leukemia. *Cancer metastasis reviews* 39, 161–171; 10.1007/s10555-019-09841-1 (2020).
- 19. Hauer, J., Fischer, U. & Borkhardt, A. Toward prevention of childhood ALL by early-life immune training. *Blood* 138, 1412–1428; 10.1182/blood.2020009895 (2021).
- 20. Lee, P., Bhansali, R., Izraeli, S., Hijiya, N. & Crispino, J. D. The biology, pathogenesis and clinical aspects of acute lymphoblastic leukemia in children with Down syndrome. *Leukemia* **30**, 1816–1823; 10.1038/leu.2016.164 (2016).
- 21. Zhang, M. Y. *et al.* Germline ETV6 mutations in familial thrombocytopenia and hematologic malignancy. *Nature genetics* **47**, 180–185; 10.1038/ng.3177 (2015).
- 22. Mullighan, C. G. *et al.* Deletion of IKZF1 and prognosis in acute lymphoblastic leukemia. *The New England journal of medicine* **360**, 470–480; 10.1056/NEJMoa0808253 (2009).
- 23. Auer, F. *et al.* Inherited susceptibility to pre-B-ALL caused by germline transmission of PAX5 c.547GA. *Leukemia* **28**, 1136–1138; 10.1038/leu.2013.363 (2014).
- 24. Gorlov, I. P. *et al.* Gene characteristics predicting missense, nonsense and frameshift mutations in tumor samples. *BMC bioinformatics* **19**, 430; 10.1186/s12859-018-2455-0 (2018).
- 25. Churchman, M. L. *et al.* Germline Genetic IKZF1 Variation and Predisposition to Childhood Acute Lymphoblastic Leukemia. *Cancer cell* **33**, 937-948.e8; 10.1016/j.ccell.2018.03.021 (2018).
- 26. Rampersaud, E. *et al.* Germline deletion of ETV6 in familial acute lymphoblastic leukemia. *Blood advances* **3**, 1039–1046; 10.1182/bloodadvances.2018030635 (2019).
- 27. Ripperger, T. & Schlegelberger, B. Acute lymphoblastic leukemia and lymphoma in the context of constitutional mismatch repair deficiency syndrome. *European journal of medical genetics* **59,** 133–142; 10.1016/j.ejmg.2015.12.014 (2016).

- 28. Treviño, L. R. *et al.* Germline genomic variants associated with childhood acute lymphoblastic leukemia. *Nature genetics* **41,** 1001–1005; 10.1038/ng.432 (2009).
- 29. Papaemmanuil, E. *et al.* Loci on 7p12.2, 10q21.2 and 14q11.2 are associated with risk of childhood acute lymphoblastic leukemia. *Nature genetics* **41,** 1006–1010; 10.1038/ng.430 (2009).
- 30. Inaba, H., Greaves, M. & Mullighan, C. G. Acute lymphoblastic leukaemia. *The Lancet* **381**, 1943–1955; 10.1016/S0140-6736(12)62187-4 (2013).
- 31. Schäfer, D. *et al.* Five percent of healthy newborns have an ETV6-RUNX1 fusion as revealed by DNA-based GIPFEL screening. *Blood* **131**, 821–826; 10.1182/blood-2017-09-808402 (2018).
- 32. Fischer, U. *et al.* Genomics and drug profiling of fatal TCF3-HLF-positive acute lymphoblastic leukemia identifies recurrent mutation patterns and therapeutic options. *Nature genetics* **47**, 1020–1029; 10.1038/ng.3362 (2015).
- 33. Richardson, D. *et al.* Ionizing radiation and leukemia mortality among Japanese Atomic Bomb Survivors, 1950-2000. *Radiation research* **172**, 368–382; 10.1667/RR1801.1 (2009).
- Shimizu, Y., Kato, H., Schull, W. J. & Hoel, D. G. Studies of the Mortality of A-Bomb Survivors.
 Mortality, 1950-1985: Part 3. Noncancer Mortality Based on the Revised Doses (DS86).
 Radiation research 130, 249; 10.2307/3578283 (1992).
- 35. Kinlen, L. J. Epidemiological evidence for an infective basis in childhood leukaemia. *British journal of cancer* **71**, 1–5; 10.1038/bjc.1995.1. (1995).
- 36. Greaves, M. Infection, immune responses and the aetiology of childhood leukaemia. *Nature reviews. Cancer* **6**, 193–203; 10.1038/nrc1816. (2006).
- 37. Kang, S., Im, H. J., Bae, K. & Park, S.-S. Influence of Musculoskeletal Manifestations as the Only Presenting Symptom in B-Cell Acute Lymphoblastic Leukemia. *The Journal of pediatrics* **182**, 290-295.e1; 10.1016/j.jpeds.2016.11.072 (2017).
- 38. Redaelli, A., Laskin, B. L., Stephens, J. M., Botteman, M. F. & Pashos, C. L. A systematic literature review of the clinical and epidemiological burden of acute lymphoblastic leukaemia (ALL). *European journal of cancer care* **14**, 53–62; 10.1111/j.1365-2354.2005.00513.x (2005).
- 39. Bhatti, F. A., Hussain, I. & Ali, M. Z. Adult B lymphoblastic leukaemia/lymphoma with hypodiploidy (-9) and a novel chromosomal translocation t(7;12)(q22;p13) presenting with severe eosinophilia case report and review of literature. *Journal of hematology & oncology* 2, 26; 10.1186/1756-8722-2-26 (2009).

- 40. Bennett, J. M. *et al.* Proposed revised criteria for the classification of acute myeloid leukemia. A report of the French-American-British Cooperative Group. *Annals of internal medicine* **103**, 620–625; 10.7326/0003-4819-103-4-620 (1985).
- 41. Omman, R. A. & Kini, A. R. Acute leukemias. In *Rodak's Hematology* (Elsevier2020), pp. 540–554.
- 42. Siegele, B. J. & Nardi, V. Laboratory testing in BCR-ABL1-like (Philadelphia-like) B-lymphoblastic leukemia/lymphoma. *American journal of hematology* **93**, 971–977; 10.1002/ajh.25126 (2018).
- 43. Porwit, A. & Béné, M.-C. Acute lymphoblastic leukemia/lymphoma and mixed phenotype acute leukemias. In *Blood and Bone Marrow Pathology* (Elsevier2011), pp. 289–301.
- 44. Gaipa, G., Basso, G., Biondi, A. & Campana, D. Detection of minimal residual disease in pediatric acute lymphoblastic leukemia. *Cytometry. Part B, Clinical cytometry* **84,** 359–369; 10.1002/cyto.b.21101 (2013).
- 45. Cuéllar-Mendoza, M. E., Chávez-Sánchez, F. R., Dorantes-Acosta, E., Arsuaga-Jiménez, B. M. & Zapata-Tarrés, M. Inmunofenotipos aberrantes en la leucemia linfoblástica aguda. *Boletin medico del Hospital Infantil de Mexico* 77, 287–292; 10.24875/BMHIM.20000171 (2020).
- 46. Dworzak, M. N. *et al.* AIEOP-BFM consensus guidelines 2016 for flow cytometric immunophenotyping of Pediatric acute lymphoblastic leukemia. *Cytometry. Part B, Clinical cytometry* **94,** 82–93; 10.1002/cyto.b.21518 (2018).
- 47. Woo, J. S., Alberti, M. O. & Tirado, C. A. Childhood B-acute lymphoblastic leukemia: a genetic update. *Experimental hematology & oncology* **3,** 16; 10.1186/2162-3619-3-16 (2014).
- 48. Braoudaki, M. & Tzortzatou-Stathopoulou, F. Clinical cytogenetics in pediatric acute leukemia: an update. *Clinical lymphoma, myeloma & leukemia* **12**, 230–237; 10.1016/j.clml.2012.04.004 (2012).
- 49. Bennett, J. M. *et al.* Proposals for the classification of the acute leukaemias. French-American-British (FAB) co-operative group. *British journal of haematology* **33**, 451–458; 10.1111/j.1365-2141.1976.tb03563.x (1976).
- 50. Randolph, T. R. Advances in acute lymphoblastic leukemia. *American Society for Clinical Laboratory Science* **17**, 235–245 (2004).
- 51. Ajithkumar, T. V. & Hatcher, H. M. Cancers of the haematopoietic system. In *Specialist Training* in *Oncology* (Elsevier2011), pp. 298–319.
- 52. Swerdlow, S. H. *et al.* (eds.). *WHO classification of tumours of haematopoietic and lymphoid tissues*. 4th ed. (International Agency for Research on Cancer, Lyon, 2017).

- 53. Heikamp, E. B. & Pui, C.-H. Next-Generation Evaluation and Treatment of Pediatric Acute Lymphoblastic Leukemia. *The Journal of pediatrics* **203,** 14-24.e2; 10.1016/j.jpeds.2018.07.039 (2018).
- 54. Inaba, H. & Mullighan, C. G. Pediatric acute lymphoblastic leukemia. *Haematologica* **105**, 2524–2539; 10.3324/haematol.2020.247031 (2020).
- 55. Adams, B. D., Parsons, C., Walker, L., Zhang, W. C. & Slack, F. J. Targeting noncoding RNAs in disease. *The Journal of clinical investigation* **127**, 761–771; 10.1172/JCI84424 (2017).
- 56. Zhang, P., Wu, W., Chen, Q. & Chen, M. Non-Coding RNAs and their Integrated Networks. *Journal of integrative bioinformatics* **16**; 10.1515/jib-2019-0027 (2019).
- 57. Cech, T. R. & Steitz, J. A. The noncoding RNA revolution-trashing old rules to forge new ones. *Cell* **157**, 77–94; 10.1016/j.cell.2014.03.008 (2014).
- 58. Peschansky, V. J. & Wahlestedt, C. Non-coding RNAs as direct and indirect modulators of epigenetic regulation. *Epigenetics* **9**, 3–12; 10.4161/epi.27473 (2014).
- 59. Latowska, J. *et al.* Non-coding RNAs in Brain Tumors, the Contribution of lncRNAs, circRNAs, and snoRNAs to Cancer Development-Their Diagnostic and Therapeutic Potential. *International journal of molecular sciences* **21**; 10.3390/ijms21197001 (2020).
- 60. Esmaeili, M. *et al.* Role of non-coding RNAs as novel biomarkers for detection of colorectal cancer progression through interaction with the cell signaling pathways. *Gene* **753**, 144796; 10.1016/j.gene.2020.144796 (2020).
- 61. Sanger, H. L., Klotz, G., Riesner, D., Gross, H. J. & Kleinschmidt, A. K. Viroids are single-stranded covalently closed circular RNA molecules existing as highly base-paired rod-like structures. *Proceedings of the National Academy of Sciences of the United States of America* 73, 3852–3856; 10.1073/pnas.73.11.3852 (1976).
- 62. Jeck, W. R. *et al.* Circular RNAs are abundant, conserved, and associated with ALU repeats. *RNA (New York, N.Y.)* **19,** 141–157; 10.1261/rna.035667.112 (2013).
- 63. Lei, K. *et al.* The mechanism and function of circular RNAs in human diseases. *Experimental cell research* **368**, 147–158; 10.1016/j.yexcr.2018.05.002 (2018).
- 64. Arnberg, A. C., van Ommen, G.-J., Grivell, L. A., van Bruggen, E. & Borst, P. Some yeast mitochondrial RNAs are circular. *Cell* 19, 313–319; 10.1016/0092-8674(80)90505-X (1980).
- 65. Kos, A., Dijkema, R., Arnberg, A. C., van der Meide, P. H. & Schellekens, H. The hepatitis delta (delta) virus possesses a circular RNA. *Nature* **323**, 558–560; 10.1038/323558a0 (1986).
- 66. Nigro, J. M. et al. Scrambled exons. Cell 64, 607–613; 10.1016/0092-8674(91)90244-S (1991).

- 67. Cocquerelle, C., Mascrez, B., Hétuin, D. & Bailleul, B. Mis-splicing yields circular RNA molecules. *FASEB journal : official publication of the Federation of American Societies for Experimental Biology* **7**, 155–160; 10.1096/fasebj.7.1.7678559 (1993).
- 68. Salzman, J., Chen, R. E., Olsen, M. N., Wang, P. L. & Brown, P. O. Cell-type specific features of circular RNA expression. *PLoS genetics* **9**, e1003777; 10.1371/journal.pgen.1003777 (2013).
- 69. Salzman, J., Gawad, C., Wang, P. L., Lacayo, N. & Brown, P. O. Circular RNAs are the predominant transcript isoform from hundreds of human genes in diverse cell types. *PloS one* 7, e30733; 10.1371/journal.pone.0030733 (2012).
- 70. Holdt, L. M., Kohlmaier, A. & Teupser, D. Circular RNAs as Therapeutic Agents and Targets. *Frontiers in physiology* **9**, 1262; 10.3389/fphys.2018.01262 (2018).
- 71. Szabo, L. & Salzman, J. Detecting circular RNAs: bioinformatic and experimental challenges. *Nature reviews. Genetics* **17**, 679–692; 10.1038/nrg.2016.114 (2016).
- 72. Li, X., Yang, L. & Chen, L.-L. The Biogenesis, Functions, and Challenges of Circular RNAs. *Molecular cell* 71, 428–442; 10.1016/j.molcel.2018.06.034 (2018).
- 73. Qiu, L.-P. *et al.* The Emerging Role of Circular RNAs in Hepatocellular Carcinoma. *Journal of Cancer* **9**, 1548–1559; 10.7150/jca.24566 (2018).
- 74. Hanan, M., Soreq, H. & Kadener, S. CircRNAs in the brain. *RNA biology* **14,** 1028–1034; 10.1080/15476286.2016.1255398 (2017).
- 75. Zhang, C. *et al.* Rapid Development of Targeting circRNAs in Cardiovascular Diseases. *Molecular therapy. Nucleic acids* **21**, 568–576; 10.1016/j.omtn.2020.06.022 (2020).
- Ragan, C., Goodall, G. J., Shirokikh, N. E. & Preiss, T. Insights into the biogenesis and potential functions of exonic circular RNA. *Scientific reports* 9, 2048; 10.1038/s41598-018-37037-0 (2019).
- 77. Kristensen, L. S. *et al.* The biogenesis, biology and characterization of circular RNAs. *Nature reviews. Genetics* **20**, 675–691; 10.1038/s41576-019-0158-7 (2019).
- 78. Starke, S. *et al.* Exon circularization requires canonical splice signals. *Cell reports* **10**, 103–111; 10.1016/j.celrep.2014.12.002 (2015).
- 79. Ashwal-Fluss, R. *et al.* circRNA biogenesis competes with pre-mRNA splicing. *Molecular cell* **56**, 55–66; 10.1016/j.molcel.2014.08.019 (2014).
- 80. Wen, J. et al. Circular RNA HIPK3: A Key Circular RNA in a Variety of Human Cancers. Frontiers in oncology 10, 773; 10.3389/fonc.2020.00773 (2020).

- 81. Zhao, W. *et al.* Circular RNAs: A novel target among non-coding RNAs with potential roles in malignant tumors (Review). *Molecular medicine reports* **20,** 3463–3474; 10.3892/mmr.2019.10637 (2019).
- 82. Hansen, T. B. *et al.* Natural RNA circles function as efficient microRNA sponges. *Nature* **495**, 384–388; 10.1038/nature11993 (2013).
- 83. Abdelmohsen, K. *et al.* Identification of HuR target circular RNAs uncovers suppression of PABPN1 translation by CircPABPN1. *RNA biology* **14,** 361–369; 10.1080/15476286.2017.1279788 (2017).
- 84. Zheng, Q. *et al.* Circular RNA profiling reveals an abundant circHIPK3 that regulates cell growth by sponging multiple miRNAs. *Nature communications* **7**, 11215; 10.1038/ncomms11215 (2016).
- 85. Tang, W. et al. Silencing CDR1as inhibits colorectal cancer progression through regulating microRNA-7. OncoTargets and therapy 10, 2045–2056; 10.2147/OTT.S131597 (2017).
- 86. Du, W. W. *et al.* Foxo3 circular RNA promotes cardiac senescence by modulating multiple factors associated with stress and senescence responses. *European heart journal* **38,** 1402–1412; 10.1093/eurheartj/ehw001 (2017).
- 87. Holdt, L. M. *et al.* Circular non-coding RNA ANRIL modulates ribosomal RNA maturation and atherosclerosis in humans. *Nature communications* **7**, 12429; 10.1038/ncomms12429 (2016).
- 88. Li, Z. *et al.* Exon-intron circular RNAs regulate transcription in the nucleus. *Nature structural & molecular biology* **22**, 256–264; 10.1038/nsmb.2959 (2015).
- 89. Verduci, L., Tarcitano, E., Strano, S., Yarden, Y. & Blandino, G. CircRNAs: role in human diseases and potential use as biomarkers. *Cell death & disease* **12**, 468; 10.1038/s41419-021-03743-3 (2021).
- 90. Liu, B. et al. Circular RNA circ_ABCB10 in cancer. Clinica chimica acta; international journal of clinical chemistry **518**, 93–100; 10.1016/j.cca.2021.03.010 (2021).
- 91. Rajappa, A., Banerjee, S., Sharma, V. & Khandelia, P. Circular RNAs: Emerging Role in Cancer Diagnostics and Therapeutics. *Frontiers in molecular biosciences* 7, 577938; 10.3389/fmolb.2020.577938 (2020).
- 92. Zhang, X. *et al.* Circular RNA circNRIP1 acts as a microRNA-149-5p sponge to promote gastric cancer progression via the AKT1/mTOR pathway. *Molecular cancer* **18**, 20; 10.1186/s12943-018-0935-5 (2019).

- 93. Hu, Z.-Q. *et al.* Circular RNA Sequencing Identifies CircASAP1 as a Key Regulator in Hepatocellular Carcinoma Metastasis. *Hepatology (Baltimore, Md.)* **72,** 906–922; 10.1002/hep.31068 (2020).
- 94. Boeckel, J.-N. *et al.* Identification and Characterization of Hypoxia-Regulated Endothelial Circular RNA. *Circulation research* **117**, 884–890; 10.1161/CIRCRESAHA.115.306319 (2015).
- 95. Hu, Y. *et al.* A circular RNA from APC inhibits the proliferation of diffuse large B-cell lymphoma by inactivating Wnt/β-catenin signaling via interacting with TET1 and miR-888. *Aging* **11**, 8068–8084; 10.18632/aging.102122 (2019).
- 96. Klionsky, D. J. Autophagy revisited: a conversation with Christian de Duve. *Autophagy* **4,** 740–743; 10.4161/auto.6398 (2008).
- 97. Glick, D., Barth, S. & Macleod, K. F. Autophagy: cellular and molecular mechanisms. *The Journal of pathology* **221**, 3–12; 10.1002/path.2697 (2010).
- 98. Kocaturk, N. M. & Gozuacik, D. Crosstalk Between Mammalian Autophagy and the Ubiquitin-Proteasome System. *Frontiers in cell and developmental biology* **6,** 128; 10.3389/fcell.2018.00128 (2018).
- 99. Lilienbaum, A. Relationship between the proteasomal system and autophagy. *International Journal of Biochemistry and Molecular Biology* **4**, 1–26 (2013).
- 100. King, J. S., Veltman, D. M. & Insall, R. H. The induction of autophagy by mechanical stress. Autophagy 7, 1490–1499; 10.4161/auto.7.12.17924 (2011).
- 101. Rosenfeldt, M. T. & Ryan, K. M. The multiple roles of autophagy in cancer. *Carcinogenesis* **32**, 955–963; 10.1093/carcin/bgr031 (2011).
- 102. Li, W., Li, J. & Bao, J. Microautophagy: lesser-known self-eating. *Cellular and molecular life sciences: CMLS* **69**, 1125–1136; 10.1007/s00018-011-0865-5 (2012).
- 103. Dice, J. F. Chaperone-mediated autophagy. *Autophagy* 3, 295–299; 10.4161/auto.4144 (2007).
- 104. Alfaro, I. E. *et al.* Chaperone Mediated Autophagy in the Crosstalk of Neurodegenerative Diseases and Metabolic Disorders. *Frontiers in endocrinology* **9,** 778; 10.3389/fendo.2018.00778 (2018).
- 105. Parzych, K. R. & Klionsky, D. J. An overview of autophagy: morphology, mechanism, and regulation. *Antioxidants & redox signaling* **20**, 460–473; 10.1089/ars.2013.5371 (2014).
- 106. Carlsson, S. R. & Simonsen, A. Membrane dynamics in autophagosome biogenesis. *Journal of cell science* **128**, 193–205; 10.1242/jcs.141036 (2015).

- 107. Germic, N., Hosseini, A., Yousefi, S., Karaulov, A. & Simon, H.-U. Regulation of eosinophil functions by autophagy. *Seminars in immunopathology* **43**, 347–362; 10.1007/s00281-021-00860-1 (2021).
- 108. Wesselborg, S. & Stork, B. Autophagy signal transduction by ATG proteins: from hierarchies to networks. *Cellular and molecular life sciences: CMLS* **72**, 4721–4757; 10.1007/s00018-015-2034-8 (2015).
- 109. Towler, M. C. & Hardie, D. G. AMP-activated protein kinase in metabolic control and insulin signaling. *Circulation research* **100**, 328–341; 10.1161/01.RES.0000256090.42690.05 (2007).
- 110. Ganley, I. G. *et al.* ULK1.ATG13.FIP200 complex mediates mTOR signaling and is essential for autophagy. *The Journal of biological chemistry* **284,** 12297–12305; 10.1074/jbc.M900573200 (2009).
- 111. Takahara, T., Amemiya, Y., Sugiyama, R., Maki, M. & Shibata, H. Amino acid-dependent control of mTORC1 signaling: a variety of regulatory modes. *Journal of biomedical science* **27**, 87; 10.1186/s12929-020-00679-2 (2020).
- 112. Fan, X.-Y. *et al.* Activation of the AMPK-ULK1 pathway plays an important role in autophagy during prion infection. *Scientific reports* **5**, 14728; 10.1038/srep14728 (2015).
- 113. Chavez-Dominguez, R., Perez-Medina, M., Lopez-Gonzalez, J. S., Galicia-Velasco, M. & Aguilar-Cazares, D. The Double-Edge Sword of Autophagy in Cancer: From Tumor Suppression to Pro-tumor Activity. *Frontiers in oncology* 10, 578418; 10.3389/fonc.2020.578418 (2020).
- 114. Wilkinson, S. & Ryan, K. M. Autophagy: an adaptable modifier of tumourigenesis. *Current opinion in genetics & development* **20**, 57–64; 10.1016/j.gde.2009.12.004 (2010).
- 115. Poillet-Perez, L., Despouy, G., Delage-Mourroux, R. & Boyer-Guittaut, M. Interplay between ROS and autophagy in cancer cells, from tumor initiation to cancer therapy. *Redox biology* **4,** 184–192; 10.1016/j.redox.2014.12.003 (2015).
- 116. Lorin, S., Hamaï, A., Mehrpour, M. & Codogno, P. Autophagy regulation and its role in cancer. Seminars in cancer biology 23, 361–379; 10.1016/j.semcancer.2013.06.007 (2013).
- 117. Huang, F.-L., Yu, S.-J. & Li, C.-L. Role of Autophagy and Apoptosis in Acute Lymphoblastic Leukemia. *Cancer control: journal of the Moffitt Cancer Center* **28**, 10732748211019138; 10.1177/10732748211019138 (2021).
- 118. Polak, R. *et al.* Autophagy inhibition as a potential future targeted therapy for ETV6-RUNX1-driven B-cell precursor acute lymphoblastic leukemia. *Haematologica* **104**, 738–748; 10.3324/haematol.2018.193631 (2019).

- 119. Mathew, R. & White, E. Autophagy, stress, and cancer metabolism: what doesn't kill you makes you stronger. *Cold Spring Harbor symposia on quantitative biology* **76**, 389–396; 10.1101/sqb.2012.76.011015 (2011).
- 120. Degenhardt, K. *et al.* Autophagy promotes tumor cell survival and restricts necrosis, inflammation, and tumorigenesis. *Cancer cell* **10**, 51–64; 10.1016/j.ccr.2006.06.001 (2006).
- 121. Du, W. W. et al. A circular RNA circ-DNMT1 enhances breast cancer progression by activating autophagy. *Oncogene* **37**, 5829–5842; 10.1038/s41388-018-0369-y (2018).
- 122. Grácio, D., Magro, F., T. Lima, R. & Máximo, V. An overview on the role of autophagy in cancer therapy. *Hematol Med Oncol* 2; 10.15761/HMO.1000117 (2017).
- 123. Ye, X., Zhou, X.-J. & Zhang, H. Exploring the Role of Autophagy-Related Gene 5 (ATG5) Yields Important Insights Into Autophagy in Autoimmune/Autoinflammatory Diseases. *Frontiers in immunology* **9**, 2334; 10.3389/fimmu.2018.02334 (2018).
- 124. Itakura, E. & Mizushima, N. Characterization of autophagosome formation site by a hierarchical analysis of mammalian Atg proteins. *Autophagy* **6,** 764–776; 10.4161/auto.6.6.12709 (2010).
- 125. Yousefi, S. *et al.* Calpain-mediated cleavage of Atg5 switches autophagy to apoptosis. *Nature cell biology* **8,** 1124–1132; 10.1038/ncb1482 (2006).
- 126. Miller, B. C. *et al.* The autophagy gene ATG5 plays an essential role in B lymphocyte development. *Autophagy* **4**, 309–314; 10.4161/auto.5474 (2008).
- 127. Pua, H. H., Dzhagalov, I., Chuck, M., Mizushima, N. & He, Y.-W. A critical role for the autophagy gene Atg5 in T cell survival and proliferation. *The Journal of experimental medicine* **204**, 25–31; 10.1084/jem.20061303 (2007).
- 128. Zhao, Z. *et al.* Autophagosome-independent essential function for the autophagy protein Atg5 in cellular immunity to intracellular pathogens. *Cell host & microbe* **4,** 458–469; 10.1016/j.chom.2008.10.003 (2008).
- 129. Kimmey, J. M. *et al.* Unique role for ATG5 in neutrophil-mediated immunopathology during M. tuberculosis infection. *Nature* **528**, 565–569; 10.1038/nature16451 (2015).
- 130. Kuma, A. *et al.* The role of autophagy during the early neonatal starvation period. *Nature* **432**, 1032–1036; 10.1038/nature03029 (2004).
- 131. Pyo, J.-O. *et al.* Overexpression of Atg5 in mice activates autophagy and extends lifespan. *Nature communications* **4,** 2300; 10.1038/ncomms3300 (2013).
- 132. Liu, H., He, Z. & Simon, H.-U. Autophagy suppresses melanoma tumorigenesis by inducing senescence. *Autophagy* **10**, 372–373; 10.4161/auto.27163 (2014).

- 133. Weber, K., Bartsch, U., Stocking, C. & Fehse, B. A multicolor panel of novel lentiviral "gene ontology" (LeGO) vectors for functional gene analysis. *Molecular therapy: the journal of the American Society of Gene Therapy* **16**, 698–706; 10.1038/mt.2008.6 (2008).
- 134. Liang, D. & Wilusz, J. E. Short intronic repeat sequences facilitate circular RNA production. *Genes & development* **28**, 2233–2247; 10.1101/gad.251926.114 (2014).
- 135. Moffat, J. *et al.* A lentiviral RNAi library for human and mouse genes applied to an arrayed viral high-content screen. *Cell* **124**, 1283–1298; 10.1016/j.cell.2006.01.040 (2006).
- 136. Dudekula, D. B. *et al.* CircInteractome: A web tool for exploring circular RNAs and their interacting proteins and microRNAs. *RNA biology* **13**, 34–42; 10.1080/15476286.2015.1128065 (2016).
- 137. Howe, K. L. *et al.* Ensembl 2021. *Nucleic acids research* **49,** D884-D891; 10.1093/nar/gkaa942 (2021).
- 138. Zhu, H. *et al.* miR-1299 suppresses cell proliferation of hepatocellular carcinoma (HCC) by targeting CDK6. *Biomedicine & pharmacotherapy = Biomedecine & pharmacotherapie* **83**, 792–797; 10.1016/j.biopha.2016.07.037 (2016).
- 139. Kaiyuan, D., Lijuan, H., Xueyuan, S. & Yunhui, Z. The role and underlying mechanism of miR-1299 in cancer. *Future science OA* 7, FSO693; 10.2144/fsoa-2021-0014 (2021).
- 140. Cao, S., Li, L., Li, J. & Zhao, H. MiR-1299 Impedes the Progression of Non-Small-Cell Lung Cancer Through EGFR/PI3K/AKT Signaling Pathway. *OncoTargets and therapy* **13**, 7493–7502; 10.2147/OTT.S250396 (2020).
- 141. Li, F., Yang, Q., He, A. T. & Yang, B. B. Circular RNAs in cancer: Limitations in functional studies and diagnostic potential. *Seminars in cancer biology* **75**, 49–61; 10.1016/j.semcancer.2020.10.002 (2021).
- 142. Codogno, P. & Meijer, A. J. Atg5: more than an autophagy factor. *Nature cell biology* **8**, 1045–1047; 10.1038/ncb1006-1045 (2006).
- 143. Zheng, W. *et al.* ATG5 and ATG7 induced autophagy interplays with UPR via PERK signaling. *Cell communication and signaling : CCS* **17**, 42; 10.1186/s12964-019-0353-3 (2019).
- 144. He, J. *et al.* Circular RNA MAPK4 (circ-MAPK4) inhibits cell apoptosis via MAPK signaling pathway by sponging miR-125a-3p in gliomas. *Molecular cancer* **19,** 17; 10.1186/s12943-019-1120-1 (2020).
- 145. Ou, R. *et al.* circRNA-AKT1 Sequesters miR-942-5p to Upregulate AKT1 and Promote Cervical Cancer Progression. *Molecular therapy. Nucleic acids* **20**, 308–322; 10.1016/j.omtn.2020.01.003 (2020).

- 146. Wang, Y., Wang, Z., Lu, J. & Zhang, H. Circular RNA circ-PTEN elevates PTEN inhibiting the proliferation of non-small cell lung cancer cells. *Human cell* **34**, 1174–1184; 10.1007/s13577-021-00526-y (2021).
- 147. Zang, Y., Li, J., Wan, B. & Tai, Y. circRNA circ-CCND1 promotes the proliferation of laryngeal squamous cell carcinoma through elevating CCND1 expression via interacting with HuR and miR-646. *Journal of cellular and molecular medicine* **24**, 2423–2433; 10.1111/jcmm.14925 (2020).
- 148. Li, Z., Kearse, M. G. & Huang, C. The nuclear export of circular RNAs is primarily defined by their length. *RNA biology* **16**, 1–4; 10.1080/15476286.2018.1557498 (2019).
- 149. Zhou, M., Xiao, M.-S., Li, Z. & Huang, C. New progresses of circular RNA biology: from nuclear export to degradation. *RNA biology* 18, 1365–1373; 10.1080/15476286.2020.1853977 (2021).
- 150. Jiang, C. et al. The Emerging Picture of the Roles of CircRNA-CDR1as in Cancer. Frontiers in cell and developmental biology 8, 590478; 10.3389/fcell.2020.590478 (2020).
- 151. Hanniford, D. *et al.* Epigenetic Silencing of CDR1as Drives IGF2BP3-Mediated Melanoma Invasion and Metastasis. *Cancer cell* **37**, 55-70.e15; 10.1016/j.ccell.2019.12.007 (2020).
- 152. Du, W. W. et al. Foxo3 circular RNA retards cell cycle progression via forming ternary complexes with p21 and CDK2. *Nucleic acids research* **44**, 2846–2858; 10.1093/nar/gkw027 (2016).
- 153. Qiu, J. et al. MiR-557 works as a tumor suppressor in human lung cancers by negatively regulating LEF1 expression. *Tumour biology: the journal of the International Society for Oncodevelopmental Biology and Medicine* **39,** 1010428317709467; 10.1177/1010428317709467 (2017).
- 154. Wang, Y. *et al.* MicroRNA-1299 is a negative regulator of STAT3 in colon cancer. *Oncology reports* **37**, 3227–3234; 10.3892/or.2017.5605 (2017).
- 155. Qiao, Z. et al. Hsa-miR-557 Inhibits Osteosarcoma Growth Through Targeting KRAS. Frontiers in genetics 12, 789823; 10.3389/fgene.2021.789823 (2021).
- 156. He, J. *et al.* Circular RNA circHERC4 as a novel oncogenic driver to promote tumor metastasis via the miR-556-5p/CTBP2/E-cadherin axis in colorectal cancer. *Journal of hematology & oncology* **14**, 194; 10.1186/s13045-021-01210-2 (2021).
- 157. Zhou, R., Luo, Z., Yin, G., Yu, L. & Zhong, H. MiR-556-5p modulates migration, invasion, and epithelial-mesenchymal transition in breast cancer cells via targeting PTHrP. *J Mol Histol* 53, 297–308; 10.1007/s10735-021-10056-4 (2022).

- 158. Zhao, W., Cao, L., Zeng, S., Qin, H. & Men, T. Upregulation of miR-556-5p promoted prostate cancer cell proliferation by suppressing PPP2R2A expression. *Biomedicine & pharmacotherapy* = *Biomedecine & pharmacotherapie* 75, 142–147; 10.1016/j.biopha.2015.07.015 (2015).
- 159. Cao, L. *et al.* MiR-324-5p Suppresses Hepatocellular Carcinoma Cell Invasion by Counteracting ECM Degradation through Post-Transcriptionally Downregulating ETS1 and SP1. *PloS one* **10**, e0133074; 10.1371/journal.pone.0133074 (2015).
- 160. Zheng, Z., Li, J., An, J., Feng, Y. & Wang, L. High miR-324-5p expression predicts unfavorable prognosis of gastric cancer and facilitates tumor progression in tumor cells. *Diagnostic* pathology **16**, 5; 10.1186/s13000-020-01063-2 (2021).
- 161. Gao, A.-M., Yuan, C., Hu, A.-X. & Liu, X.-S. circ_ARF3 regulates the pathogenesis of osteosarcoma by sponging miR-1299 to maintain CDK6 expression. *Cellular signalling* **72**, 109622; 10.1016/j.cellsig.2020.109622 (2020).
- 162. Liu, L.-H., Tian, Q.-Q., Liu, J., Zhou, Y. & Yong, H. Upregulation of hsa_circ_0136666 contributes to breast cancer progression by sponging miR-1299 and targeting CDK6. *Journal of cellular biochemistry* **120**, 12684–12693; 10.1002/jcb.28536 (2019).
- 163. Fraiberg, M. & Elazar, Z. Genetic defects of autophagy linked to disease. *Progress in molecular biology and translational science* **172**, 293–323; 10.1016/bs.pmbts.2020.04.001 (2020).
- 164. Wang, Y. *et al.* Crosstalk between autophagy and microbiota in cancer progression. *Molecular cancer* **20**, 163; 10.1186/s12943-021-01461-0 (2021).
- 165. Mathew, R., Karantza-Wadsworth, V. & White, E. Role of autophagy in cancer. *Nature reviews*. *Cancer* 7, 961–967; 10.1038/nrc2254 (2007).
- 166. Wang, Y. *et al.* The influence of circular RNAs on autophagy and disease progression. *Autophagy* **18**, 240–253; 10.1080/15548627.2021.1917131 (2022).
- 167. Liang, G. *et al.* Autophagy-associated circRNA circCDYL augments autophagy and promotes breast cancer progression. *Molecular cancer* **19**, 65; 10.1186/s12943-020-01152-2 (2020).
- 168. Molteni, M., Gemma, S. & Rossetti, C. The Role of Toll-Like Receptor 4 in Infectious and Noninfectious Inflammation. *Mediators of inflammation* **2016**, 6978936; 10.1155/2016/6978936 (2016).
- 169. Huang, B. *et al.* Toll-like receptors on tumor cells facilitate evasion of immune surveillance. *Cancer research* **65**, 5009–5014; 10.1158/0008-5472.CAN-05-0784 (2005).
- 170. Kelly, M. G. *et al.* TLR-4 signaling promotes tumor growth and paclitaxel chemoresistance in ovarian cancer. *Cancer research* **66**, 3859–3868; 10.1158/0008-5472.CAN-05-3948 (2006).

- 171. Da Cruz, L. L. P. *et al.* TLR4 expression and functionality are downregulated in glioblastoma cells and in tumor-associated macrophages: A new mechanism of immune evasion? *Biochimica et biophysica acta. Molecular basis of disease* **1867**, 166155; 10.1016/j.bbadis.2021.166155 (2021).
- 172. Chen, W., Liang, R., Yi, Y., Zhu, J. & Zhang, J. P38α deficiency in macrophages ameliorates murine experimental colitis by regulating inflammation and immune process. *Pathology, research and practice* **233**, 153881; 10.1016/j.prp.2022.153881 (2022).
- 173. Ouyang, S. *et al.* The Double-Edged Sword of SIRT3 in Cancer and Its Therapeutic Applications. *Frontiers in pharmacology* **13**, 871560; 10.3389/fphar.2022.871560 (2022).
- 174. Xi, S., Chen, W. & Ke, Y. Advances in SIRT3 involvement in regulating autophagy-related mechanisms. *Cell division* **19**, 20; 10.1186/s13008-024-00124-y (2024).
- 175. Li, Y. *et al.* Role of SIRT3 in neurological diseases and rehabilitation training. *Metabolic brain disease* **38**, 69–89; 10.1007/s11011-022-01111-4 (2023).

8 Acknowledgements

First, I would like to thank my supervisor Prof. Dr. Arndt Borkhardt for giving me the opportunity to complete my doctoral thesis in the Department of Pediatric Oncology, Hematology and Immunology, and for this fascinating topic.

Furthermore, I am profoundly grateful to Prof. Dr. Sebastian Wesselborg for being my second supervisor.

I want to thank Prof. Dr. Björn Stock and Dr. Ute Fischer for your excellent supervision and guidance. Thank you for proofreading this thesis. Thanks Dr. Ute Fischer for always finding the time to discuss my questions and supporting me in my professional Interests.

Moreover, I want to thank the Düsseldorf School of Oncology for financial Support. Here I would like to address my warm thanks to Dr Cornelia Hoener.

I would like to thank Daniel Picard for analyzing RNA-seq data, Dr. Lena Blümel and Dr. Mareike Dörrenberg for proofreading.

Also, thanks to Dr. Cai Chen, Dr. Daniel Rickert, Dr. Daniel Hein, Dr. Jasmin Bartl, Dr. Nan Qin and Dr. Cyrill Schipp for various forms of support.

A big thanks to Daniel, Kai, Melf, Melina and Julian with whom I shared the same office throughout my PhD. In this regard, I also want to thank all present and past colleagues I met at the KMT lab. You made the lab a very friendly place to work at.

Last but not least, I would like to thank my parents, who never cease to support me from afar with their prayers. Finally, big thanks to my family: My wife Aline and my children Magdalena, Yannick, and Leonie, without whom all this would never have been possible. You gave me the motivation to go ahead. Thank you for everything.

9 Appendix

9.1 Abbreviations

Abbreviation	Full name	
ALL	Acute lymphatic leukemia	
AML	Acute myeloid leukemia	
APS	Ammoniumpersulfat	
ATG	Autophagy-related genes	
ATG5	Autophagy Related 5	
ATP	Adenosine triphosphate	
B-ALL	B-cell acute lymphoblastic leukemia	
BCP-ALL	B-Cell Precursor Acute Lymphoblastic Leukemia	
BM	Bone marrow	
BMFZ	Biologisch-Medizinisches Forschungszentrum	
bp	Base pair	
BSA	Bovine serum albumin	
CDK6	Cyclin Dependent Kinase 6	
cDNA	Complementary deoxyribonucleic acid	
CFSE	Carboxyfluorescein succinimidyl ester	
cIgM	Cytoplasmic immunoglobulin M	
CircRNA	Circular ribonucleic acid	
CircSRY	CircRNA in testes sex-determining region Y	
CLL	Chronic lymphoblastic leukemia	
CLP	Common lymphoid progenitor	
CMA	Chaperone-mediated autophagy	
CML	Chronic myeloid leukemia	
CNS	Central nervous system	
CPM	Counts per millions	
CMP	Common myeloid progenitor	
CMV	Cytomegalovirus	
Ct	Cycle threshold	
Cyto	Cytoplasm	
DAPI	4',6-diamidino-2-phenylindole	
DKFZ	Deutsche Krebsforschungszentrum	
DMSO	Dimethylsulfoxide	

DMEM Dulbecco's Modified Eagle Medium

DNA Deoxyribonucleic acid

dNTP Deoxyribonucleotide triphosphate

dsRNA Double-stranded-RNA

EBSS Earle's Balanced Salt Solution

E. coli Escherichia coliEcircRNAs Exonic circRNAs

EDTA Ethylenediaminetetraacetic

EIciRNAs Exon-intron circRNAs

EmGFP Emerald green fluorescent protein

ER endoplasmic reticulum
eRNA Enhancer-associated RNA

FAB French-American-British

FBS Fetal bovine serum

FISH Fluorescence *in-situ* hybridization

FITC Fluorescein isothiocyanate

GAPDH Glycerinaldehyd-3-phosphat-Dehydrogenase

GFP Green fluorescent protein

HIV Human immunodeficiency virus

HSV-TK Herpes Simplex Virus type 1 Thymidine Kinase

HQC Hydroxychloroquine IcircRNA intronic circRNA

IDT Integrated DNA Technologies

IgG Immunoglobulin G

KD Knockdown

LB Lysogeny broth

LBL lymphoblastic lymphoma

LSC Leukemic stem cell

mAb Monoclonal antibodies

MEPs megakaryocyte/erythrocyte progenitors

MFC multi-channel flow cytometry

miRNA Micro RNA

MKP megakaryocyte progenitor
MRD Minimal residual disease

mRNA Messenger RNA
MS Mass spectrometry
ncRNA Non-coding RNA

NGS Next Generation Sequencing

nt Nucleotide

OE Overexpression

ori Origin of replication

OE Overexpression

pAb Polyclonal antibody

PBS Phosphate-buffered saline PCR Polymerase chain reaction

piRNA PIWI-interacting RNA

PI Propidium iodide
Pre-miRNA Precursor miRNA
RBP RNA-binding protein

RNA-seq RNA sequencing
RNA Ribonucleic acid

RNA FISH RNA Fluorescence in situ hybridization

rRNA Ribosomal ribonucleic acid

RT-qPCR Real-time PCR SCF Stem cell factor

SDS Sodiumdodecylsulfate

SFFV spleen focus-forming virus

siRNA Small interfering RNA snoRNA Small nucleolar RNA snRNA Small nuclear RNA SV40 Simian-Virus 40

TBST Tris-buffered saline with Tween20

TMED Tetramethylethylendiamin

tRNA Transfer RNA

WBC White blood cell count

WHO World Health Organization

WT Wild type

9.2 Table Directory

Table 1: Immunophenotype of B- and T-ALL and their subtypes	15
Table 2: 2016 World Health Organization classification of B- and T-acute lymphoblastic leukemia/lymphoma 11	17
Table 3: Risk factors in pediatric acute lymphoblastic leukemia ⁵⁴	18
Table 4: Media and cell culture supplements	31
Table 5: Reagents and chemicals	32
Table 6: Kits and ladders	34
Table 7: Commercially available oligonucleotides	35
Table 8: Oligonucleotides	35
Table 9: RNA FISH probes	36
Table 10: siRNAs	36
Table 11: Plasmids	37
Table 12: Antibodies.	41
Table 13: Enzymes	41
Table 14: Other consumables	42
Table 15: Software	43
Table 16: Hardware	43
Table 17: RNase R treatment	46
Table 18: cDNA Synthesis using M-MLV reverse transcriptase.	47
Table 19: RT-qPCR compositions	48
Table 20: RT-qPCR conditions (GoTaq®)	48
Table 21: Polyadenylation, first-strand synthesis, and RT-qPCR of miRNAs	49
Table 22: PCR reaction using Phusion HF (High Fidelity)	50
Table 23: PCR conditions	50
Table 24: PCR for Sanger sequencing	51
Table 25: PCR condition	51
Table 26: Composition of the double digestion mix	52
Table 27: Composition of transfection mix	53
Table 28: Overview of significantly dysregulated genes upon circATG5 4-5 overexpression	74

9.3 Figure Directory

Figure 1: Most prevalent cancer types presenting in childhood (age <18 years) in Germany	10
Figure 2: Scheme of hematopoiesis.	11
Figure 3: Classification of non-coding RNAs.	19
Figure 4: Pathways of circular RNA biogenesis	21
Figure 5: CircRNA functions 89	23
Figure 6: Schematic illustration of microautophagy and chaperone-mediated autophagy in mammalian, Infrom 105	_
Figure 7: Mammalian autophagy pathway. Image taken from ¹⁰⁷ .	
Figure 8: pcDNA3.1(+) CircRNA Mini Vector card.	
Figure 9: Autophagy LC3 HiBiT Reporter vector card from Promega	
Figure 10: LeGO-IG2, mammalian expression, lentiviral	
Figure 11: Autophagy LC3 HiBiT Reporter Assay system (Promega)	
Figure 12: Identification of circATG5 4-5 in RNA seq data (Cai Chen and Daniel Picard)	
Figure 13: Schematic presentation of circRNAs derived from the human gene ATG5	
Figure 14: The circATG5 4-5 can be validated by PCR and Sanger sequencing	
Figure 15: Expression of circATG5 4-5 in leukemia cell lines	
Figure 16: Analysis of the subcellular localization of circATG5 4-5 by RNA-FISH	
Figure 17: CircATG5 4-5 overexpression construct	
Figure 18: The expression of circATG5 4-5 can be upregulated (an example of a non-lentiviral vector pcD)	
Mini vector)	1 1
Figure 19: The generated circATG5 4-5 is resistant RNase R	
Figure 20: Overexpression of circATG5 4-5 using lentiviral vector.	
Figure 21: circATG5 4-5 and ATG5 mRNA tend to move in tandem	
Figure 22: The overexpression of circATG5 4-5 positively influences ATG5	
Figure 23: The circATG5 4-5 knockdown is associated with a downregulation of ATG5	
Figure 24: CircATG5 4-5 influences the stability of ATG5	
Figure 25: The overexpression of circATG5 4-5 has an impact on several genes	
Figure 26: Top significantly dysregulated genes through circATG5 4-5 overexpression (RNA-Seq)	
Figure 27: CircATG5 4-5 affects cellular autophagy activity	
Figure 28: Potential circATG5 4-5-miRNA interactions	
Figure 29: Expression of miRNAs in HEK293, 697 and HAL-01 cell lines	
Figure 30: Impact of circATG5 4-5 on miRNA expression in HEK293, 697 and HAL-01	
Figure 31: Overexpression of circATG5 4-5 is associated with increased CDK6 mRNA levels	
Figure 32: Correlation of circATG5 4-5 and ATG5 mRNA with CDK6	
Figure 33: The overexpression of circATG5 4-5 promotes cell viability	
Figure 34: CircATG5 4-5 regulates cell proliferation.	
Figure 35: Overexpression of circ ATG5 4-5 leads to G2M	85

Publications

Daniel Rickert1, Jasmin Bartl1, Daniel Picard1, Flavia Bernardi, Nan Qin1, Marta Lovino, Stéphanie Puget, Frauke-Dorothee Meyer, Idriss Mahoungou Koumba et al., Circular RNA profiling distinguishes medulloblastoma groups and shows aberrant RMST overexpression in WNT medulloblastoma. Acta Neuropathol 141, 975–978 (2021). Doi: 10.1007/s00401-021-02306-2

Jasmin Bartl, Marco Zanini, Flavia Bernardi, Antoine Forget, Lena Blümel, Julie Talbot, Daniel Picard, Nan Qin, Gabriele Cancila, Qingsong Gao, Soumav Nath, Idriss Mahoungou Koumba et al., The *HHIP-AS1* IncRNA promotes tumorigenicity through stabilization of dynein complex 1 in human SHH-driven tumors. *Nat Commun* 13, 4061 (2022). Doi: 10.1038/s41467-022-31574-z

Affirmation

Hereby, I declare on oath that I composed this dissertation independently by myself. I used only the references and resources indicated in this thesis. With the exception of such quotations, the work presented in this thesis is my own. I have accredited all the sources of help. This PhD thesis was never submitted or presented in a similar form to any other institution or examination board. I have not undertaken a doctoral examination without success so far.

Düsseldorf, 18.03.2025

Idriss Edler Koumba Mahoungou